



# 16ENV10 MetroRADON

## Deliverable D1

Method for the traceable calibration of radon ( $^{222}\text{Rn}$ ) measurement instruments at low activity concentrations ( $100 \text{ Bq/m}^3$  to  $300 \text{ Bq/m}^3$ ) with relative uncertainties  $\leq 5 \%$  ( $k = 1$ )

Physikalisch-Technische Bundesanstalt, Braunschweig, Germany (PTB)

Due date: February 2020

Submission: May 2020

**EMPIR**



The EMPIR initiative is co-funded by the European Union's Horizon 2020 research and innovation programme and the EMPIR Participating States

## Table of contents

1. Introduction .....	3
2. Development of new $^{222}\text{Rn}$ and $^{220}\text{Rn}$ radioactive reference sources with stable and known radon emanation capacity .....	3
3. Establishment of constant and stable $^{222}\text{Rn}$ radon activity concentrations in reference chambers and development of procedures for the calibration of radon measurement instruments at low activity concentrations .....	4
4. Annex .....	5

## 1. Introduction

This document, titled, “Method for the traceable calibration of radon ( $^{222}\text{Rn}$ ) measurement instruments at low activity concentrations (100 Bq/m<sup>3</sup> to 300 Bq/m<sup>3</sup>) with relative uncertainties  $\leq 5\%$  ( $k = 1$ )” represents the deliverable D1 of the EMPIR joint research project 16ENV10 MetroRADON. This report is comprised of a short overview section and several detailed project reports that are attached to this document as Annexes.

The calibration procedures in the activity concentration range from 100 Bq/m<sup>3</sup> to 300 Bq/m<sup>3</sup> were developed using  $^{222}\text{Rn}$  gas and emanation standards developed within MetroRADON. The results are described in the combined report of A1.3.1 and A1.3.2 in the Annex.

The development of novel procedures for the traceable calibration of radon ( $^{222}\text{Rn}$ ) measurement instruments at low activity concentrations (100 Bq/m<sup>3</sup> to 300 Bq/m<sup>3</sup>) with relative uncertainties  $\leq 5\%$  ( $k = 1$ ) was organized in WP1 in two parts described in Task 1.1: Development of new  $^{222}\text{Rn}$  and  $^{220}\text{Rn}$  radioactive reference sources with stable and known radon emanation capacity and Task 1.3: Establishment of constant and stable  $^{222}\text{Rn}$  radon activity concentrations in reference chambers and development of procedures for the calibration of radon measurement instruments at low activity concentrations. The procedures described here are linked to Task 5.3: Validation of the traceability of European radon calibration facilities at stable radon atmospheres in the range from 100 Bq/m<sup>3</sup> to 300 Bq/m<sup>3</sup> that will be discussed in detail in Deliverables D7 and D8.

## 2. Development of new $^{222}\text{Rn}$ and $^{220}\text{Rn}$ radioactive reference sources with stable and known radon emanation capacity (Task 1.1)

The aim of this task was to develop reference radon sources for  $^{222}\text{Rn}$  (radon) and  $^{220}\text{Rn}$  (thoron) with constant, stable measured emanations traceable to primary standards, based on three different technologies and to compare these sources with decaying radon gas standards. The activity ranges of the emanation sources depend on the volumes of the calibration chambers in which they were used, and they are built in order to generate radon activity concentrations between 100 Bq/m<sup>3</sup> and 300 Bq/m<sup>3</sup> in the specific calibration chambers of BfS, BFKH, IFIN-HH, IRSN, METAS and SUJCHBO.

PTB, supported by JRC has developed  $^{222}\text{Rn}$  and  $^{220}\text{Rn}$  emanation sources including a detector system for the continuous monitoring of the emanated activity of  $^{222}\text{Rn}$  relative to the activity of the  $^{226}\text{Ra}$  source (and emanated  $^{220}\text{Rn}$  relative to activity of  $^{228}\text{Th}$  source) traceable to primary standards. The results are described in activity report A1.1.1 in the Annex.

CEA has developed  $^{222}\text{Rn}$  and  $^{220}\text{Rn}$  emanation sources using polymers. The results are described in activity report A1.1.2 in the Annex. The radon emanation of the sources is not quantitative. These sources are used by CEA and METAS for the development of a method for direct and traceable measurement of the activity concentration of  $^{222}\text{Rn}$  and  $^{220}\text{Rn}$  in an air flow. The results are described in activity report A1.1.4 in the Annex.

CMI with support from SUJCHBO has developed a long term stable  $^{222}\text{Rn}$  low activity emanation flow-through standard source based on a metering flow controller and dispenser generating a known  $^{222}\text{Rn}$  concentration in an air flow. The results are described in activity report A1.1.3 in the Annex.

The quantitative emanations from the two types of sources, developed at PTB and CMI, were compared with the results obtained with the “in air flow measurement system” developed at CEA. The results are described in the combined report of A1.1.5 and A1.1.6 in the Annex.

### **3. Establishment of constant and stable $^{222}\text{Rn}$ radon activity concentrations in reference chambers and development of procedures for the calibration of radon measurement instruments at low activity concentrations (Task 1.3)**

The aim of this task was

- i. to use the  $^{222}\text{Rn}$  radon sources developed in Task 1.1 to establish traceable stable radon activity concentrations in reference chambers in the laboratories at BfS, BFKH, IFIN-HH, IRSN, METAS and SUJCHBO,
- ii. to develop calibration procedures for these reference chambers for the radon activity concentration range from  $100 \text{ Bq/m}^3$  to  $300 \text{ Bq/m}^3$ ,
- iii. to use these new reference  $^{222}\text{Rn}$  fields to calibrate radon measurement instruments, including those instruments that will then be used in WP5 to validate the traceability of European radon calibration facilities, and to determine their accuracy,
- iv. based on this information, to document a method for the traceable calibration of radon ( $^{222}\text{Rn}$ ) measurement instruments at low activity concentrations ( $100 \text{ Bq/m}^3$  to  $300 \text{ Bq/m}^3$ ) with relative uncertainties  $\leq 5 \%$  ( $k = 1$ ).

The new  $^{222}\text{Rn}$  emanation sources developed and compared in A1.1.1-A1.1.5 together with existing certified reference volumes were installed at BfS, BFKH, IFIN-HH, IRSN, METAS and SUJCHBO reference chambers in order to establish constant and traceable  $^{222}\text{Rn}$  activity concentrations.

BfS, IFIN-HH, BFKH, IRSN, METAS and SUJCHBO developed calibration procedures for their reference chambers in the activity concentration range from  $100 \text{ Bq/m}^3$  to  $300 \text{ Bq/m}^3$  using  $^{222}\text{Rn}$  gas and emanation standards developed and compared in A1.1.1-A1.1.6. The results are described in the combined report of A1.3.1 and A1.3.2 in the Annex. The result is not one single and unified calibration method but very similar methods using slightly different sizes of calibration chambers and a bit different instrumentation of sensors, flow controllers, etc. The comparability of the calibrations at the six mentioned facilities is documented in Deliverable D7 "Validation report on the traceability of primary and secondary radon calibration facilities in Europe". The goal to develop procedures for the calibration of radon measurement instruments at low activity concentrations (in the activity concentration range from  $100 \text{ Bq/m}^3$  to  $300 \text{ Bq/m}^3$ ) with sufficiently low relative uncertainties  $\leq 5 \%$  was reached. Time stable activity concentrations in this range have been established with the following uncertainties ( $k = 1$ ) at: BfS with 1.0 %, IRSN with 2 %, METAS with 1.5 %, and SUJCHBO with 2 %. Long exposure times of about 40 hours were used to realize uncertainties of the calibration factors for radon measurement instruments close to the uncertainties of the activity concentrations.

IRSN, IFIN-HH, BFKH, BfS, SUJCHBO and METAS have determined the accuracy of commonly used integrated radon measurement instruments (alpha-track detectors, electrets, etc.) and novel detectors using their radon reference chambers upgraded in A1.3.1 and the calibration procedures from A1.3.2. The results are described in activity report A1.3.3 in the Annex.

## **4. Annex**

- 4.1 Report of Activity A1.1.1
- 4.2 Report of Activity A1.1.2
- 4.3 Report of Activity A1.1.3
- 4.4 Report of Activity A1.1.4
- 4.5 Combined report of Activities A1.1.5 and A1.1.6
- 4.6 Combined report of Activities A1.3.1 and A1.3.2
- 4.7 Report of Activity A1.3.3



# 16ENV10 MetroRADON

Activity A1.1.1

$^{222}\text{Rn}$  and  $^{220}\text{Rn}$  emanation source development

PTB, JRC Geel

Due date: January 2019  
Submission: February 2020

**EMPIR**



The EMPIR initiative is co-funded by the European Union's Horizon 2020 research and innovation programme and the EMPIR Participating States

## Table of contents

1	$^{222}\text{Rn}$ and $^{220}\text{Rn}$ emanation source development at JRC and PTB.....	4
2	Description of the task.....	4
3	Radon emanation source preparation approaches at JRC .....	4
3.1	JRC measurement setups.....	5
3.2	Drop deposition source preparation at JRC.....	5
3.3	Chemical adsorption (chemisorption) .....	5
3.4	Conclusions of JRC .....	6
4	Source Production at PTB .....	7
4.1	Determination of deposited $^{226}\text{Ra}$ activity.....	10
4.2	Determination of the emanation coefficient.....	12
4.3	Influence of humidity.....	16
4.4	Conclusions of PTB.....	18
5	References .....	19

## List of Figures:

Figure 1: Manganese-dioxide discs as radon emanation source in a closed airtight glass vessel.....	6
Figure 2: Apparatus for the electrodeposition of $^{226}\text{Ra}$ .....	7
Figure 3: SEM pictures of the deposit with different magnifications.....	9
Figure 4: Autoradiograph of source 2018-1441 with 0.04 mm <sup>2</sup> pixel size. The coordinate systems origin refers to the center of the circular stainless-steel disc carrying the deposit .....	9
Figure 5: Typical alpha-particle spectrum of electrodeposited sources. FWHM of the 4786 keV Ra-226 Peak is 21 keV .....	12
Figure 6: LaBr <sub>3</sub> $\gamma$ -spectrum of a sealed $^{226}\text{Ra}$ source.....	16
Figure 7: Evolution of the emanation power $\chi$ and relative humidity %rH with time .....	17
Figure 8: Emanation power of an electrodeposited $^{226}\text{Ra}$ source represented by count rate ratios and relative humidity as function of time .....	17
Figure 9: Drying process of an electrodeposited $^{226}\text{Ra}$ emanation source.....	18

## List of Tables:

Table 1: Radon emanation sources and their main features. Measurements were performed using AlphaGuard 2000 radon detector.....	6
Table 2: Overview over produced $^{226}\text{Ra}$ sources, activity determinations and the respective emanation coefficients $\chi$ .....	8
Table 3: Overview over produced $^{228}\text{Th}$ sources with activity determinations .....	10
Table 4: Uncertainty budget for $^{226}\text{Ra}$ activity determination of source 2017-1709.....	11
Table 5: Uncertainty budget for an 86400 s measurement of source 2017-1709 .....	13
Table 6: Uncertainty budget for the determination of the effective emanation coefficient $\chi$ derived using the count rate approach .....	15
Table 7: Uncertainty budget for the determination of the activity concentration in the reference volume at a specified position of taking the sample.....	15

## 1 $^{222}\text{Rn}$ and $^{220}\text{Rn}$ emanation source development at JRC and PTB

### 2 Description of the task

PTB, supported by JRC who have experience of emanation sources, will develop  $^{222}\text{Rn}$  and  $^{220}\text{Rn}$  emanation sources (with a relative target uncertainty  $\leq 5\%$  ( $k = 1$ )) at PTB, including a detector system for the continuous monitoring of the emanated activity of  $^{222}\text{Rn}$  relative to the activity of the  $^{226}\text{Ra}$  source (and emanated  $^{220}\text{Rn}$  relative to activity of  $^{228}\text{Th}$  source) which is traceable to primary standards. The sources will consist of the radionuclide, based on a radium/thorium salt, and deposited on exchangeable carriers.

Using the new emanation sources PTB and JRC then will evaluate the influence of changes in temperature, humidity and air pressure on the emanation rate.

The new emanation standards for  $^{220}\text{Rn}$  have been produced by electrolytic deposition from a  $^{228}\text{Th}$  solution onto solid metal discs (Linzmaier & Röttger, 2013, 2014). For the activity determination and the determination of the emanation coefficient  $\chi$  apply the same techniques as for the  $^{222}\text{Rn}$  emanation sources, which are described below, accordingly.

New emanation standards for  $^{222}\text{Rn}$  have been produced by electrodeposition of  $^{226}\text{Ra}$  onto solid metal discs (Mertes et al., 2020). Activity determination of deposited  $^{226}\text{Ra}$  on these discs is carried out by defined solid-angle  $\alpha$ -particle spectrometry as a primary measurement technique (Dersch, 2004; Picolo, 1996; Picolo et al., 2000). The emanation coefficient  $\chi$  is deduced from  $\gamma$ -ray spectrometry comparing the measured full-energy peak count-rates in the  $^{226}\text{Ra}$  decay chain of open and sealed electrodeposited  $^{226}\text{Ra}$  sources. The resulting emanation sources can be used as primary standards for the  $^{222}\text{Rn}$  activity concentration, since the  $^{226}\text{Ra}$  activity is measured by an absolute technique and the emanation coefficient  $\chi$  is determined without the need for another  $^{222}\text{Rn}$  standard.

### 3 Radon emanation source preparation approaches at JRC

For making high quality radon emanation sources the feasibility of several source preparation approaches was studied like electrodeposition, drop deposition, chemical adsorption and precipitation. Since other project partners had already invested extensive work in certain source preparation approaches (e.g. PTB chose to develop electrodeposited sources and LNHB tested precipitated source preparation), JRC decided to focus on drop deposition and chemisorption source preparations to avoid duplication of these works within the MetroRADON project.

Apart from the main *Activity* objectives, JRC set some extra requirements for preparing radon emanation sources as listed below:

- Prepare multi-purpose radon sources that can be used for radon-in-air as well as radon-in-water experiments.
- “Green/environmentally friendly approach”: to reduce use of and energy, chemicals and eventually waste.
- Reusable electrolyte that could be used several times for source preparation just by feeding the necessary initial  $^{226}\text{Ra}$  activity.

These requirements were considered when drop deposition and chemisorption source preparation approaches were tested and further refined.

### 3.1 JRC measurement setups

The following radon measurement devices were available at JRC during the project: RAD 7 (DurrIDGE Ltd.), Alphaguard2000 (Saphymo GmbH) and Radim type (SMM Prague) active radon monitors, high-purity germanium (HPGe)  $\gamma$ -ray detectors.

For absolute activity measurements defined solid angle alpha particle spectrometry as primary measurement technique and liquid scintillation counters were also available. However, due to other project priorities we were not able to use them to characterize our emanation sources for  $^{226}\text{Ra}$  activity measurements. Therefore, we had to rely on the manufacturer's certificates of the standardised radioactive material.

### 3.2 Drop deposition source preparation at JRC

The first source preparation approach was a very simple straightforward method, based on depositing a known activity of  $^{226}\text{Ra}$  on a substrate (paper filter, glass backing etc.) and encapsulate it in a radon permeable material. In this way  $^{226}\text{Ra}$  is fixed and encapsulated in a solid matrix and cannot contaminate its environment. One of the pitfalls is that radon permeability strongly depends on environmental parameters like temperature, humidity and pressure. Therefore, for such emanation sources the experimental conditions must stay stable and fully controlled during the experiments.

Approximately 586 Bq  $^{226}\text{Ra}$  was deposited on a paper filter, dried and sealed in a commercially available light density polyethylene (LDPE) foil. The LDPE foil thickness was found to be  $(46 \pm 4) \mu\text{m}$ , which was sufficiently thin for being radon permeable. The  $^{226}\text{Ra}$  standardized solution was obtained from the Czech Metrology Institute (Eurostandard).

The highest emanation power of a drop deposited radon source was moderate (66 %) and needed more than two days to reach the maximum saturation activity concentration in the small volume test chamber (1.5 L).

Therefore, we plan to further adjust this approach by changing some parameters listed below:

- Target materials: glass, metal (Ni steel),
- Pre-treated with a seeding agent including colloidal silica to obtain more homogeneous radium source,
- Thermal treatment: convert radium to oxide to make the source physically more bound to the target substrate,
- Covering with thin co-polymer VYNS (polyvinyl chloride-acetate copolymer) foil  $< 20 \mu\text{g}/\text{cm}^2$  thickness,  $^{222}\text{Rn}$  can escape but radium stays. However, VYNS foil needs to be replaced time to time due to physical degradation.

### 3.3 Chemical adsorption (chemisorption)

For  $^{226}\text{Ra}$  chemisorption manganese-dioxide ( $\text{MnO}_2$ ) based discs from TrisKem International were used (TrisKem). These discs are thick polyamide substrates covered with manganese-dioxide. The procedure and application of manganese-dioxide coated polyamide discs were originally described by Heinz Surbeck (Nucfilm, Switzerland). In contact with water manganese-dioxide discs works as a highly selective cation exchanger for alkaline-earth ions (including radium). Thus, radium can be adsorbed to the surface and bound strongly on the disc. One of the emanation sources obtained from chemisorption experiment is presented in Figure 1.

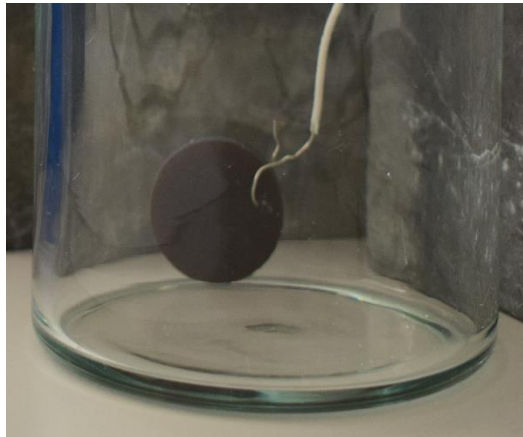


Figure 1: Manganese-dioxide discs as radon emanation source in a closed airtight glass vessel

The deposited activity was homogeneously distributed over the disc surface, which makes this source preparation approach a very good candidate for preparing good quality homogeneous emanation sources. As a disadvantage, we still observe very low  $^{226}\text{Ra}$  adsorption yield from the initial  $^{226}\text{Ra}$  bearing stock solution (< 10 % - 30 %) and low emanation power which suggests further method refinement. Furthermore, the manufacturer indicates 2 years as shelf life of the product. Therefore, the degradation of emanation source can be expected, and the source stability has to be checked on a regular basis. The main features of the radon emanation sources are summarized in Table 1.

Table 1: Radon emanation sources and their main features.  
Measurements were performed using AlphaGuard 2000 radon detector.

Source name	Preparation mode	Emanation power	Relative uncertainty
RnDdep	Drop deposition	$0.67 \pm 0.05$	7.4%
Metro-Rn01	Chemisorption	$0.20 \pm 0.03$	15%
Metro-Rn02	Drop deposition (filter)	$0.74 \pm 0.04$	5.6%
Metro-Rn03	Drop deposition (laminated filter)	$0.10 \pm 0.03$	30%
Metro-Rn04	Chemisorption	$0.18 \pm 0.03$	17%
Metro-Rn04	Chemisorption	$0.25 \pm 0.04$	16%

Source: JRC, 2019.

It is planned to further refine chemisorption and testing new emanation source preparation options (e.g.  $^{226}\text{Ra}$  sorption on resins or inorganic materials) and encapsulate them in stable solid cases.

### 3.4 Conclusions of JRC

After a preliminary literature study and consultation with the other project partners, JRC-Geel decided to investigate the feasibility of using drop deposition and chemisorption methods for radon emanation source

preparation. After the tests, we concluded that both tested emanation source preparation methods could be used as a simple radon emanation source preparation approach, but they still have their limitations. Therefore, this suggests further experiments to improve source quality in the future that could include

- optimization of source preparations,
- more accurate emanation power determination with cooperation of a metrology institute,
- further tests of JRC's sources in larger volume calibration chambers.

#### 4 Source Production at PTB

Parker et al. investigated the suitability of electro-deposition of a wide variety of isotopes from slightly acidic organic media at high voltages, and coined the term "molecular plating" for this technique (Getoff et al., 1967; Parker et al., 1964a, 1964b). A non-metallic form of deposition was postulated since the standard reduction potentials of the deposited metals and the overall transported charge are too low to allow for reductive plate-out. With a standard reduction potential of  $-2.8$  V this is especially true for  $\text{Ra}^{2+}$  (Bratsch, 1989).

Whitehead et al. (Whitehead et al., 1992) and Hancock and Martin (Hancock & Martin, 1991) published comparable protocols for the molecular-plating of  $^{226}\text{Ra}$  for environmental samples, which have been used for the production of sources in the range of several 100 Bq  $^{226}\text{Ra}$  from a  $^{226}\text{Ra}$  standard solution. Vargas and De Soto have shown that  $^{226}\text{Ra}$  deposited in such a way will allow for  $^{222}\text{Rn}$  emanation, the amount limited by the thickness of the resulting layer (Vargas and De Soto, 1996; Vargas, 2000). Since  $\text{Ba}^{2+}$  would co-deposit with  $\text{Ra}^{2+}$  (Vargas & De Soto, 1995) and all available  $^{226}\text{Ra}$  standard solutions had  $\text{Ba}^{2+}$  carriers (3 - 6 orders of magnitude more  $\text{Ba}^{2+}$  than  $\text{Ra}^{2+}$ ), the  $\text{Ba}^{2+}$  content was reduced by extraction chromatography prior to deposition in the present study.

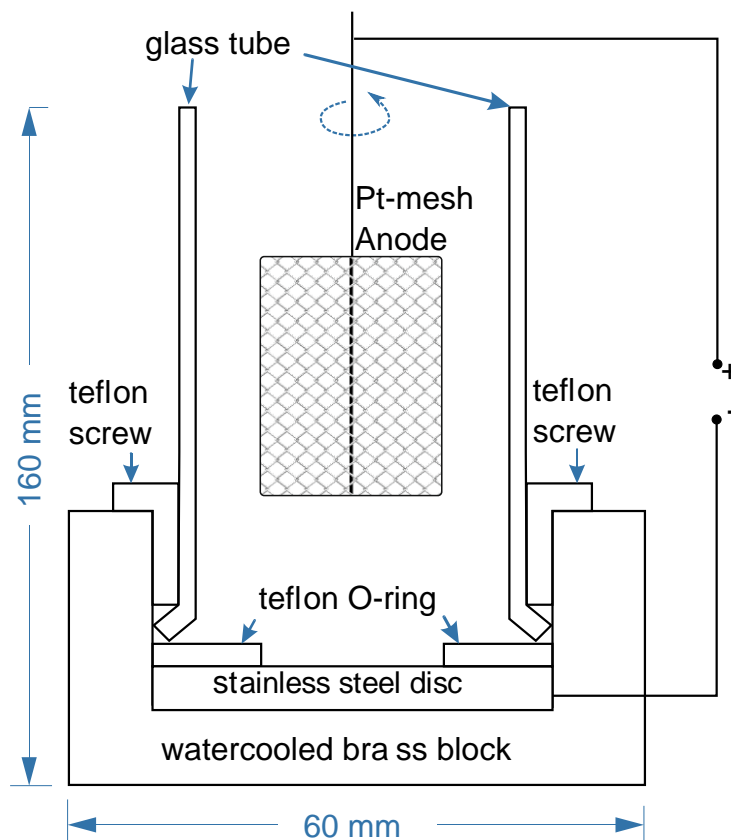


Figure 2: Apparatus for the electrodeposition of  $^{226}\text{Ra}$

The initial chemical composition of the  $^{226}\text{Ra}$  solution (PTB standard  $^{226}\text{Ra}$  solution) employed was nominally 71 kBq  $^{226}\text{Ra}$  as  $\text{RaCl}_2$  in  $0.1 \text{ mol}\cdot\text{L}^{-1}$   $\text{HCl}$  with  $5.7 \text{ mg}\cdot\text{mL}^{-1}$   $\text{Ba}^{2+}$  as  $\text{BaCl}_2\cdot 6 \text{ H}_2\text{O}$  and  $(12.90 \pm 0.13)$  kBq of  $^{133}\text{Ba}$  with the same carrier solution added gravimetrically from a PTB  $^{133}\text{Ba}$  standard solution as a radioactive tracer for inactive  $\text{Ba}^{2+}$ . The resulting solution was evaporated to dryness on a sand-bath ( $90 \text{ }^\circ\text{C}$ ), and 2 mL of 65 %  $\text{HNO}_3$  (Merck, EMSURE<sup>®</sup>, analysis grade) were added to the residue and subsequently removed by evaporation to convert the chlorides into the respective nitrates. The resulting residue was dissolved in 1 mL of 0.6 M  $\text{HNO}_3$  and passed onto a pre-conditioned (30 mL of 0.6 M  $\text{HNO}_3$ ) column of 3 Sr-Resin cartridges (4,4'(5')-bis(tertbutylcyclohexano)-18-crown-6 in 1-Butanol, dispersed on  $\text{SiO}_2$ -particles, purchased from Triskem International). While the resin was initially developed for the preparation of Sr-samples (Philip Horwitz et al., 1992), it has been shown to be an effective chromatography system for the separation of  $\text{Ba}^{2+}$  and  $\text{Ra}^{2+}$  as well (Chabaux et al., 1994). Radium was eluted from the column with 0.6 M  $\text{HNO}_3$  at a flow rate of  $1 \text{ mL}\cdot\text{min}^{-1}$ . Fractions of 10 mL were taken from the eluate and were investigated using gamma-ray spectrometry with a HPGe-Detector. The detection efficiency was deduced from measuring PTB  $^{133}\text{Ba}$  and  $^{226}\text{Ra}$  standard solutions in the same geometry.

Since no  $^{133}\text{Ba}$  could be detected in the first fraction by gamma-ray spectrometry, the  $\text{Ba}^{2+}$  content in this fraction was measured by ICP-MS and found to be  $(86 \pm 5)$  ppb (m/m). The  $^{226}\text{Ra}$  content in this fraction was  $(84 \pm 1)$  ppb (m/m) or  $(3.13 \pm 0.05)$  kBq $\cdot\text{mL}^{-1}$ , as determined by the described gamma-ray spectrometry method. As more significant levels of  $\text{Ba}^{2+}$  were found as detectable  $^{133}\text{Ba}$  in the later fractions, only the first fraction was used in the production of the sources.

To prepare each source, the deposition apparatus shown in was filled with 9 mL of analytical grade ethanol (EtOH, Merck, EMSURE<sup>®</sup>) or 2-propanol (IPA, Merck, EMSURE<sup>®</sup>), respectively. A desired amount of activity of  $^{226}\text{Ra}$  was transferred directly from the first fraction to the cell by means of a pipette. The amount of added  $^{226}\text{Ra}$  was determined gravimetrically. A potential was applied by a Keithley Model 2410 SMU in 2-electrode operation mode. Depositions at constant current density and constant potential were both carried out. While no direct advantage of potentiostatic over galvanostatic deposition was identified, higher voltages and 2-propanol as a solvent seemed to lead to higher deposition efficiency. Deposition times were approximately 1 hour for each source in an open-bench setup. The diameter of the deposit is fixed by a Teflon aperture covering the steel disc with an opening of nominally 15 mm in diameter. A total of 8 sources were produced by this method.

Table 2: Overview over produced  $^{226}\text{Ra}$  sources, activity determinations and the respective emanation coefficients  $\chi$

Source ID	$A_{\text{Ra-226}} / \text{Bq}$ (recovered $A_{\text{Ra-226}}$ )	$\chi$ (N)	Deposition Method / Solvent
2017-1709	$48.01 \pm 0.17$ (49 %)	$0.8260 \pm 0.0013$ (22)	potentiostatic 35 V / EtOH
2017-1710	$58.5 \pm 1.7^a$ (17 %)	$0.7363 \pm 0.0028$ (9)	potentiostatic 35 V / EtOH
2017-1074	$57.5 \pm 2.5^a$ (29 %)	$0.893 \pm 0.003$ (13)	potentiostatic 35 V / EtOH
2018-1437	$104.4 \pm 0.4$ (36 %)	$0.637 \pm 0.005$ (3)	galvanostatic $1 \text{ mA}\cdot\text{cm}^{-2}$ / IPA
2018-1438	$182.2 \pm 0.7$ (43%)	$0.7813 \pm 0.0019$ (4)	galvanostatic $1 \text{ mA}\cdot\text{cm}^{-2}$ / IPA
2018-1439	$184.3 \pm 0.5$ (81 %)	$0.6535 \pm 0.0023$ (9)	potentiostatic 200 V / IPA
2018-1440	$193.9 \pm 0.7$ (65 %)	$0.6533 \pm 0.0023$ (10)	potentiostatic 200 V / IPA
2018-1441	$665.5 \pm 1.9$ (67 %)	$0.7645 \pm 0.0009$ (32)	potentiostatic 90 V / IPA

a: comparative gamma-ray spectrometric determination with 2017-1709 as a reference

Table 2 shows the respective deposition parameters, the resulting activity of the produced sources and their emanation coefficients  $\chi$  as determined by the measurements presented later. SEM-images of the deposit are depicted in Figure 3 and show a highly porous deposit, offering a large surface area for  $^{222}\text{Rn}$  to escape.

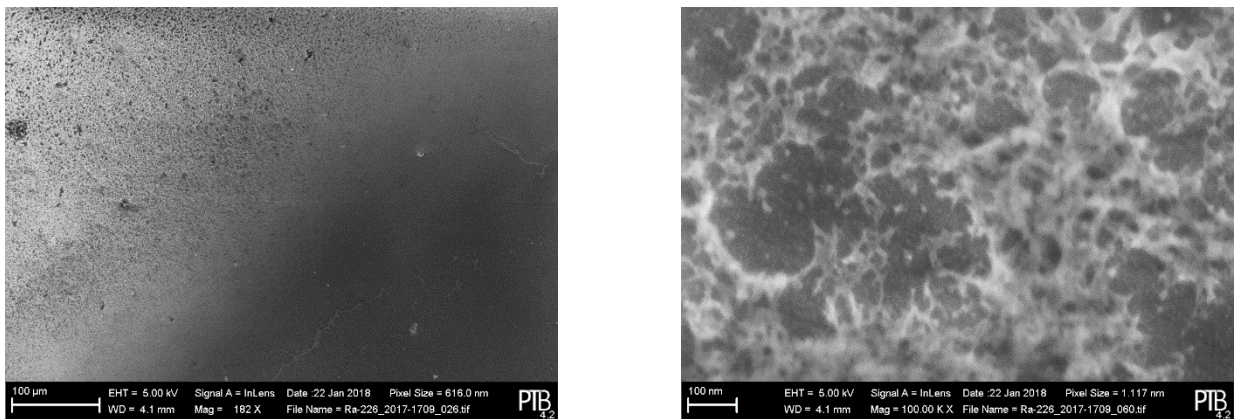


Figure 3: SEM pictures of the deposit with different magnifications

Digital autoradiographs of the sources are taken with a Fujifilm FLA-9000. These yield the relative activity distribution,  $w_{dA}$ , on the source per  $0.04 \text{ mm}^2$  square pixel. A typical radiograph of the produced sources is shown in Figure 4.

The radiographs show that the method does not produce homogeneous deposits, however this is accounted for in the measurement of the  $^{226}\text{Ra}$  activity and is described in more detail below.

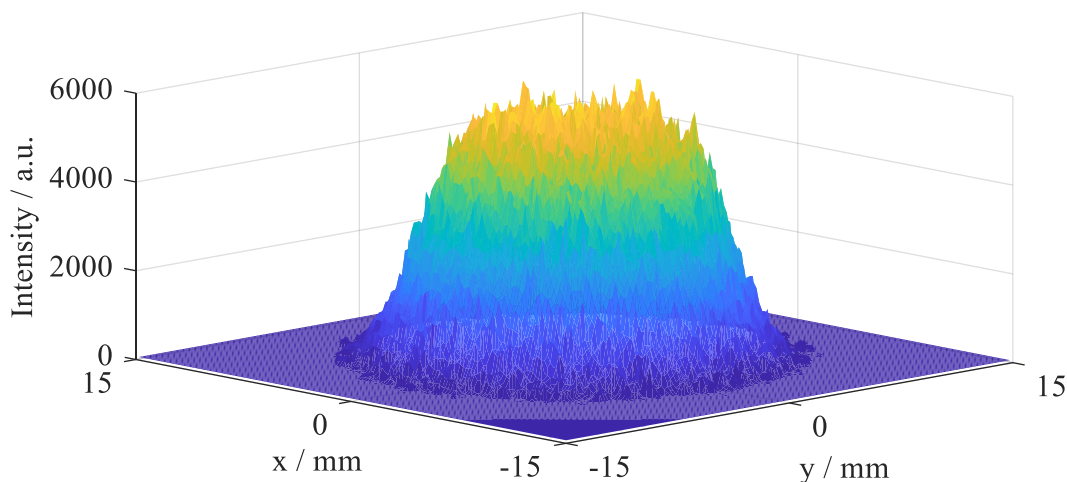


Figure 4: Autoradiograph of source 2018-1441 with  $0.04 \text{ mm}^2$  pixel size. The coordinate systems origin refers to the center of the circular stainless-steel disc carrying the deposit

One of the produced sources was sealed against  $^{222}\text{Rn}$  emanation after alpha-particle- and gamma-ray-spectrometric measurements by gluing a stainless-steel sheet (nominally  $0.05 \text{ mm}$  thickness) onto the source disc with a 2-component epoxy resin (DELO-DUOPOX 01 rapid). Tightness of the seal against  $^{222}\text{Rn}$  emanation was investigated using a calibrated AlphaGuard (Saphymo, Model PQ2000) in diffusion mode that was placed in a noble gas tight reference volume ( $50 \text{ L}$ ) and flushed with aged air. No significant increase in the  $^{222}\text{Rn}$  level was identified after the sealed source was introduced into this reference volume. Given the statistical fluctuation of the AlphaGuard's background reading, its detection limit would allow to detect a leak in the seal down to  $0.5 \%$  of emanating  $^{222}\text{Rn}$ .

Table 3: Overview over produced  $^{228}\text{Th}$  sources with activity determinations

Source ID	$A_{\text{Th-228}} / \text{Bq}$	Deposition Method
ME 2001-1134	1.01E+01	electrolysis
ME 2001-1455	5.73E+00	electrolysis
ME 2001-1456	1.14E+00	electrolysis
ME 2012-1574	9.48E+04	electrolysis
ME 2012-1575	9.48E+04	electrolysis
ME 2012-1576	9.48E+04	electrolysis
ME 2012-1577	9.48E+04	electrolysis
ME 2012-1578	9.48E+04	electrolysis
ME 2012-1579	9.48E+04	electrolysis
ME 2012-1580	9.48E+04	electrolysis

#### 4.1 Determination of deposited $^{226}\text{Ra}$ activity

The deposited  $^{226}\text{Ra}$  activity on each source was determined by defined solid-angle alpha-particle spectrometry. The setup consists of a passivated implanted planar silicon (PIPS) detector ( $300 \text{ mm}^2$ , specified at 17 keV FWHM at 5.5 MeV) and a source holder, which features two apertures that define the solid angle between source and detector. The apertures are at a fixed distance of  $(50.03 \pm 0.03) \text{ mm}$  to one another and have a diameter of their openings of  $(28.00 \pm 0.20) \text{ mm}$  and  $(20.002 \pm 0.010) \text{ mm}$ . The PIPS detector is  $(2.0 \pm 0.5) \text{ mm}$  above the second aperture, whereas the source disc is pressed onto the lower aperture by a spring. All relevant geometrical parameters and assigned uncertainties of the setup are known, traceable to PTB standards. This includes a possible shift of the source against the rotational axis, the distance between the apertures, the distance between the detector and the top aperture, the diameters of the aperture openings and the tilting angles of the apertures against the rotational axis and the detector plane. Measurements are carried out at an air pressure of  $10^{-3} \text{ mbar}$  to suppress the recoil implantation of  $^{222}\text{Rn}$  and decay products into the detector.

The geometry factor  $G$ , which defines the counting efficiency of the setup is given by equation (1).  $G$  is calculated separately by Monte-Carlo integration for each source to account for the different activity distributions on each source. For this purpose, origin points  $(x, y)$  for the trajectories of alpha particles on the source are sampled directly from the associated experimental autoradiography data. Therefore, the inhomogeneity of each deposit is included in its resulting geometry factor  $G$ . This sampling is done by mapping two uniform random floats in the interval  $[0,1]$  to the normalized row- or respectively column-wise cumulative density functions of the autoradiography data. Polar angles  $\theta$  and azimuthal angles  $\phi$  are sampled from a spherical distribution with a bias on  $\theta$  towards the detector. For each pair of  $x, y, \theta$  and  $\phi$ , the given trajectory is checked for intersections with one of the apertures and the detector. After each  $10^7$  iterations, the geometrical parameters of the detector and the apertures are sampled from gaussian distributions given by the known geometrical parameters and associated uncertainties.  $G$  is obtained by counting the trajectories that hit the detector and calculating the fraction of detector hits and total samples and correcting for the applied bias on  $\theta$ . Since the parameters of the geometry are iteratively changed, the distribution of  $G$  around its mean value is obtained by computing a histogram of the calculated values for  $G$ . The technique is in accordance with GUM Supplement 1 (Joint Committee for Guides in Metrology, 2008). A comparable approach has been described in (Arinc et al., 2016).

$$G = \frac{\int_A \Omega_{dA} \cdot w_{dA} dA}{4\pi \int_A w_{dA} dA} \quad (1)$$

where  $\Omega_{dA}$  describes the solid angle subtended between the detector and a surface element,  $dA$ , on the source, and  $w_{dA}$  describes the relative amount of activity in the surface element  $dA$ .

Dead time was corrected by a high-precision pulse generator which is connected to the detector pre-amplifier and is traceable to the PTB frequency standard. Because of the good energy resolution of the resultant alpha-particle spectra with typically 20 keV - 30 keV FWHM in the 4.87 MeV  $^{226}\text{Ra}$  peak, it is assumed that self-absorption in the source and scattering of alpha particles on the source backing is negligible. A GEANT4 simulation (Allison, 2006) of the setup at an estimated source thickness and composition of 500 nm  $\text{BaNO}_3$  and  $5 \cdot 10^8$  alpha-particles with 5 MeV showed that these assumptions can introduce an estimated uncertainty of up to 0.3 %. An extensive analysis of uncertainties in defined solid-angle alpha-particle spectrometry is given in (Pommé, 2015), where a comparable effect of scattering and self-absorption was estimated. Rotation of the source between taking the autoradiograph and performing alpha-particle spectrometry measurements is disregarded since the setup features a very high degree of rotational symmetry. Table 4 shows an example uncertainty budget for the determination of the Ra-226 activity.

Table 4: Uncertainty budget for  $^{226}\text{Ra}$  activity determination of source 2017-1709

Quantity	Value (k = 1)	relative contribution
$N_{\text{Ra-226}}$	$199.5 \cdot 10^3 \pm 6 \cdot 10^2$	66.5 %
$N_{\text{Pulser}}$	$21.595 \cdot 10^6 \pm 5 \cdot 10^3$	0.4 %
$N_{\text{Ra-226,bg}}$	$1.1 \cdot 10^3 \pm 4 \cdot 10^2$	0.9 %
$N_{\text{Pulser,bg}}$	$129.5737 \cdot 10^6 \pm 1.14 \cdot 10^4$	$5 \cdot 10^{-8}$ %
$f$	$(49.995670 \pm 5 \cdot 10^{-6}) \cdot \text{s}^{-1}$	$1 \cdot 10^{-6}$ %
$G$	$9.597 \cdot 10^{-3} \pm 1.8 \cdot 10^{-5}$	28.2 %
$C_{\text{scatter}}$	$0.9985 \pm 0.0009$	6.0 %
$A$	$(48.01 \pm 0.17) \cdot \text{Bq}$	

Equation (2) is used for the analysis of the resultant alpha-particle spectra.

$$A = \frac{f}{G} \cdot \left( \frac{N_{\text{Ra-226}}}{N_{\text{Pulser}}} \cdot c_{\text{scatter}} - \frac{N_{\text{Ra-226,bg}}}{N_{\text{Pulser,bg}}} \right) \quad (2)$$

where  $f$  denotes the frequency of the pulse generator,  $G$  denotes the geometrical efficiency as defined by equation (1) and  $N_{\text{Ra-226}}$ ,  $N_{\text{Ra-226,bg}}$ ,  $N_{\text{Pulser}}$  and  $N_{\text{Pulser,bg}}$  denote the  $^{226}\text{Ra}$  peak net area and the pulser peak net area of the measurement and the background spectra, respectively.  $c_{\text{scatter}}$  denotes a correction factor for possible self-absorption in the source and scattering of  $\alpha$ -particles.

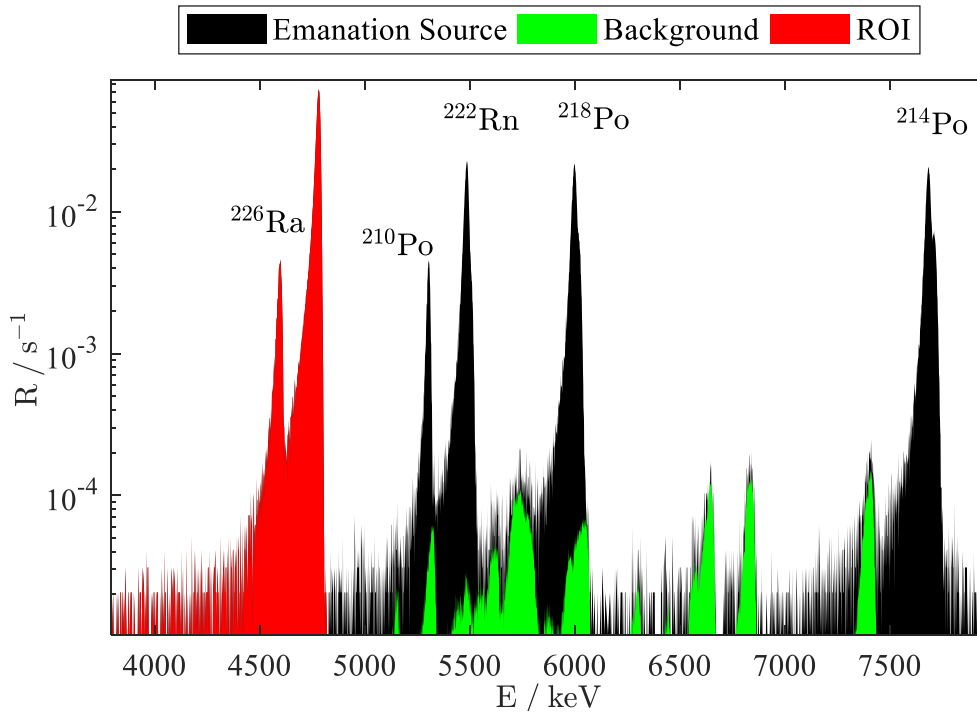


Figure 5: Typical alpha-particle spectrum of electrodeposited sources. FWHM of the 4786 keV  $^{226}\text{Ra}$  Peak is 21 keV

#### 4.2 Determination of the emanation coefficient

The emanation coefficient  $\chi$ , the fraction of emanating  $^{222}\text{Rn}$ , is determined by assessing the distorted equilibrium in the  $^{226}\text{Ra}$  decay chain due to  $^{222}\text{Rn}$  emanation, as shown in equation (3). The method is adapted from (Linzmaier & Röttger, 2014).

$$\chi = 1 - \frac{A_{\text{Rn-222}}}{A_{\text{Ra-226}}} = 1 - \frac{A_{\text{Pb-214}}}{A_{\text{Ra-226}}} \quad (3)$$

where  $\chi$  denotes the emanation coefficient and  $A_{\text{Rn-222}}$ ,  $A_{\text{Ra-226}}$  and  $A_{\text{Pb-214}}$  denote the activity of  $^{222}\text{Rn}$ ,  $^{226}\text{Ra}$  and  $^{214}\text{Pb}$  in the source respectively.

The emanation coefficient  $\chi$  was then determined with equation (4), below, by comparison of the full-energy peak count rate ratios of the respective gamma-ray spectra of the emanation sources and the produced sealed source of the same type and geometry. This leads to significantly lower uncertainty in the emanation coefficient  $\chi$  compared to traditional gamma-ray spectrometric measurement using detector efficiency and transition probabilities as these factors cancel out. The detection efficiency is otherwise commonly amongst the highest contributors to the combined uncertainty in gamma-ray spectrometric measurements.

The measurements of the emanation coefficient  $\chi$  were carried out using 2 HPGe detectors (EG&G Ortec, GEM-F8020P4 and GXP-115220-S) inside lead castles. The sources are mounted in a noble gas tight stainless-steel source holder which is connected in a loop to a reservoir volume to prevent  $^{222}\text{Rn}$  from entering the laboratory and to accumulate  $^{222}\text{Rn}$  inside this volume. The use of the source holder further ensures reproducibility of the measuring geometry. Humidity, pressure and temperature are not controlled inside of the loop. Convection in the loop is forced by a circulating pump at nominally  $1 \text{ L} \cdot \text{min}^{-1}$ . The sources are mounted inside the source holder such that the emerging gamma-rays are passing the layer of epoxy-resin and the stainless-steel sheet to reach the HPGe crystal in case of the sealed source. The possible imperfect seal and thus imperfect secular equilibrium of the sealed source is accounted for by a correction factor  $c_{\text{seal}}$ , which is estimated between 0.995 and 1 because of the detection limit of the AlphaGuard that was used to investigate the tightness of the sealed source as described previously.  $c_{\text{abs}}$  denotes a correction factor which accounts for

the absorption that occurs in the sealed source due to the layer of epoxy-resin and the stainless-steel sheet on the source, and is analytically estimated from the Lambert-Beer law and the respective mass-attenuation coefficients obtained through XCOM (Berger et al., 2019).

$$\varepsilon = 1 - \frac{R_{open}^{Pb-214} - R_{bg}^{Pb-214}}{R_{open}^{Ra-226} - R_{bg}^{Ra-226}} \cdot \frac{R_{sealed}^{Ra-226} - R_{bg}^{Ra-226}}{R_{sealed}^{Pb-214} - R_{bg}^{Pb-214}} \cdot c_{seal} \cdot c_{abs} \quad (4)$$

where  $R_{open}$  and  $R_{sealed}$  denote the respective full-energy peak count rates of the open and the sealed sources and  $R_{bg}$  denotes the associated background count rates. As described above,  $c_{seal}$  and  $c_{abs}$  denote correction factors.

Equation (4) was applied using the  $^{214}\text{Pb}$  peak at 351.9 keV and the  $^{226}\text{Ra}$  peak at 186.2 keV. An example of an uncertainty budget for a day-wise measurement and evaluation of these peaks is shown Table 5. Peak areas and associated uncertainties were determined by subtracting a linear background. Determined values for the emanation coefficient  $\chi$  are given for each source in Table 2. Uncertainties of the emanation coefficient  $\chi$  listed in Table 2 are calculated with the uncertainty of the mean values of the full-energy peak count rate ratios of N day-wise measurements. Background spectra were measured before measuring each source and showed stability in the  $^{222}\text{Rn}$  progeny count rates. Within the measurement uncertainties, the emanation coefficient  $\chi$  appeared stable over the N day-wise measurements taken for each source.

Table 5: Uncertainty budget for an 86400 s measurement of source 2017-1709

Quantity	Value / $\text{s}^{-1}$ ( $k = 1$ )	relative contribution
$R_{sealed}^{Ra-226}$	$0.2869 \pm 0.0026$	10.2 %
$R_{sealed}^{Pb-214}$	$1.7812 \pm 0.0026$	0.2 %
$R_{open}^{Ra-226}$	$0.0856 \pm 0.0016$	58.8 %
$R_{open}^{Pb-214}$	$0.0825 \pm 0.0013$	25.1 %
$R_{bg}^{Ra-226}$	$0.0146 \pm 0.0005$	2.5 %
$R_{bg}^{Pb-214}$	$0.0023 \pm 0.0004$	2.1 %
$c_{seal}$	$0.9950 \pm 0.0029$	0.9 %
$c_{abs}$	$1.0041 \pm 0.0014$	0.2 %
$\chi$	$0.827 \pm 0.005$	

With respect to  $^{220}\text{Rn}$  the emanation coefficient  $\chi$  has to be extended to an effective emanation coefficient  $\chi_e$  (Röttger et al., 2010) and is given by

$$\chi_e = \frac{A(\text{Rn} - 220)}{A(\text{Th} - 228)} = 1 - \frac{R_2 \cdot A(\text{Pb} - 212)}{R_1 \cdot A(\text{Ra} - 224)}, \quad (5)$$

where  $R_1$  represents the recoil correction of  $^{224}\text{Ra}$  activity. During the  $\alpha$ -decay of  $^{228}\text{Th}$ , the produced  $^{224}\text{Ra}$  nuclei can be recoiled from the open source and implanted in other surfaces nearby. The same is true in principle in the case of the  $\alpha$ -decay of  $^{216}\text{Po}$ , resulting in the correction term  $R_2$ . This effect results in a small activity loss and also in an additional background, which in this publication will be called the background of second order (that is, the background of first order, which is the conventional background of  $\gamma$ -ray spectrometry, plus the additional background produced from deposited activity inside the emanation housing

from recoil and wall-attached thoron progenies). Both effects, the recoil-induced loss of activity and the two types of background can be measured and included in the uncertainty budget for the respective isotopes  $^{224}\text{Ra}$  as well as the thoron progenies.

The choice of  $^{224}\text{Ra}$  and  $^{212}\text{Pb}$  for observing the gas-flow-induced disequilibrium was made because of their  $\gamma$ -transitions, s. (Bé M.-M. Chisté V., 2004):  $^{224}\text{Ra}$  has an emission at 240.986 keV (with 4.12 % emission probability) whereas  $^{212}\text{Pb}$  has one at 238.632 keV with an emission probability of 46.3 %. These energies are so close to each other that the number of counts in each peak is practically independent of the relative efficiency of the detector.

Working on this assumption, there are two approaches to provide traceability for the determination of the transfer thoron gas activity. The first one is the conventional line of traceability for  $\gamma$ -ray spectrometry including the emission probabilities of the respective isotopes. Since only transitions after the decay of  $^{228}\text{Th}$  are compared, this procedure is independent of the recoil correction. The second one, which here is called the count rate approach, is based on the comparison to the  $\gamma$ -spectra of the open source and a gas-tight sealed source in the same geometry. In this case no emission probabilities have to be included. This reduces the resulting uncertainty significantly, though we have here a dependency on the recoil.

Both approaches can be applied to the online supervision, to the activity transferred to the reference volume.

The conventional approach yields

$$\chi = 1 - \frac{\dot{Z}_m(\text{Pb} - 212) - \dot{Z}_{bg2,A,t}(\text{Pb} - 212)}{\dot{Z}_m(\text{Ra} - 224) - \dot{Z}_{bg2,A,t}(\text{Ra} - 224)} \cdot \frac{p_\gamma(\text{Ra} - 224)}{p_\gamma(\text{Pb} - 212)}, \quad (6)$$

in which  $\dot{Z}$  gives the count rates of the respective  $\gamma$ -lines, the index  $m$  represents the measurement with the open source while creating a reference atmosphere, the background count rate of second order is given by  $\dot{Z}_{bg2,A,t}$ , since this background is dependent on the activity and the state of equilibrium reached inside the emanation housing.

This results in an effective emanation coefficient for the  $^{228}\text{Th}$  source ( $A(^{228}\text{Th}) = (8.18 \pm 0.12) \text{ kBq}$ ) of  $\chi = 0.405 \pm 0.014$  for  $k = 1$ . The uncertainty of the result is dominated by the uncertainties of the emission probabilities  $p_\gamma(\text{Ra} - 224)$  (57 %) and  $p_\gamma(\text{Pb} - 212)$  (35 %).

Thus, the conventional approach will always be limited to a relative standard uncertainty above 3 %.

The count rate approach yields

$$\chi = 1 - \left( R_2 \frac{\dot{Z}_k(\text{Ra} - 224) - \dot{Z}_{bg1}(\text{Ra} - 224)}{\dot{Z}_k(\text{Pb} - 212) - \dot{Z}_{bg1}(\text{Pb} - 212)} \right) / \left( R_1 \cdot \frac{\dot{Z}_m(\text{Ra} - 224) - \dot{Z}_{bg2,A,t}(\text{Ra} - 224)}{\dot{Z}_m(\text{Pb} - 212) - \dot{Z}_{bg2,A,t}(\text{Pb} - 212)} \right), \quad (7)$$

in which  $\dot{Z}$  indicates the count rates of the respective  $\gamma$ -lines, the index  $k$  represents the calibration with the sealed source, the index  $m$  represents the measurement with the open source while creating a reference atmosphere and the two types of background are indicated by the indices  $bg1$  and  $bg2,A,t$ , since the background of second order is also dependent of the activity and the state on equilibrium reached inside the emanation housing. In the uncertainty budget of Table 6, the background of the second order is given at the time of certified activity and corrected later for the time difference of certified activity and time of application,  $t_A$ .

The result for the effective emanation of the same  $^{228}\text{Th}$  source is  $\chi = 0.4105 \pm 0.0016$  for  $k = 1$  (see also Table 6). The uncertainty budget is dominated by the stability of the count rates during the emanation measurements and the statistical limit of the calibration with the closed source. In this example, the count rate approach results in a relative standard uncertainty of 0.4 %. This uncertainty is an order of magnitude smaller than the conventional approach.

With this concept, a realization of a true reference atmosphere for  $^{220}\text{Rn}$  (primary standard) has been accomplished for the first time (Röttger et al., 2010).

Table 6: Uncertainty budget for the determination of the effective emanation coefficient  $\chi$  derived using the count rate approach

$X_i$	$x_i$	$u(x_i)$	$C_i \cdot u(x_i)$	Relative contribution
$Z_k(\text{Ra-224})$	$2395 \cdot 10^2$	$5 \cdot 10^2$	$-1.2 \cdot 10^{-3}$	62.8 %
$Z_k(\text{Pb-212})$	$2581.2 \cdot 10^3$	$1.6 \cdot 10^3$	$370 \cdot 10^{-6}$	5.5 %
$Z_m(\text{Ra-224})$	$6776 \cdot 10^2$	$6 \cdot 10^2$	$500 \cdot 10^{-6}$	10.1 %
$Z_m(\text{Pb-212})$	$4333 \cdot 10^3$	$6 \cdot 10^3$	$-730 \cdot 10^{-6}$	21.6 %
$t_k$	$23553 \cdot 10^1 \text{ s}$	$6 \cdot 10^1 \text{ s}$	$660 \cdot 10^{-9}$	0.0 %
$t_m$	$77640 \cdot 10^1 \text{ s}$	$6 \cdot 10^1 \text{ s}$	$-130 \cdot 10^{-9}$	0.0 %
$t_{bg1}$	$182340 \cdot 10^1 \text{ s}$	$6 \cdot 10^1 \text{ s}$	$-85 \cdot 10^{-9}$	0.0 %
$t_{\Delta}$	$222196 \cdot 10^4 \text{ s}$	$5 \cdot 10^4 \text{ s}$	$1.0 \cdot 10^{-6}$	0.0 %
$Z_{bg1}(\text{Ra-224})$	$123.8 \cdot 10^2$	$1.2 \cdot 10^2$	$36 \cdot 10^{-6}$	0.1 %
$Z_{bg1}(\text{Pb-212})$	$435.3 \cdot 10^2$	$2.1 \cdot 10^2$	$-6.2 \cdot 10^{-6}$	0.0 %
$\dot{Z}_{bg2}(\text{Ra-224}, t=0)$	$8691 \cdot 10^{-5} \text{ 1/s}$	$9 \cdot 10^{-5} \text{ 1/s}$	$-4.8 \cdot 10^{-6}$	0.0 %
$\dot{Z}_{bg2}(\text{Pb-212}, t=0)$	$342.7 \cdot 10^{-3} \text{ 1/s}$	$2.4 \cdot 10^{-3} \text{ 1/s}$	$20 \cdot 10^{-6}$	0.0 %
$R_1$	1.004517	$25 \cdot 10^{-6}$	$15 \cdot 10^{-6}$	0.0 %
$R_2$	1.00000	$1 \cdot 10^{-5}$	$15 \cdot 10^{-6}$	0.0 %
$\lambda$	$12.42 \cdot 10^{-9} \text{ 1/s}$	$4 \cdot 10^{-11} \text{ 1/s}$	$12 \cdot 10^{-6}$	0.0 %
$\chi$	0.4105	$1.6 \cdot 10^{-3}$		

Table 7: Uncertainty budget for the determination of the activity concentration in the reference volume at a specified position of taking the sample

$X_i$	$x_i$	$u(x_i)$	$c_i \cdot u(x_i)$	Relative contribution
A	596.5 Bq	1.2 Bq	16	0.6 %
$\chi$	0.4105	$1.6 \cdot 10^{-3}$	30	2.2 %
V	$30.16 \cdot 10^{-3} \text{ m}^3$	$7 \cdot 10^{-5} \text{ m}^3$	-17	0.0 %
$\varphi$	0.981	0.025	200	96.6 %
C	$7.96 \cdot 10^3 \text{ Bq/m}^3$	$2.1 \cdot 10^2 \text{ Bq/m}^3$		

In this realization the maximum variation in the mean value of activity concentration is 4.5 %. Therefore, it is necessary to specify the position of the measurement precisely and to include a small correction in case of sampling near to the wall. This correction is included in the uncertainty budget in Table 7 in the form of a homogeneity function  $\varphi$  and has a minimum uncertainty of 2.5 %.

### 4.3 Influence of humidity

It was observed, that varying humidity can impact the emanation coefficient  $\chi$  of  $^{222}\text{Rn}$  from electrodeposited  $^{226}\text{Ra}$ , where lower humidity leads to decreased emanation.

Since the magnitude of this effect can have very complex covariance on multiple different parameters, namely temperature, pressure, history of the source, plating conditions and chemical impurities, it is infeasible to correct for these dependencies by measuring all possible combinations of them. The alternative is to measure the emanation coefficient of the sources using an on-line measurement setup based on low-cost, high-resolution scintillation detectors, consisting of the inorganic crystals  $\text{LaBr}_3$ ,  $\text{CeBr}_3$  or  $\text{SrI}_2$ . PTB has investigated the application of these scintillators for this purpose by measuring the emanation coefficients of a subset of the produced electrodeposited sources with a setup, where the sources are installed in between the respective scintillator and a HPGe detector.

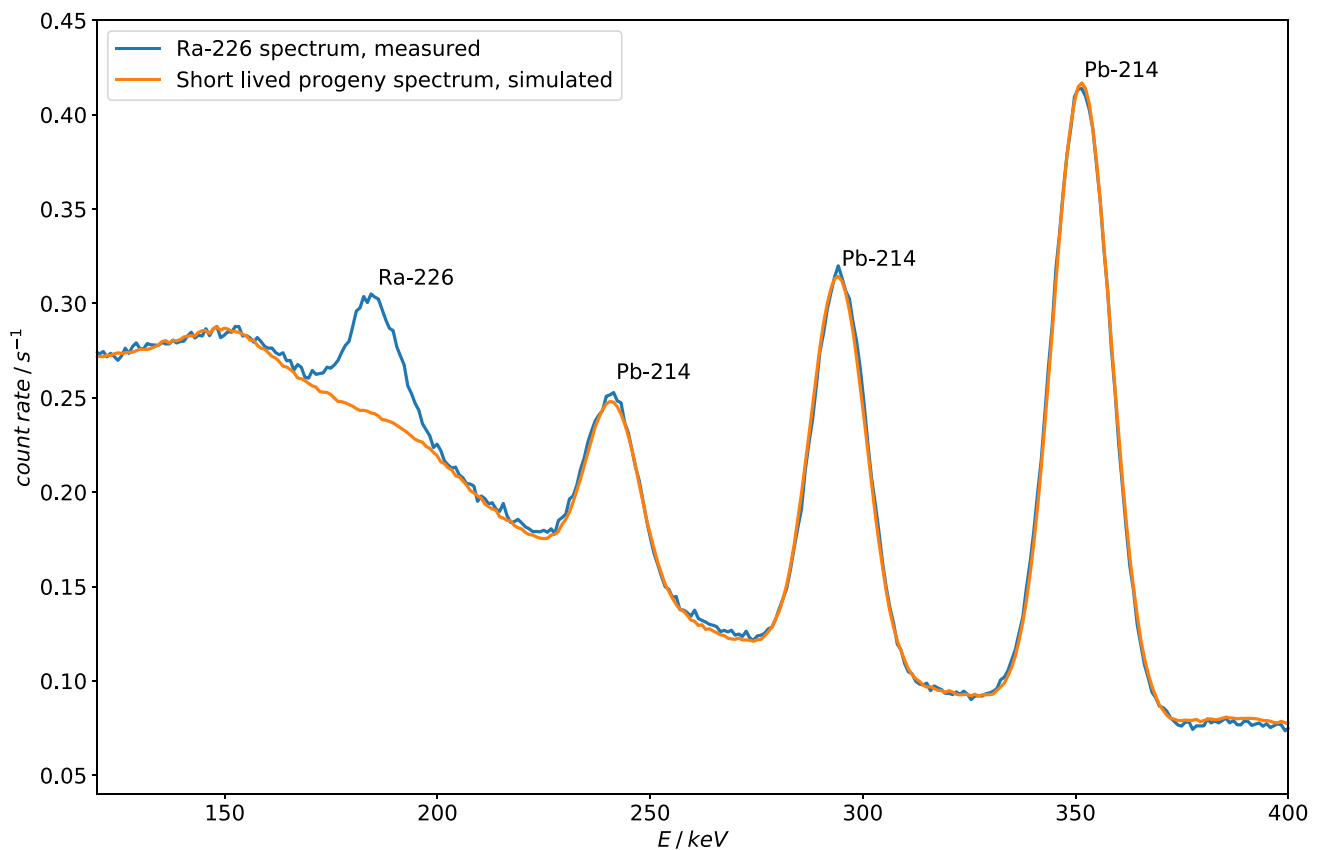


Figure 6:  $\text{LaBr}_3$   $\gamma$ -spectrum of a sealed  $^{226}\text{Ra}$  source

Thereby, it was found that the conventional approach outlined in equation (3) is not readily applicable to these scintillators, because of deviations of the thus determined  $\chi$  by over 5 %, as compared to the values from the HPGe measurements, where observed. It was shown, that this effect is due to peak overlaps in the region of the  $^{226}\text{Ra}$  peak. One possible solution to this issue is to substitute the  $^{226}\text{Ra}$  count rate ratio in equation ((4)) with the known activity ratio to obtain the equations ((8)). Then, the achievable uncertainty for the emanation coefficient determination by this system is limited to the uncertainty of the ratio of  $^{226}\text{Ra}$  activities achievable by DSA  $\alpha$ -spectrometry. For the  $\gamma$ -ray spectra of scintillation detectors, equation ((8)) needs to be used instead. With this adapted analysis, deviations from the values determined by HPGe detectors vanish.

$$\chi = 1 - \frac{A_{Ra-226(closed)}}{A_{Ra-226(open)}} \cdot \frac{R_{Pb-214(open)}}{R_{Pb-214(closed)}} \quad (8)$$

Based on these results, a portable system consisting of a 2" LaBr<sub>3</sub> detector was implemented and used for the first time in Task 1.1.5. A  $\gamma$ -spectrum of the relevant energy range with <sup>226</sup>Ra peak and the <sup>214</sup>Pb progeny peaks with their simulation, for the evaluation of their count rates is shown in Figure 6.

Using the classical way of producing emanation sources, drop deposition on a filter encased in polyethylene foils, a dependency of the emanation, relative to ambient temperature and relative humidity are expected, due to diffusion processes. This effect is shown in Figure 7.

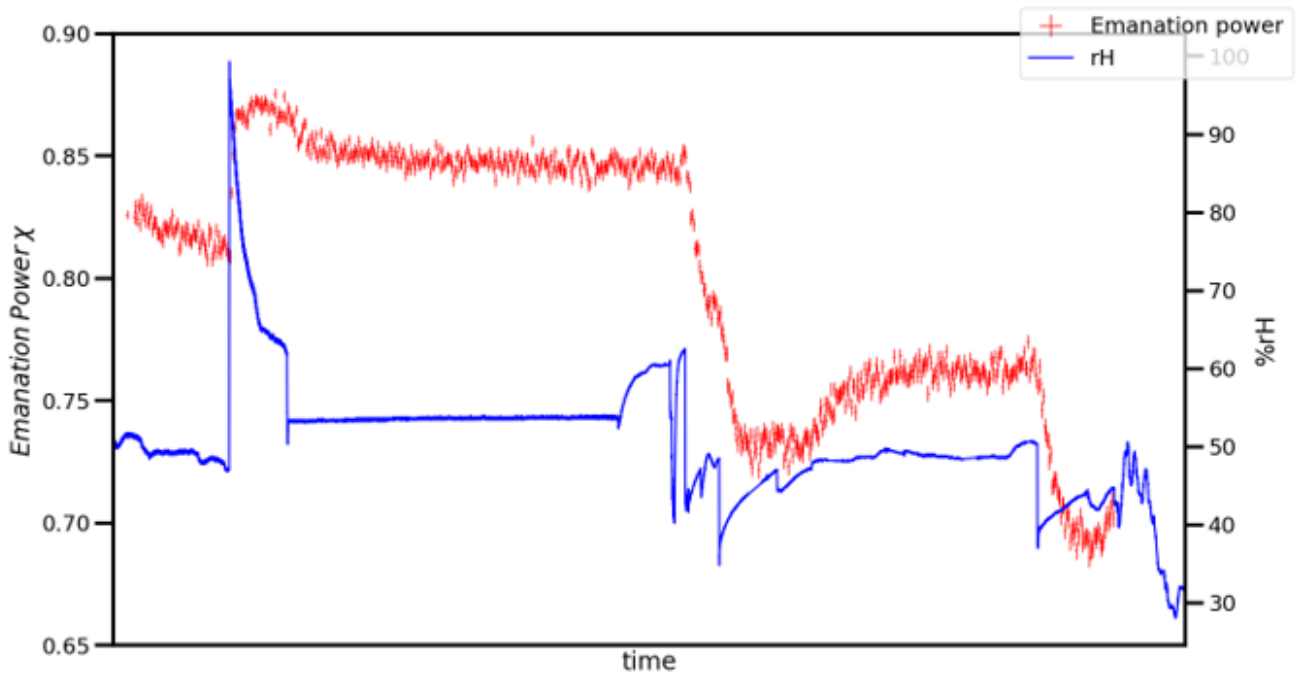


Figure 7: Evolution of the emanation power  $\chi$  and relative humidity %rH with time

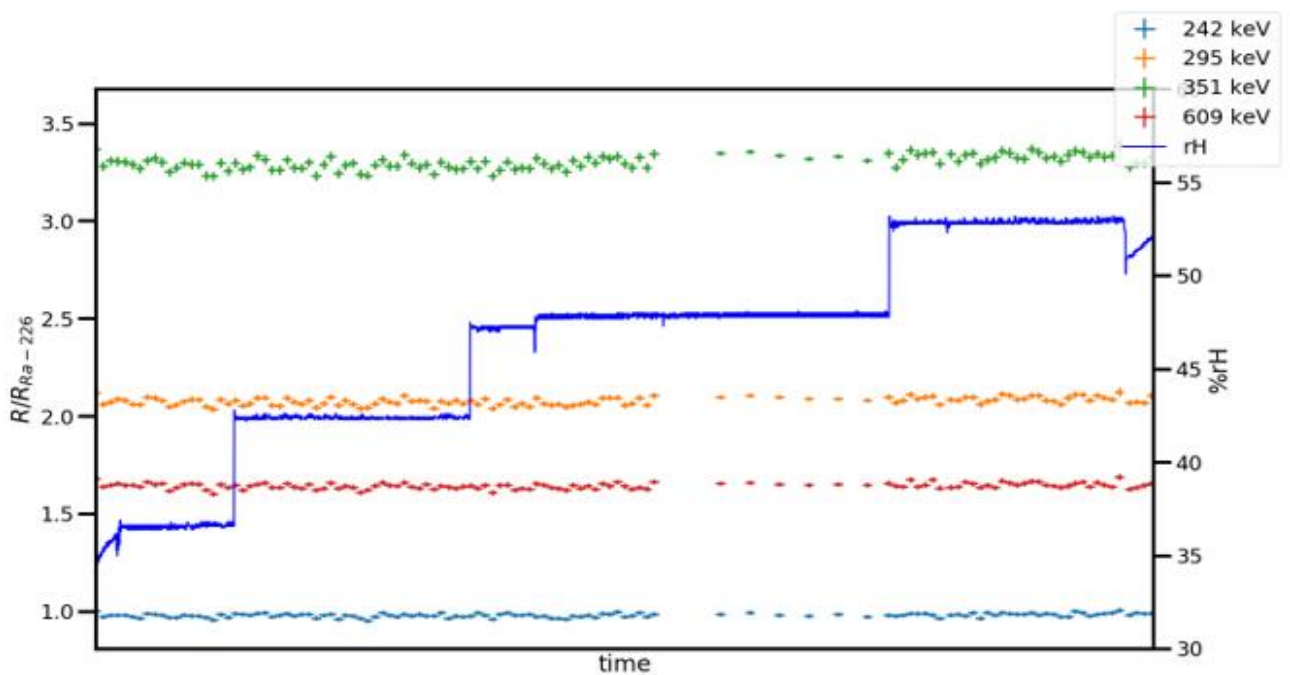


Figure 8: Emanation power of an electrodeposited <sup>226</sup>Ra source represented by count rate ratios and relative humidity as function of time

Using electrodeposition of  $^{226}\text{Ra}$  on a stainless-steel deposit this effect should be less prominent, unless the source becomes completely dry. Figure 8 shows the evolution of the count rate ratios of several  $^{222}\text{Rn}$  progenies, relative to the count rate of the  $^{226}\text{Ra}$  emission with time of a  $^{226}\text{Ra}$  ion implanted source. While the relative humidity is changing between 35 %rH and 55 %rH. No change in the count rate ratio and therefore no change in the emanation power is observed.

Using electrodeposited  $^{226}\text{Ra}$  sources and drying the source to a relative humidity below 30 %rH, special drying effects are observed over longer periods of time, that are not yet fully understood.

The dependency of the electrodeposited source is derived from the process of drying a source from rH 30 % to a rH 20 %. The change of the emanation power  $\chi$  is shown in Figure 9.

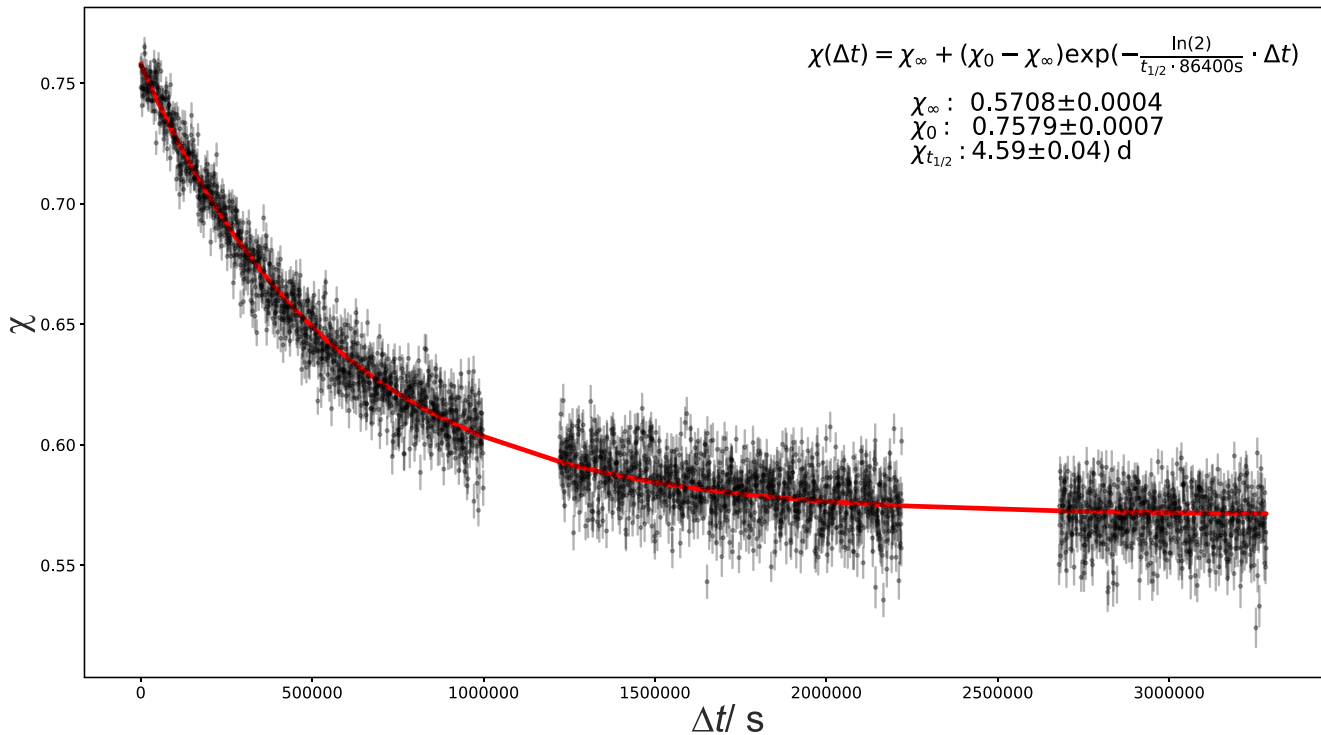


Figure 9: Drying process of an electrodeposited  $^{226}\text{Ra}$  emanation source.

The data points given are the  $1/\sigma^2$ -weighted means of the  $\chi$  values determined from all the  $\gamma$ -emitting progenies of  $^{222}\text{Rn}$ . The decrease of  $\chi$  is composed of the drying of the source and the build-up of the  $^{222}\text{Rn}$  progenies, which of course is delayed with the half-life of  $^{222}\text{Rn}$ . Both processes are hard to disentangle. A change of the emanation from extrapolated 76 % to 57 % is observed.

#### 4.4 Conclusions of PTB

It was shown that thin-film deposition using molecular-plating techniques allows the manufacture of  $^{226}\text{Ra}$  sources from which a high fraction of generated  $^{222}\text{Rn}$  can emanate. Emanation coefficients between 0.6 and 0.9 were observed for the produced sources. A possible explanation for the varying emanation coefficients are the different plating conditions that were employed because these conditions impact the kinetics of particle growth of the deposit. The kinetics in turn determine the microstructure of the film, which can cause different emanation characteristics. From the amount of deposited  $^{226}\text{Ra}$  and the emanation coefficient  $\chi$ , a known and stable activity concentration of  $^{222}\text{Rn}$  in air can be produced with the sources. The  $^{226}\text{Ra}$  activity is determined with an absolute technique, and the emanation coefficient is determined without the need for another  $^{222}\text{Rn}$  standard, which allows the use of these sources as primary standards for activity concentration of  $^{222}\text{Rn}$  in air. The combined uncertainty of the resulting activity concentration using these sources does not exceed 2 % ( $k = 1$ ) under the assumption that a precisely known reference volume is available. Because of the thin-layer and highly porous  $^{226}\text{Ra}$  deposit, with particles in the range of a couple of nm in diameter, it is suggested that the

recoil energy of  $^{222}\text{Rn}$  (86 keV) is an important factor in the emanation from the sources. However, as the surface-to-volume ratio increases, humidity might readily adsorb onto the particles which can cause the emanation coefficient to change with respect to changes in humidity. Within the collected data and associated uncertainties, however, such an effect was not observed even though the humidity was uncontrolled during the measurements of the emanation coefficient. Further, up to 50 % of the emerging  $^{222}\text{Rn}$  nuclei are implanted into the steel backing by their recoil. Whether these  $^{222}\text{Rn}$  nuclei can subsequently diffuse out of the metal is unknown. Further studies will be conducted to investigate the effect of changing humidity and temperature on the emanation characteristics from such deposits.

## 5 References

- Allison, J. and others. (2006). Geant4. *Nuclear Science, IEEE Transactions on (Volume:53, Issue: 1)*.  
<https://doi.org/10.1109/TNS.2006.869826>
- Arinc, A., Parfitt, M. J., Keightley, J. D., & Wilson, A. (2016). Defined solid angle alpha counting at NPL. *Applied Radiation and Isotopes*, 109, 198–204. <https://doi.org/10.1016/j.apradiso.2015.11.073>
- Bé M.-M. Chisté V., D. C. B. E. C. V. K. N. H. R. N. A. S. E. D. R. (2004). *Monographie BIPM-5, Table of radionuclides*.
- Berger, M. J., Hubbell, J. H., Seltzer, S. M., Chang, J., Coursey, J. S., Sukumar, R., Zucker, D. S., & Olsen, K. (2019). *XCOM: Photon Cross Section Database version 1.5, National Institute of Standards and Technology, Gaithersburg, MD*.
- Bratsch, S. G. (1989). Standard Electrode Potentials and Temperature Coefficients in Water at 298.15 K. *Journal of Physical and Chemical Reference Data*, 18(1), 1–21. <https://doi.org/10.1063/1.555839>
- Chabaux, F., Othman, D. Ben, & Birck, J. L. (1994). A new RaBa chromatographic separation and its application to Ra mass-spectrometric measurement in volcanic rocks. *Chemical Geology*, 114(3–4), 191–197. [https://doi.org/10.1016/0009-2541\(94\)90052-3](https://doi.org/10.1016/0009-2541(94)90052-3)
- Dersch, R. (2004). Primary and secondary measurements of  $^{222}\text{Rn}$ . *Applied Radiation and Isotopes*, 60(2–4), 387–390. <https://doi.org/10.1016/j.apradiso.2003.11.046>
- Getoff, N., Bildstein, H., & Proksch, E. (1967). Molecular plating, V. The influence of some experimental factors on the deposition yield. *Nuclear Instruments and Methods*, 46(2), 305–308. [https://doi.org/10.1016/0029-554X\(67\)90088-2](https://doi.org/10.1016/0029-554X(67)90088-2)
- Hancock, G. J., & Martin, P. (1991). Determination of Ra in environmental samples by  $\alpha$ -particle spectrometry. *International Journal of Radiation Applications and Instrumentation. Part, 42*(1), 63–69. [https://doi.org/10.1016/0883-2889\(91\)90125-K](https://doi.org/10.1016/0883-2889(91)90125-K)
- Joint Committee for Guides in Metrology. (2008). *Evaluation of measurement data — Supplement 1 to the JCGM 101*, 90.
- Jurado Vargas, M., & Fernández De Soto, F. (1996). A study of  $^{222}\text{Rn}$  emanation in electrodeposited sources of  $^{226}\text{Ra}$  with barium. *Nuclear Instruments and Methods in Physics Research, Section A: Accelerators, Spectrometers, Detectors and Associated Equipment*, 368(2), 488–491. [https://doi.org/10.1016/0168-9002\(95\)00854-3](https://doi.org/10.1016/0168-9002(95)00854-3)
- Linzmaier, D., & Röttger, A. (2013). Development of a low-level radon reference atmosphere. *Applied Radiation and Isotopes*, 81, 208–211. <https://doi.org/10.1016/j.apradiso.2013.03.032>
- Linzmaier, D., & Röttger, A. (2014). Development of a transfer standard for the measurement of low Rn-222 activity concentration in air. *Applied Radiation and Isotopes*, 87, 306–309. <https://doi.org/10.1016/j.apradiso.2013.11.076>
- Mertes, F., Röttger, S., & Röttger, A. (2020). A new primary emanation standard for Radon-222. *Applied Radiation and Isotopes*, 156(October 2019). <https://doi.org/10.1016/j.apradiso.2019.108928>
- Parker, W., Bildstein, H., & Getoff, N. (1964a). Molecular plating I, a rapid and quantitative method for the electrodeposition of thorium and uranium. *Nuclear Instruments and Methods*, 26(C), 55–60. [https://doi.org/10.1016/0029-554X\(64\)90049-7](https://doi.org/10.1016/0029-554X(64)90049-7)
- Parker, W., Bildstein, H., & Getoff, N. (1964b). Molecular plating III the rapid preparation of radioactive reference samples. *Nuclear Instruments and Methods*, 26(C), 314–316. [https://doi.org/10.1016/0029-554X\(64\)90095-3](https://doi.org/10.1016/0029-554X(64)90095-3)

- Philip Horwitz, E., Dietz, M. L., & Chiarizia, R. (1992). A novel strontium-selective extraction chromatographic resin. *Solvent Extraction and Ion Exchange*, *10*(2), 313–336.  
<https://doi.org/10.1080/07366299208918107>
- Picolo, J. L. (1996). Absolute measurement of radon-222 activity. *Nuclear Instruments and Methods in Physics Research Section A*, *369*(2–3), 452–457.
- Picolo, J. L., Pressyanov, D., Blanchis, P., Barbier, M., Michielsen, N., Grassin, D., Voisin, V., & Turek, K. (2000). A radon-222 traceability chain from primary standard to field detectors. *Applied Radiation and Isotopes*, *52*(3), 427–434. [https://doi.org/10.1016/S0969-8043\(99\)00190-6](https://doi.org/10.1016/S0969-8043(99)00190-6)
- Pommé, S. (2015). The uncertainty of counting at a defined solid angle. *Metrologia*, *52*(3), S73–S85.  
<https://doi.org/10.1088/0026-1394/52/3/S73>
- Röttger, A., Honig, A., Dersch, R., Ott, O., & Arnold, D. (2010). A primary standard for activity concentration of <sup>220</sup>Rn (thoron) in air. *Applied Radiation and Isotopes*, *68*(7–8), 1292–1296.  
<https://doi.org/10.1016/j.apradiso.2010.01.004>
- Vargas, M. J. (2000). Model to explain simultaneously the <sup>222</sup>Rn and <sup>220</sup>Rn emanation from thin electrodeposited sources. *Nuclear Instruments and Methods in Physics Research, Section A: Accelerators, Spectrometers, Detectors and Associated Equipment*, *447*(3), 608–613. [https://doi.org/10.1016/S0168-9002\(99\)01289-9](https://doi.org/10.1016/S0168-9002(99)01289-9)
- Vargas, M. J., & De Soto, F. F. (1995). Influence of Ba on the electrodeposition of <sup>226</sup>Ra. *Journal of Radioanalytical and Nuclear Chemistry Articles*, *198*(1), 143–150. <https://doi.org/10.1007/BF02038252>
- Whitehead, N. E., Ditchburn, R. G., McCabe, W. J., & Van Der Raaij, R. (1992). Factors affecting the electrodeposition of <sup>226</sup>Ra. *Journal of Radioanalytical and Nuclear Chemistry Articles*, *160*(2), 477–485.  
<https://doi.org/10.1007/BF02037123>



# 16ENV10 MetroRADON

Activity A1.1.2

Emanation sources of  $^{222}\text{Rn}$  and  $^{220}\text{Rn}$

CEA

Due date: January 2019  
Submission: February 2020

**EMPIR**



The EMPIR initiative is co-funded by the European Union's Horizon 2020 research and innovation programme and the EMPIR Participating States

## Table of contents

List of figures.....	2
List of Tables .....	2
1. Introduction .....	3
2. Source preparation .....	3
3. Activity source measurement.....	3
4. Preparation for emanation measurements .....	4
5. Influence of the parameters .....	5
6. Supplement.....	7
7. References .....	8

## List of figures

Figure 1 – Powder in the middle of the first filter. ....	3
Figure 2 – View of the source placed for its activity measurement in front of a HPGe detector<. ....	4
Figure 3 – Scheme of the source mounting.....	4
Figure 4 – View of the source support with metal grid. ....	5
Figure 5 – The source between two valves. ....	5
Figure 6 – Device with the source inside. ....	5
Figure 7 – Influence of the humidity on the $^{220}\text{Rn}$ production. ....	6
Figure 8 – Influence of the temperature on the $^{220}\text{Rn}$ production. ....	6
Figure 9 – Influence of the pressure on the $^{220}\text{Rn}$ production.....	7
Figure 10 – New design of the source holder. ....	7
Figure 11 – Picture of the finalized source holder design. ....	8

## List of Tables

Table 1: Overview of GeHP detector calibration at LNHB. ....	3
--	---

## 1. Introduction

CEA had to develop  $^{222}\text{Rn}$  and  $^{220}\text{Rn}$  emanation sources using polymers and evaluate the influence of the temperature, humidity and pressure on the emanation rate.

## 2. Source preparation

The CEA-LNHB laboratory has adapted a chemical protocol to produce these emanation sources. To produce the  $^{220}\text{Rn}$  emanation sources, a radioactive solution of  $^{228}\text{Th}$  was used and diluted in a solution of chloride barium ( $\text{BaCl}_2, 2\text{H}_2\text{O}$ ) in methanol. This mixture is then mixed with a sodium stearate solution (in methanol) and the  $^{228}\text{Th}$  activity is fixed in the barium stearate coprecipitate. The mixture is then filtered under low vacuum on cellulose/glass fiber filter and the desired amount of coprecipitate (which has a powder form) was deposit between two membranes of cellulose acetate mixed with glass fibers (Figure 1) in order to obtain sources which emanate  $^{220}\text{Rn}$ . The same procedure was used with  $^{226}\text{Ra}$  solution to obtain a  $^{222}\text{Rn}$  emanation source.



Figure 1 – Powder in the middle of the first filter.

The second member was fixed with glue around the perimeter in order to keep all the powder inside and so the sources are ready to be measured.

## 3. Activity source measurement

The activity of  $^{228}\text{Th}$  or  $^{226}\text{Ra}$  deposited between the two membranes was measured with an HPGe detector (Figure 2). These measurements are typically performed at LNHB for the production of certificate following ISO17025 rules. The different characteristics for the calibration and use of our HPGe are presented in Table 1.

Table 1: Overview of GeHP detector calibration at LNHB.

<b><i>Method for efficiency calibration and transfer</i></b>	<b><i>Radionuclides used for calibration</i></b>	<b><i>Traceability</i></b>	<b><i>Corrections applied</i></b>	<b><i>Software for spectra analysis</i></b>
Calibration curve from 3 different volume sources and point sources	23 Radionuclides with 141 energy points	Primary standard methods from LNE-LNHB with SIR (BIPM) submission	True coincidence, Density (with attenuation measurement), Geometry (ETNA calculation code from LNHB)	Interwinner 7.0, Colegram 3.1

In order to reduce the uncertainty on the measurement (especially due to coincidence and geometry transfer), we placed the filter inside a 3D printed holder at 10 cm of the detector. The efficiency of such geometry is then calculated from our reference calibration curve at 10 cm with punctual sources and the  $^{228}\text{Th}$  or  $^{226}\text{Ra}$  source characteristics.

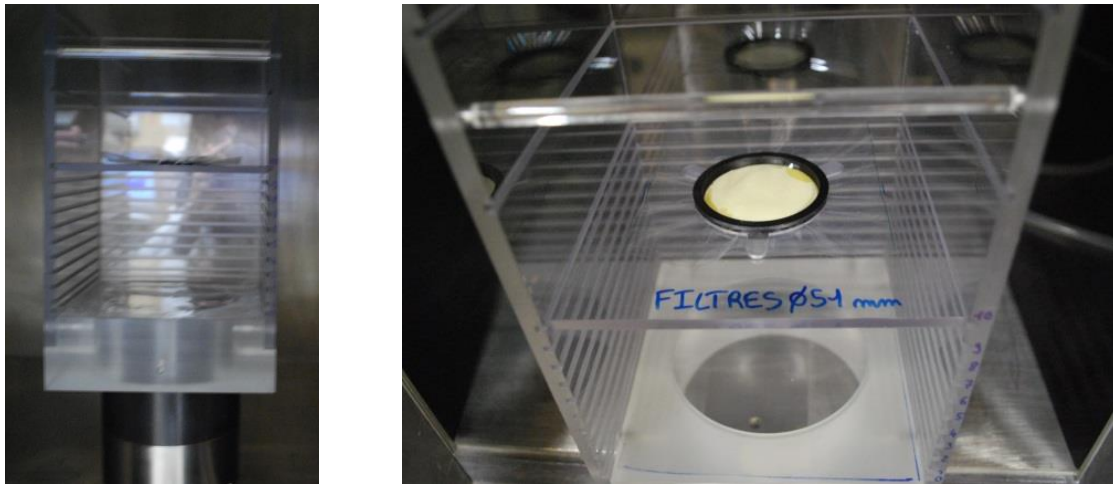


Figure 2 – View of the source placed for its activity measurement in front of a HPGe detector.

Using the directed measurement of total absorption peak from either  $^{228}\text{Th}$  or  $^{226}\text{Ra}$  we can then determine the activity deposited between the membranes. With such measurement, if the activity was high enough, it is possible to reach a relative standard uncertainty of 1% on the activity of  $^{228}\text{Th}$  or  $^{226}\text{Ra}$ .

#### 4. Preparation for emanation measurements

In order to measure the emanation rate, we chose mechanical parts to make the measurements efficient and enough safe. In order to ensure there is now release of the material (i.e.  $^{228}\text{Th}$  or  $^{226}\text{Ra}$ ) in the atmosphere, we have placed two membrane filters at the inlet (to clean incoming air from potential dust that may destroy the source) and at the outlet in case there is any release of the material (Figure 3).

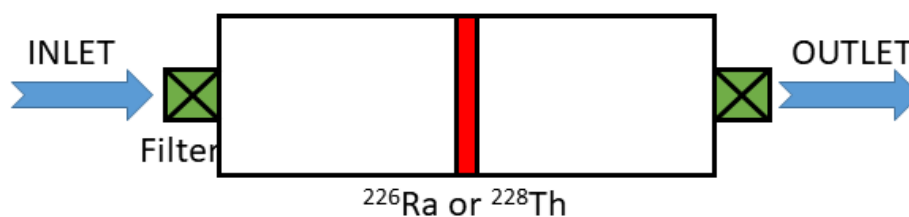


Figure 3 – Scheme of the source mounting.

In this case, the material between the membranes was directly impacted by the air flow, this can be dangerous, because it may destroy the membranes. As a result, the membranes containing the material were placed between two stainless steel grids to protect them (Figure 4).

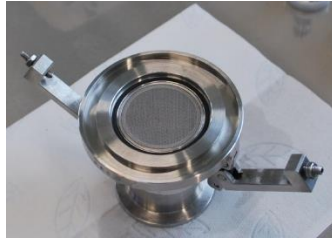


Figure 4 – View of the source support with metal grid.

The source was then placed between two valves and the protection filter holders (Figure 5).



Figure 5 – The source between two valves.

This closed device (Figure 6) can be adapted very easily in loops of measurements, also it is possible to use them even if you switch air inlet and air outlet as it is geometrically symmetrical.



Figure 6 – Device with the source inside.

In order to make sure the source is tight, we performed over pressure test and helium test (using Adixen GraphD mass spectrometer). The tightness was ensured by metal ring (aluminum or VCR stainless-steel silver-plated rings).

## 5. Influence of the parameters

To study the influence of the parameters on the emanation rate we decided to use our primary standard of thoron (Sabot, 2016) directly connected to the source where clean air was circulating (free of particles).

These tests were performed in a „prototype“ atmosphere loop developed in 2015 at LNHB (Sabot, 2015) where we are able to change the relative humidity, temperature and pressure. Figure 7, Figure 8 and Figure 9 show the influence of the humidity, temperature and pressure on the counting rate of  $^{220}\text{Rn}$ , i.e. the emanation rate of the  $^{228}\text{Th}$  source.

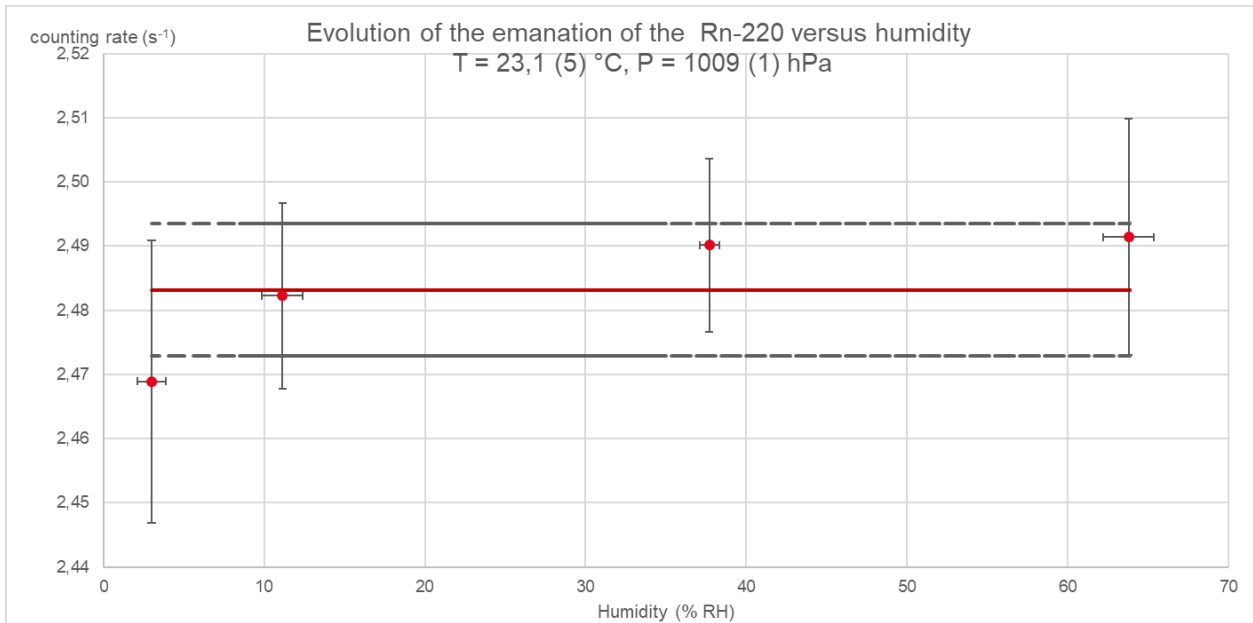


Figure 7 – Influence of the humidity on the <sup>220</sup>Rn production.

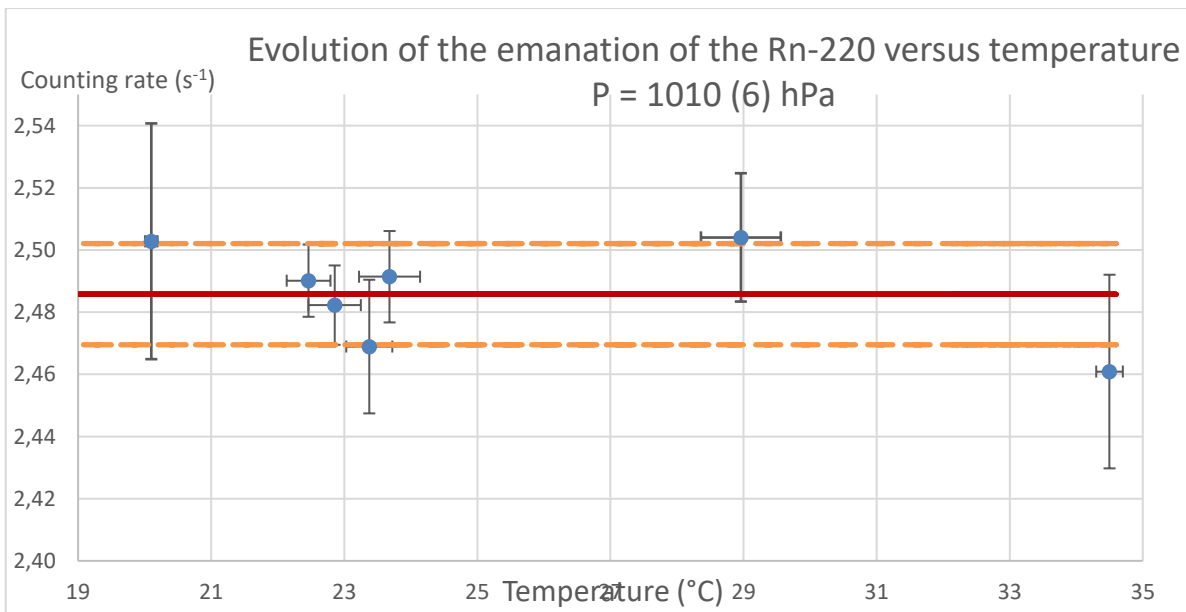


Figure 8 – Influence of the temperature on the <sup>220</sup>Rn production.

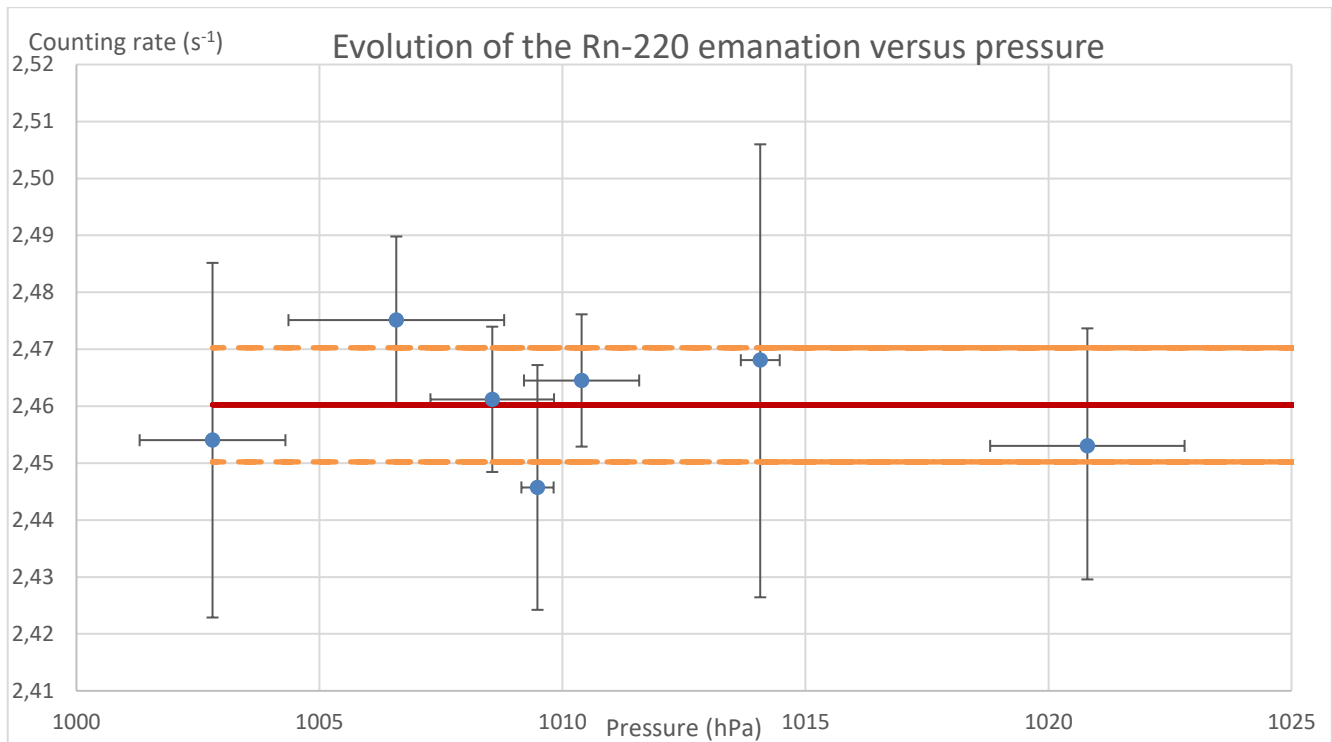


Figure 9 – Influence of the pressure on the <sup>220</sup>Rn production.

To conclude, we can see that these parameters have not a big influence on the results according to the uncertainty of the measurement.

## 6. Supplement

During the project and with the help of new technologies, we decided to design a more complexe source holder inside the main pipe. This was to make sure there is no possibility of membrane destruction and radioactive material dispersion with very high flowrate. To performe such thing, we designed a holder which was printed in 3D with PETG to make sure we can place up to three sources inside one, this time parallel to the flowrate (Figure 10 and Figure 11). The choice of the material PETG was made because it is transparent to radon noble gases and can support very high humidity.



Figure 10 – New design of the source holder.

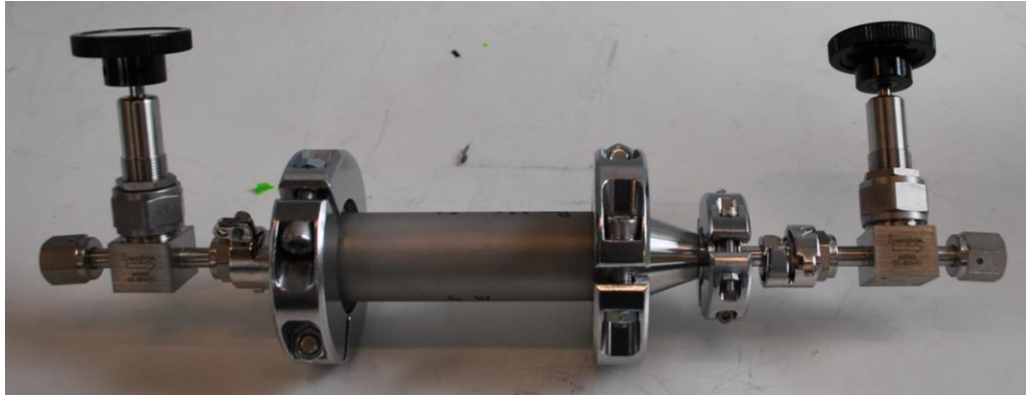


Figure 11 – Picture of the finalized source holder design.

This older is also a way to upgrade a source by adding more membranes with material easily and also can be used for mixed material ( $^{228}\text{Th}$  and  $^{226}\text{Ra}$ ) without mixing solution but separated source holder. These new designed source were then place in the new loop for noble gases atmosphere production developed at LNHB and which was presented at the ICRM conference in 2019 but also is published in an open source publication (Sabot, 2020).

## 7. References

- Sabot, B. (2015). *Calibration of Thoron ( $^{220}\text{Rn}$ ) Activity Concentration Monitors*. PhD thesis. NNT: 2015SACLS122, pp. 97–100.
- Sabot, B. P. (2016). *A new thoron atmosphere reference measurement system*. *Appl. Radiat. Isot.* 109, 205–209.
- Sabot, B. R. (2020). *Experimental facility for the production of reference atmosphere of radioactive gases (Rn, Xe, Kr, and H isotopes)*. *Applied Radiation and Isotopes* 155, 108934.



# 16ENV10 MetroRADON

## Activity A1.1.3

Development of a long term stable  $^{222}\text{Rn}$  low activity emanation flow-through standard source

CMI

Due date: January 2019  
Submission: February 2020

**EMPIR**



The EMPIR initiative is co-funded by the European Union's Horizon 2020 research and innovation programme and the EMPIR Participating States

## Table of contents

1. Introduction .....	3
2. Development of a $^{222}\text{Rn}$ low activity emanation flow-through standard source .....	3

## 1. Introduction

Activity description: CMI with support from SUJCHBO, where the source will be tested, will develop a long term stable  $^{222}\text{Rn}$  low activity emanation flow-through standard source at CMI based on a metering flow controller and dispenser generating a known  $^{222}\text{Rn}$  concentration in an air flow with the relative uncertainty  $\leq 4\%$  ( $k = 1$ ).

## 2. Development of a $^{222}\text{Rn}$ low activity emanation flow-through standard source

An emulsion of salts of fatty acids in silicone rubber was formed from the weighed standard solution. The emulsion was allowed to polymerize in a steel tray of the following dimensions: 70 x 94 mm. The activity of the standard is determined by the weighting of the  $^{226}\text{Ra}$  solution, the weight of the resulting emulsion and the losses (<0.1%). The whole process was controlled by weighing and gamma spectrometry on an HPGe detector. Determination of 185 keV gamma-ray emission intensity measured with the use of the standard solution has confirmed excellent conformity with the tabulated value. [1] The source was constructed as a stainless steel cylindrical case supplied on the ends with the ball valves and the two aerosol filters connected on the output aperture of the valves. The steel tray with  $^{226}\text{Ra}$  is placed in the middle of this cylindrical case and radon releases from this thin layer.

The emanation coefficient of the source was determined by measuring the activity of the  $^{222}\text{Rn}$  daughter products ( $^{214}\text{Pb}/^{214}\text{Bi}$ ) and the activity of  $^{226}\text{Ra}$  and was almost equal 1. The detection efficiency of the gamma photons was calculated by the MCNP code.

The application of this source is calibration of detectors for activity measurements of  $^{222}\text{Rn}$  in air. The source is operated in flow through mode.

Flow-through source of  $^{222}\text{Rn}$  type RF 5 with activity 4.955(50) kBq of  $^{226}\text{Ra}$  developed by Czech Metrological Institute is accompanied by the air pressure vessel as the source of air free from the radon and the mass flow controller of type Bronkhorst EL-Flow. The old air from pressure vessel comes through the protective aerosol particle filter and the calibrated mass flow controller to the low-level radon source. The radon flux is long term stable and realized as 0.0104(1) Bq/s. The application of this source is the calibration of detectors for activity measurements of  $^{222}\text{Rn}$  in air (in the range of 100 – 300 Bq.m<sup>-3</sup>).

[1] Mazanova, M., Dryak, P., Havelka, M., 2018. Emission probability measurement of  $\gamma$ - and X-rays in Ra-226 and Pb-210 decay. Appl. Radiat. Isot. 134, 429-432. DOI: 10.1016/j.apradiso.2017.10.023.



Figure 1 - The flow-through low-level radon source developed by CMI

Ra-4 of 100



**Czech Metrology Institute**  
 Okružní 31, 838 00 Brno, Czech Republic  
 phone +420 545 555 111  
 www.cmi.cz

---

**Workplace:** Regional Inspectorate Prague, Radiová 1136/3, 102 00 Praha 10  
 Department of Radionuclide Standards Production, Radiová 1288/1a  
 phone +420 266 020 497

**CERTIFICATE**  
 of the measurement standard of activity

<b>Certificate No.:</b> 1035-SF-40456-19	<b>Type:</b> RF 5	<b>Serial No.:</b> 080419-221425
<b>Radionuclide:</b> Ra-226	<b>Half life of Ra-226:</b> 584388 (2557) days	
<b>Activity:</b> 4,955 (50) kBq	<b>Half life of Rn-222:</b> 3,823 (8) days	
<b>Radon output:</b> 0,0104 (1) Bq/s	<b>Mass of Ra-226:</b> 0,1355 (14) µg	
<b>Radionuclide impurities:</b> -	<b>Emanation power:</b> 0,999 (0)	
<b>Reference date:</b> 31.5.2019	<b>Inner volume between valves:</b> 200 (5) cm <sup>3</sup>	

**Description:**  
 The flow-through source of Ra-222 enclosed in the aluminium alloy cylindrical case with two ball valves. The radon source in the form of a polymer layer is placed in the centre of the case.

**Metrological traceability:**  
 The declared Ra-226 activity is traceable to CMI Measurement Standards of Ra-226 activity.

**Note:**  
 The source should be used in the temperature range from 0 - 40 degrees Celsius and the relative humidity 0 - 100 % (non-condensing).  
 1 g Ra-226 = 3,658E10 Bq

---

**Date of the certificate issue:** 24.5.2019      **Certificate validity:** 5 years

**Customer:**  
 ČMI-Of Praha  
 Radiová 1a  
 102 00 Praha 10



Checked by: Ing. Vlasta Zdychová





Ing. Jiří Šaroun, MBA  
 Deputy Director of RI Prague

Figure 2 – Certificate of emanation radon source developed at CMI



# 16ENV10 MetroRADON

Activity A1.1.4

Development of direct and traceable measurement of the activity concentration in an air flow

CEA

Due date: January 2019  
Submission: February 2020

**EMPIR**



The EMPIR initiative is co-funded by the European Union's Horizon 2020 research and innovation programme and the EMPIR Participating States

## Table of contents

List of figures.....	2
List of tables.....	2
1. Introduction .....	3
2. CEA-LNHB setup.....	4
3. CEA-LNHB results for source 1 387 Bq.....	7
4. CEA-LNHB results for source 1 533 Bq.....	8
5. METAS measurement setup .....	10
6. METAS measurement results for source 1 387 Bq .....	12
7. METAS measurement results for source 1 533 Bq .....	13
8. References .....	15

## List of figures

Figure 1 – Source container as described in Task 1.1.2.....	3
Figure 2 – Second source with finalized design.....	3
Figure 3 – Picture of CEA-LNHB device source 1 387 Bq .....	4
Figure 4 – Picture of CEA-LNHB device source of 1 533Bq.....	4
Figure 5 – Scheme of the device to measure the spectra. ....	5
Figure 6 – Spectrum of Ra-226-0.2 L·min <sup>-1</sup> . ....	8
Figure 7 – Emanation rate of the source of 1 533 Bq.....	10
Figure 8 – <sup>222</sup> Rn test site block diagram.....	10
Figure 9 – <sup>222</sup> Rn concentration of the source CEA 'LNHB-METAS-226Ra-01-2019' with 1 387 Bq.....	12
Figure 10 – Measurement result of the source of 1 533 Bq .....	14

## List of tables

Table 1 – Measurement of the emanation rate in 2018. ....	7
Table 2 – Measurement of the emanation rate in 2019 . ....	7
Table 3 – Calculation of the radon emanation at 0.2 L·min <sup>-1</sup> . ....	9
Table 4 – Parameters of CEA source Ra226-no1. ....	12
Table 5 – Detail overview of deviations.....	13
Table 6 – Parameters of CEAs source Ra226-no1.....	13

## 1. Introduction

CEA with support from METAS will develop a method for direct and traceable measurement of the activity concentration of  $^{222}\text{Rn}$  and  $^{220}\text{Rn}$  in an air flow. This method will be implemented at CEA and METAS. Over the project different kind of sources were used to produce the atmosphere of  $^{222}\text{Rn}$  and  $^{220}\text{Rn}$ . The first prototype presented in Figure 1 – Source container as described in Task 1.1.2. was used in CEA-LNHB measurement loop and device developed in 2015 (Sabot, 2015) (Sabot, et al., 2015) and then sent to METAS to produce atmosphere of radon in a small volume and perform measurements with Alphaguard device from Bertin instruments (Bertin, 2020).



Figure 1 – Source container as described in Task 1.1.2.

A finalized version of the source was then produced during the project (cf. Figure 2) atmosphere production was then performed in a new setup to produce radioactive gas atmospheres (Sabot, 2020). In this new setup it was possible to measure the atmosphere with Alphaguard and other devices mentioned before. The sources were then sent to METAS to produce low activity concentration level atmosphere and measure them with Alphaguard.



Figure 2 – Second source with finalized design.

## 2. CEA-LNHB setup

Figure 3 show pictures and scheme of CEA-LNHB loop used to measure the emanation rate with the first prototype of the source and describe in (Sabot, 2015). The source used to produce atmosphere of  $^{222}\text{Rn}$  has and activity of  $^{226}\text{Ra}$  of 1 387 (11) Bq the 14<sup>th</sup> of November 2018.

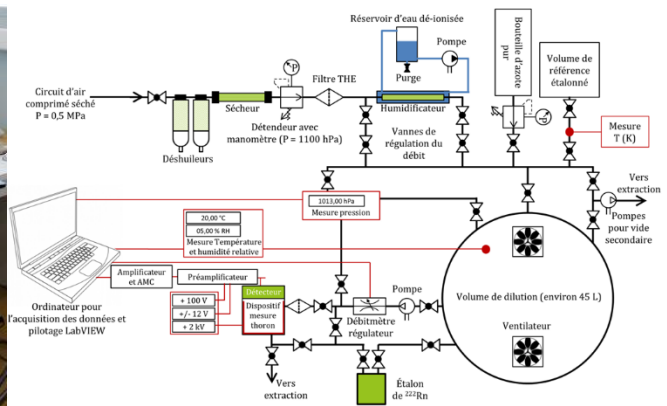


Figure 3 – Picture of CEA-LNHB device source 1 387 Bq.

Figure 4 illustrates the new device developed during the project (Sabot, 2020) with the financial support of LNE (French metrology institute) in order to perform better measurement with more possibilities. In this case we used the new source of  $^{226}\text{Ra}$  with the final design (Figure 2). The activity of  $^{226}\text{Ra}$  was 1 533 (18) Bq the 9<sup>th</sup> of October 2019 12:00 UTC.

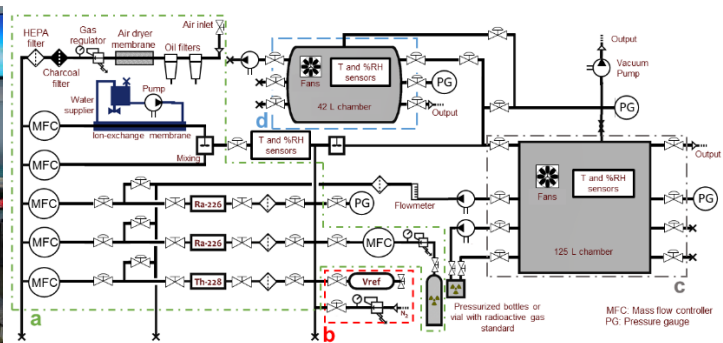


Figure 4 – Picture of CEA-LNHB device source of 1 533Bq.

The principle of this setup is entirely detailed in the open source publication (Sabot, 2020), and ensure free volume traceability with a reference volume calibrated by LNE, calibrated humidity, pressure and temperature sensors. It also allows us to place Alphaguard or any other commercial device in the chamber in order to compare with the method used by METAS.

In both loop we can either work in closed way or open way, the reference device developed by the LNHB (Sabot, 2015) and illustrated in Figure 5 was also connected directly at the source outlet in order to perform direct measurement of  $^{222}\text{Rn}$  or  $^{220}\text{Rn}$  produced by the source.

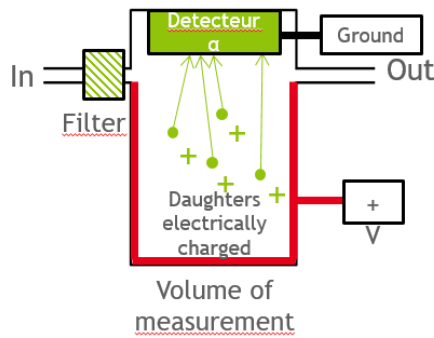


Figure 5 – Scheme of the device to measure the spectra.

This device is equipped with a PIPS detector and an electric field to catch the decay products at the surface of the silicon. Using electronics developed in LNHB, we can obtain spectra which allow us to measure directly gas or decay product from each radon isotopes. In the case of mixing, we can also separate each isotopes and deduce the activity concentration using equations (1) for  $^{220}\text{Rn}$ .

$$A_{v\ 220\text{Rn}}(0) = \frac{N_{220\text{Rn} + 212\text{Bi}} - N_{212\text{Po}} \frac{\alpha(^{212}\text{Bi})}{\beta(^{212}\text{Bi})}}{t_m V_{det} R_d\ 220\text{Rn} e^{\left(-\lambda_{220\text{Rn}} \frac{V_t}{Q}\right)}}, \quad (1)$$

With :

- ↳  $A_{v\ 220\text{Rn}}(0)$  : Volumic activity at the outlet of the source ( $\text{Bq}\cdot\text{m}^{-3}$ ),
- ↳  $N_{212\text{Po}}$  : counting of  $^{212}\text{Po}$  pic,
- ↳  $\frac{\alpha(^{212}\text{Bi})}{\beta(^{212}\text{Bi})} = 0,560$  (6): ration of emission from both isotopes,
- ↳  $N_{220\text{Rn} + 212\text{Bi}}$  : counting of  $^{220}\text{Rn}$  and  $^{212}\text{Bi}$  with tail of  $^{216}\text{Po}$  subtracted,
- ↳  $\lambda_{220\text{Rn}}$  :  $^{220}\text{Rn}$  decay constant,
- ↳  $Q$  : flow rate of the  $^{220}\text{Rn}$  atmosphere inside the device,
- ↳  $V_{det}$  : volume of the measurement device,
- ↳  $V_t$  : volume of pipe between source outlet and device inlet,
- ↳  $t_m$  : measurement time,
- ↳  $R_d\ 220\text{Rn}$  : detection efficiency of  $^{220}\text{Rn}$

The relative standard uncertainty on this measurement can be calculated using the flowing equation (2) to (4):

$$\frac{u(A_v^{220Rn})}{A_v^{220Rn}} = \sqrt{\left(\frac{u(N^{220Rn})}{N^{220Rn}}\right)^2 + \left(\frac{u(t_m)}{t_m}\right)^2 + \left(\frac{u(R_d^{220Rn})}{R_d^{220Rn}}\right)^2 + \left(\frac{u(F_{tube})}{F_{tube}}\right)^2 + \left(\frac{u(V_{det})}{V_{det}}\right)^2}, \quad (2)$$

with:

$$\left(\frac{u(F_{tube})}{F_{tube}}\right)^2 = \left(-\frac{V_t}{Q}\right)^2 u^2(\lambda_{220Rn}) + \left(\frac{-\lambda_{220Rn}}{Q}\right)^2 u^2(V_t) + \left(\frac{\lambda_{220Rn} V_t}{Q^2}\right)^2 u^2(Q), \quad (3)$$

And :

$$u^2(N^{220Rn}) = u^2(N^{220Rn + 212Bi}) + \left(\frac{\alpha(^{212}Bi)}{\beta(^{212}Bi)}\right)^2 u^2(N^{212Po}) + \left(\frac{N^{212Po}}{\beta(^{212}Bi)}\right)^2 u^2(\alpha(^{212}Bi)) + \left(\frac{N^{212Po} \alpha(^{212}Bi)}{(\beta(^{212}Bi))^2}\right)^2 u^2(\beta(^{212}Bi)), \quad (4)$$

This equation (1) can be also adapted for the activity measurement using counting rate of  $^{216}Po$  only as described in (5) where the efficiency of the  $^{216}Po$  pic is directly used.

$$A_v^{220Rn} = \frac{N^{216Po}}{t_m V_{det} R_d^{216Po} e^{\left(-\lambda_{220Rn} \frac{V_t}{Q}\right)}} \quad (5)$$

In the case of  $^{222}Rn$  the same method can be applied however the exponential component become negligible and we can also use a second decay product  $^{214}Po$  the same way than equation (5). If the counting statistic is high enough, the best relative standard uncertainty for the measurement can be 1% with gas alpha pic and 2% with the decay products pics.

The measured activity concentration was then compared to theoretical activity concentration obtained using equation (6) (Collé, 1990):

$$A_{Rn} = A_{Ra}^0 \cdot \exp(-\lambda_{Ra} \cdot t_D) \cdot f_0 \cdot x \quad (6)$$

Where:

- ↳  $f_0$  is the  $^{222}Rn$  emanation fraction,
- ↳  $A_{Ra}^0$  is the total  $^{226}Ra$  activity in the capsule at reference time  $t_R$ ,
- ↳  $\lambda_{Ra}$  is the  $^{226}Ra$  decay constant,  $\lambda_{Ra} = (4.332 \pm 0.019) \cdot 10^{-4} \text{ y}^{-1}$  (Bé, et al., 2008),
- ↳  $t_D$  is the time interval from  $t = t_R$  ( $t_R$  is the reference time) to  $t = t_0$ ,  $t_D = t_0 - t_R$ ,
- ↳  $x = 1 - \exp(-\lambda_{Rn} \cdot t_A)$ , where  $\lambda_{Rn} = (2.09822 \pm 0.00016) \cdot 10^{-6} \text{ s}^{-1}$  (Bé, et al., 2008).

Assuming previous measurement possibility the best relative standard uncertainty achievable in the case of emanation calculation could be 1.3% to 2.1%, however such results are for very high statistics. On the same way, using activity concentration measured by the Alphaguard (Bertin, 2020) inside the second chamber it is also possible to calculate the emanation rate and compare with reference device measurement.

### 3. CEA-LNHB results for source 1 387 Bq

A measurement is made in December 2018, before sending the source to IRA-METAS. The results are given Table 1.

Table 1 – Measurement of the emanation rate in 2018.

	VALUE	STAND. UNCERT.	REL. STAN. UNC.
$N_{222RN+218PO}$	20633	144	0.7%
$T_M$ (S)	1377519	1	0.000%
$V_{DET}$ (M <sup>3</sup> )	1.2556E-05	6.00E-08	0.5%
$R_D$ RN-222	0.320	0.002	0.6%
$R_D$ PO-218	0.465	0.0100	2.2%
<b>AV (BQ.M-3)</b>	<b>1519.70</b>	<b>50</b>	<b>3.5%</b>
<b>CALCULATION OF EMANATION RATE :</b>			
<b>EMANATION :</b>	<b>45.80%</b>	<b>1.5%</b>	<b>3.5%</b>

Then, the source came back from IRA-METAS and was measured again in CEA-LNHB. The results are given in Table 2.

Table 2 – Measurement of the emanation rate in 2019.

	VALUE	STAND. UNCERT.	REL. STAN. UNC.
$N_{222RN+218PO}$	12058	110	0.9%
$T_M$ (S)	1097022	1	0.000%
$V_{DET}$ (M <sup>3</sup> )	1.2556E-05	6.00E-08	0.5%
$R_D$ RN-222	0.320	0.002	0.6%
$R_D$ PO-218	0.465	0.0100	2.2%
$N_{214PO}$	9951.330231	99.7564	1.0%
<b>AV PO-214</b>	<b>1584</b>	<b>38</b>	<b>2.4%</b>
<b>CALCULATION OF EMANATION RATE :</b>			
<b>THEORITICAL ACTIVITY CONCENTRATION (BQ/M3 )</b>	<b>3493</b>	<b>34</b>	<b>1.0</b>
<b>EMANATION CALCULATED WITH <sup>214</sup>PO</b>	<b>45.35%</b>	<b>1.2%</b>	<b>2.6%</b>

Both measurements are in good agreement within their uncertainty also both measurements were performed with the same measurement device and setup.

#### 4. CEA-LNHB results for source 1 533 Bq

The second type of source was measured with 3 different flow rates: 0.2 l/min, 0.5 l/min and 0.8 l/min, as we assume the distribution of the flux inside this new source model may have an impact on the diffusion of radon and mixture. The measurements were delicate because of remaining decay products of  $^{220}\text{Rn}$  from other MetroRadon measurements that were remaining in the measurement loop as we can see in the spectrum in Figure 6 (0.2 l/min).

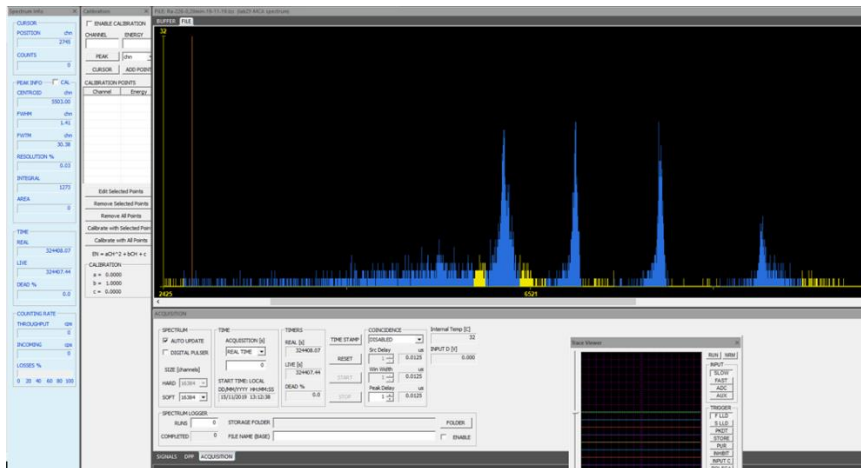


Figure 6 – Spectrum of  $^{226}\text{Ra}$  - 0.2 L·min<sup>-1</sup>.

Nevertheless, we are able to use the peak of  $^{214}\text{Po}$  and the peak of  $^{218}\text{Po}$  to calculate the emanation rate. An example of this calculation at 0.2 L·min<sup>-1</sup> is given in Table 3.

Table 3 – Calculation of the radon emanation at 0.2 L·min<sup>-1</sup>.

	VALUE	STAND. UNCERT.	REL. STAN. UNC.
<b>N<sub>218PO</sub></b>	1534	39	3%
<b>MP ROI</b>	373	19	5%
<b>N<sub>218PO</sub> - MP - CONTRIB, AUTRE</b>	897	44	5%
<b>N ROI MELANGE</b>	4014	63	2%
<b>N MP MELANGE</b>	337	18,4	5%
<b>T<sub>MP</sub></b>	600953	1	0,000%
<b>BLANC</b>	182	13	7,4%
<b>N<sub>222RN+218PO</sub></b>	2004		
<b>N<sub>222RN+218PO</sub> - BLANC</b>	1822	72	4%
<b>T<sub>M</sub> (S)</b>	324407	1	0,000%
<b>V<sub>DET</sub> (M<sup>3</sup>)</b>	1.2440E-05	6.00E-08	0.5%
<b>R<sub>D</sub> RN-222</b>	0.320	0.002	0.6%
<b>R<sub>D</sub> PO-218</b>	0.465	0.0100	2.2%
<b>N<sub>214PO</sub></b>	955	31	3.2%
<b>MP ROI <sup>214</sup>PO</b>	3		
<b>N<sub>214PO</sub> -MP</b>	953		
<b>R<sub>D</sub> PO-214</b>	0.474	0.010	2.2%
<b>A<sub>V</sub> WITH PO-218</b>	478	15	3.4%
<b>A<sub>V</sub> WITH PO-214</b>	498	18	3.9%
<b>CALCULATION OF EMANATION RATE :</b>			
<b>EMANATION LNHB FROM PEAK PO-218</b>	54.81%	2.2%	4.0%

At the same time of this measurement we had an Alphaguard and a RadonEye in the chamber, however they do not separate the radon from the thoron in this case, so we cannot use their results. For some measurements we were able to use only the <sup>218</sup>Po peak result due to time schedule and especially the equilibrium time necessary to wait for equilibrium.

The emanation rate versus the flow rate is shown in Figure 7:

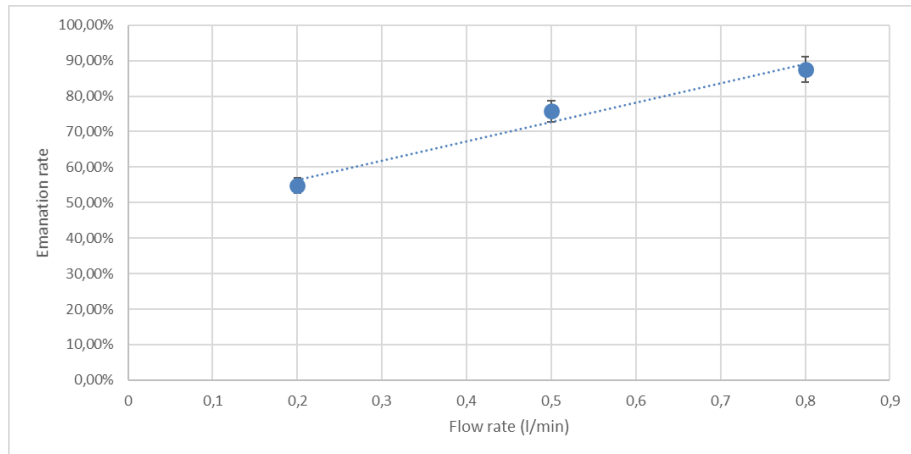


Figure 7 – Emanation rate of the source of 1 533 Bq.

## 5. METAS measurement setup

Figure 8 presents a block diagram of Swiss radon reference test site at the Federal Institute of Metrology (METAS). The Swiss radon reference test site is described in activity report A1.3.1 / A1.3.2.

### METAS $^{222}\text{Rn}$ test site

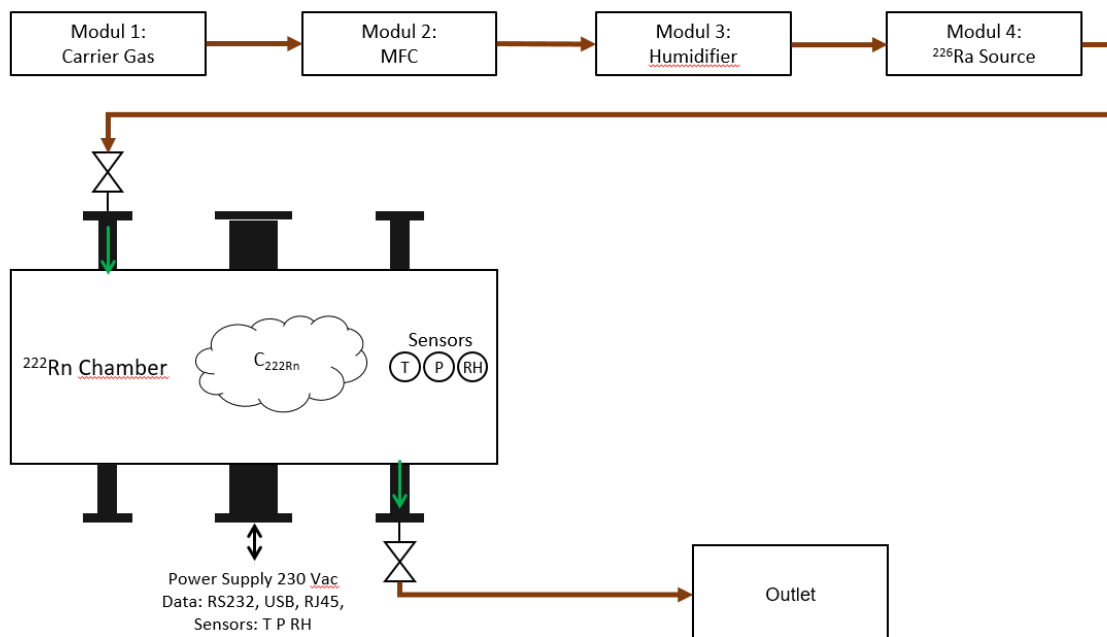


Figure 8 –  $^{222}\text{Rn}$  test site block diagram.

The final  $^{222}\text{Rn}$  activity concentrations inside the chamber is time-dependent and mathematically describable by following equation (7):

$$C_{\text{Rn-222}} = C_0 + \frac{E}{\lambda_{\text{Rn-222}} \cdot V + Q_V} \quad (7)$$

With:

$E = A_{\text{Ra-226}} \cdot \lambda_{\text{Rn-222}} \cdot \chi$ ,  $^{222}\text{Rn}$  Emanation rate [ $\text{Bq}\cdot\text{s}^{-1}$ ], with:

$A_{\text{Ra-226}} = A_{0 \text{ Ra-226}} \cdot k_D$ ,  $^{226}\text{Ra}$  Activity [ $\text{Bq}$ ] of the source at time  $t$ , with:

$A_{0 \text{ Ra-226}}$ ,  $^{226}\text{Ra}$  Reference Activity [ $\text{Bq}$ ] of the source at reference date  $t_0$  (given by the certificate of the source)

$k_D = e^{\left(-\frac{\ln(2)}{T_{1/2 \text{ Ra-226}}}(t-t_0)\right)}$ , Decay factor  $^{226}\text{Ra}$  Activity of the Source at time  $t$

$T_{1/2 \text{ Ra-226}}$ ,  $^{226}\text{Ra}$ -226 Half-live time (Bé, et al., 2008)

$t$ , Date / Time of measurement

$t_0$ , Reference Date / Time of the Activity  $A_{0 \text{ Ra-226}}$  of the source

$\lambda_{\text{Rn-222}} = \frac{\ln(2)}{T_{1/2 \text{ Rn-222}}}$ ,  $^{222}\text{Rn}$  decay constantant [ $1/\text{s}$ ]

$T_{1/2 \text{ Rn-222}}$ ,  $^{222}\text{Rn}$  Half-live time (Bé, et al., 2008)

$\chi$ , Emanation power / coefficient of the source (given by the certificate of the source)

$C_0$ ,  $^{222}\text{Rn}$  concentration of carrier gas [ $\text{Bq}$ ]

$V$ , Volume [ $\text{m}^3$ ] of the chamber

$Q_V = Q_{n,c} \cdot k_{PT}$ , Flow rate of the MFC at environmental condition

$Q_{n,c} = Q_n \cdot k_Q$ , Calibrated flow rate of the MFC

$Q_n$ , Flow rate of the MFC [ $\text{Ln}\cdot\text{min}^{-1}$ ]

$k_Q = \frac{1}{1+\Delta_{r,q}}$ , Correction factor of the MFC flow rate

$\Delta_{r,q}$ , Relative flow rate deviation of the calibrated MFC

$k_{PT} = \frac{p_0}{p_c} \cdot \frac{T_c+T_0}{T_0}$ , Correction factor for pressure-temperature of the flow rate

$p_0 = 1013.25 \text{ hPa}$ , Standard pressure according DIN 1343

$T_0 = 273.15 \text{ K}$ , Standard pressure according DIN 1343

$p_c = p \cdot k_p + k_{offset}$ , Corrected pressure

$T_c = T \cdot k_T + T_{offset}$ , Corrected temperature

## 6. METAS measurement results for source 1 387 Bq

METAS did measure the CEA source 'LNHB-METAS-226Ra-01-2019' during January and February 2019. The measurements were performed at several concentrations: 45, 90, 135, 23, 300 and 500 Bq·m<sup>-3</sup>. Three series of measurement were conducted and an additional measurement of aged and bottle air was performed with the result of < 8 Bq·m<sup>-3</sup>. The measurements were performed with a calibrated AlphaGuard PQ 2000 Pro, S/N 2142. Table 4 shows the given parameters by CEA.

Table 4 – Parameters of CEA source Ra226-no1.

Parameter	given value by CEA
<sup>226</sup> Ra activity $A_{0Ra-226}$	1387 Bq
<sup>222</sup> Rn emanation power $\chi$	0.458
<sup>226</sup> Ra reference date	14 <sup>th</sup> Nov. 2018
Combined uncertainty $u_r(A_0, Ra-226)$	0.8 % (k=1)
Combined uncertainty $u_r(\chi)$	1.6 % (k=1)

Figure 9 shows the calculated vs. the measured <sup>222</sup>Rn concentration of the CEA source 'LNHB-METAS-226Ra-01-2019'.

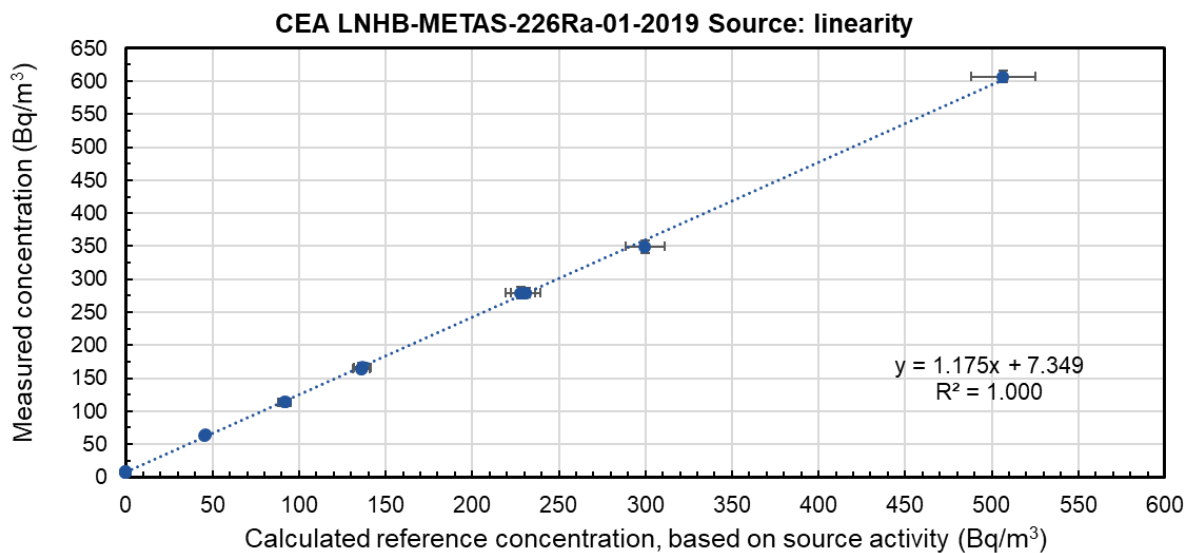


Figure 9 – <sup>222</sup>Rn concentration of the source CEA 'LNHB-METAS-226Ra-01-2019' with 1 387 Bq.

Based on the performed measurements at METAS a discrepancy between the calculated and the measured <sup>222</sup>Rn concentration was found. Following Table 5 shows the detailed deviations of each measurement sequence.

Table 5 – Detail overview of deviations.

Series of measurement	Calculated <sup>222</sup> Rn concentration $C_{ref}$ [Bq/m <sup>3</sup> ]	Calculated <sup>222</sup> Rn concentration $C_{meas}$ [Bq/m <sup>3</sup> ]	Flow Rate [Ln/min]	Relative Deviation	Duration Time [h]
2019-01-01	46	64	1.5102	40 %	18.5
2019-01-02	91	114	0.7581	25 %	67.3
2019-01-03	137	166	0.5044	22 %	17.2
2019-01-04	228	279	0.3035	22 %	16.3
2019-02-01	46	63	1.5023	38 %	19.6
2019-02-02	92	114	0.7410	24 %	19.5
2019-02-03	136	164	0.5040	21 %	56.6
2019-02-04	231	280	0.2974	21 %	25.8
2019-03-01	300	349	0.2351	20 %	47.5
2019-03-02	507	607	0.1338	17 %	24.1

The combined uncertainty of the reference concentration can give with  $u_r(C_{ref}) = 1.8\%$  ( $k = 1$ ) and for the measured concentration with  $u_r(C_{meas}) = 2.8\%$  ( $k = 1$ ). Based on the results of the measured <sup>222</sup>Rn activity concentration METAS did calculate a <sup>222</sup>Rn emanation power of 0.538 or 53.8 %.

## 7. METAS measurement results for source 1 533 Bq

METAS did measure the CEA source 'Ra226-no1' during December 2019 for 63 h in stabilized conditions according the equilibrium of <sup>222</sup>Rn and his the decay products <sup>218</sup>Po, <sup>214</sup>Pb and <sup>214</sup>Bi. During the measurement period ambient temperature was  $T_{AVG} = 21.9^\circ\text{C}$  and ambient pressure  $P_{AVG} = 944.4$  hPa. Table 6 shows the given parameters by CEA.

Table 6 – Parameters of CEAs source Ra226-no1.

Parameter	given value by CEA
<sup>226</sup> Ra activity $A_{0Ra-226}$	1533 Bq
<sup>222</sup> Rn emanation power $\chi$	unknown
<sup>226</sup> Ra reference date	09 <sup>th</sup> Oct. 2019

The flow rate through the CEA source Ra226-no1 was 150.0 mLn/min (flow rate of the mass flow controller (MFC) under standard conditions). The result of the measurement of the <sup>222</sup>Rn activity concentration is shown in Figure 10. The average of the measured <sup>222</sup>Rn activity concentration is 939.4 Bq/m<sup>3</sup>, within an uncertainty  $u_r(C_{meas}) = 5.5\%$  ( $k = 1$ ). METAS did measure the <sup>222</sup>Rn concentration with a 270 ml diffusion scintillation cell (Lucas cell), a photo multiplier tube (PMT) and a multi-channel analyzer (MCA) in pulse height analysis (PHA) mode.

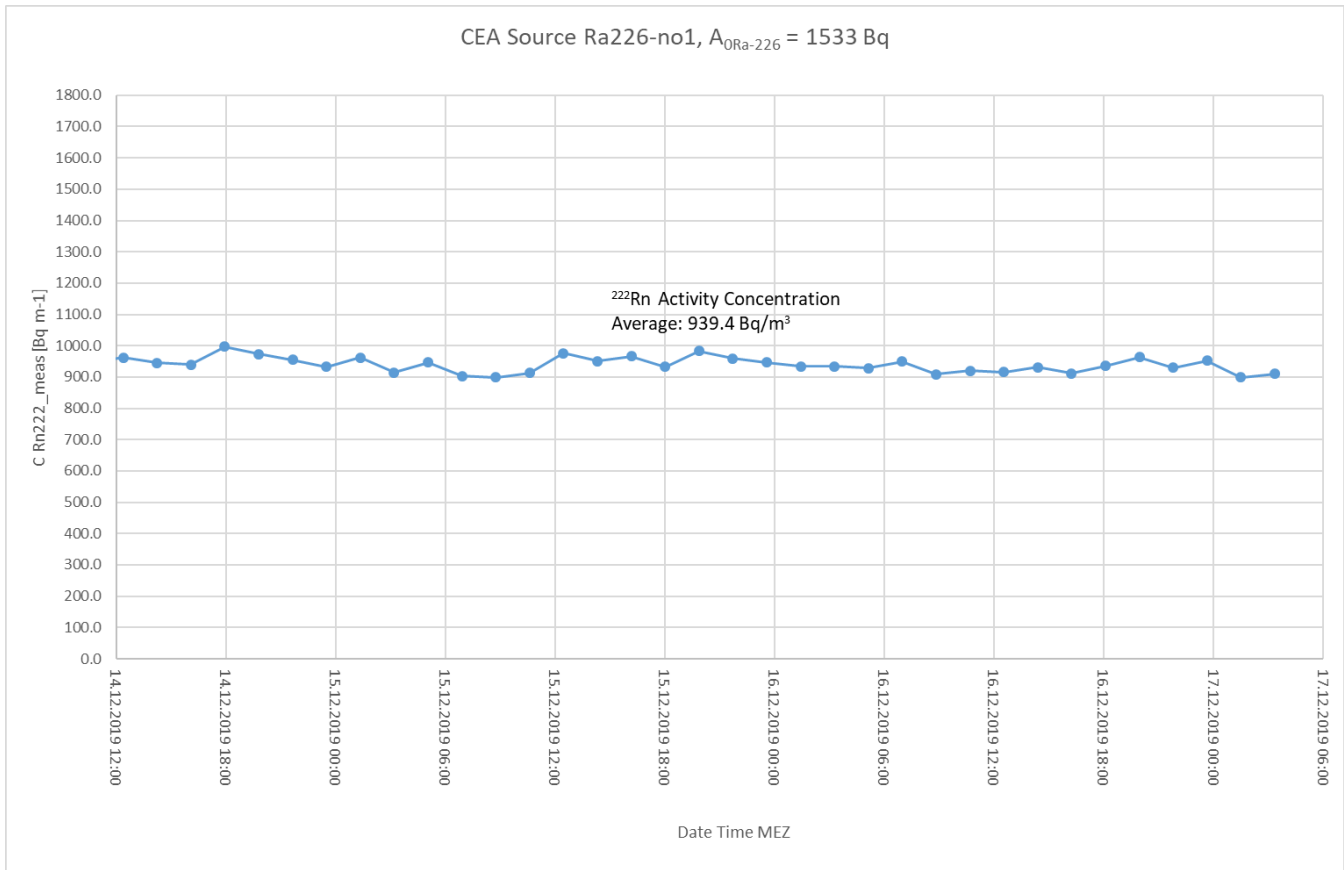


Figure 10 – Measurement result of the source of 1 533 Bq.

Based on the results of the measured  $^{222}\text{Rn}$  activity concentration METAS did calculate a  $^{222}\text{Rn}$  emanation power of 0.867 or 86.7 % for a flow rate of 150.0 mLn/min (related to standard conditions according German industry norm DIN 1343).

## 8. References

**Bé, M.-M. et al. 2008.** *Table of Radionuclides (Vol 4 - A = 133 to 252)*. s.l. : Monographie BIPM-5, Vol 4. Bureau International des Poids et Mesures, Sèvres, France., 2008.

**Bertin, Ins. 2020.** *Alphaguard, Radon Monitor*. s.l. : <https://www.bertin-instruments.com>, last access in 2020, 2020.

**Collé, R., Hutchinson, J.M.R., Unterweger, M.P. 1990.** *The NIST Primary Radon-222 Measurement System*. s.l. : J. Res. Natl. Inst. Stand. Technol., 95, 155-165, 1990.

**Sabot, B. 2015.** *Calibration of Thoron ( $^{220}\text{Rn}$ ) Activity Concentration Monitors*. s.l. : PhD thesis. NNT: 2015SACLS122, pp. 97–100, 2015.

**Sabot, B., et al. 2015.** *Development of a primary thoron activity standard for the calibration of thoron measurement instruments*. s.l. : Radiation Protection Dosimetry, Volume 167, Issue 1-3, Pages 70–74, 2015.

**Sabot, B., Pierre, S., Michielsen, N., Bondiguel, S., Casette, P. 2016.** *A new thoron atmosphere reference measurement system*. s.l. : Appl. Radiat. Isot. 109, 205–209, 2016.

**Sabot, B., Rodrigues, M., Pierre, S. 2020.** *Experimental facility for the production of reference atmosphere of radioactive gases (Rn, Xe, Kr, and H isotopes)*. s.l. : Applied Radiation and Isotopes 155, 108934, 2020.



# 16ENV10 MetroRADON

Activities A1.1.5 and A1.1.6

Comparison of activity from  $^{222}\text{Rn}$  measurements

CEA, PTB

Due date: May 2019

Submission: February 2020

**EMPIR**



The EMPIR initiative is co-funded by the European Union's Horizon 2020 research and innovation programme and the EMPIR Participating States

## Table of contents

1. Description of the task.....	3
2. Measurement of PTB source 2018-1441 in PTB .....	3
3. Measurement of PTB source 2018-1441 in CEA-LNHB.....	3
4. Measurement of PTB source 2018-1441 in both PTB and CEA-LNHB systems .....	3
5. Measurement of PTB source 2018-1441 in CEA-LNHB: result of CEA.....	5
6. Measurement of PTB source 2018-1441 in CEA-LNHB: result of PTB .....	7
7. Measurement of CMI source in CEA-LNHB.....	10
8. References .....	13
9. List of Figures .....	13

## 1. Description of the task

PTB, CEA and CMI will compare the activity from direct measurement of  $^{222}\text{Rn}$  in an air flow using the method developed in A 1.1.4 with the  $^{222}\text{Rn}$  activity of the emanation sources developed in A 1.1.1, A 1.1.2 and A 1.1.3. The approach that will be used to compare the activities will be determined once the emanation sources and the radon in the air flow method are partially developed.

CEA, PTB, CMI, SUJCHBO will compare the  $^{222}\text{Rn}$  activity from the stable emanation sources developed in A 1.1.1 - A 1.1.3 with existing decaying  $^{222}\text{Rn}$  gas standards using a known sample of radon as the transfer standard.

## 2. Measurement of PTB source 2018-1441 in PTB

In preparation of this intercomparison, the  $^{226}\text{Ra}$  source has been measured applying the DSA method described in the report of A1.1.1 in detail. The  $^{226}\text{Ra}$  activity determined for the source 2018-1441 is  $(665.5 \pm 1.9)$  Bq ( $k=1$ ).

To determine the emanation of the open source ( $^{222}\text{Rn}$  emanation source, 2018-1441), the spectra have to be compared with an equivalent but sealed  $^{226}\text{Ra}$  source (2018-1438). The  $^{226}\text{Ra}$  activity determined for this source 2018-1438 is  $(182.2 \pm 0.7)$  Bq ( $k = 1$ ). The  $^{222}\text{Rn}$  tightness of this source (2018-1438) after sealing was determined to be below 0.5 % of  $^{222}\text{Rn}$  emanating from the source – as described in the reporting of A1.1.1.

## 3. Measurement of PTB source 2018-1441 in CEA-LNHB

The PTB source is measured in the device detailed in task 1.1.4 with a flow rate of 1 L/min, but only with an Alphaguard inside the 45 L chamber. This Alphaguard has been calibrated with a standard prepared at CEA-LNHB.

The results obtain in these conditions ( $26.2\text{ }^{\circ}\text{C}$ ,  $1.472 \cdot 10^5\text{ Pa}$ ) is an emanation rate of 70.3 % with an uncertainty of 23 % ( $k = 1$ ).

## 4. Measurement of PTB source 2018-1441 in both PTB and CEA-LNHB systems

PTB device and CEA-LNHB device are inserted inside the loop (Sabot 2020, [1]) presented in the Activity reporting A 1.1.4. Figure 1 shows PTB device on the left and CEA-LNHB device on the right.



Figure 1 – PTB and CEA-LNHB devices

Details of PTB devices are shown in Figure 2, and the source more clearly showed in Figure 3.

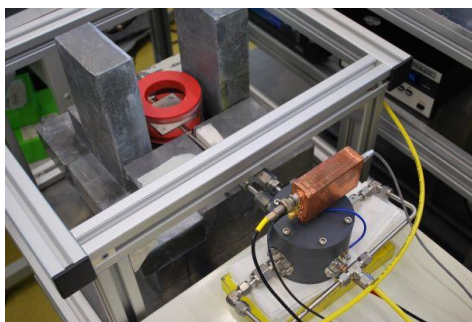


Figure 2 – PTB and CEA-LNHB devices inside the loop



Figure 3 – PTB source

The filtered air is coming through the source box, runs through the LNHB box with PIPS, and leaves towards the outside. PTB has got its own system to record the measurement (Figure 4) whereas CEA-LNHB uses his (Figure 5). The parameters (temperature, pressure, humidity, flow rate) are automatically recorded.

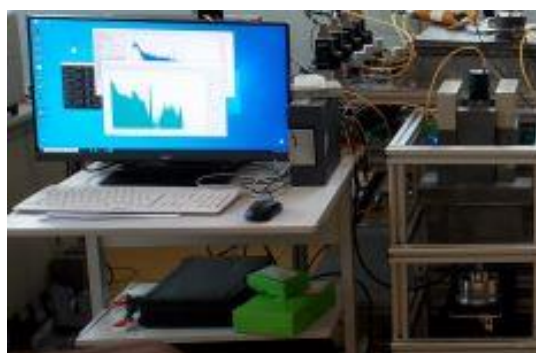


Figure 4 – PTB acquisition system



Figure 5 – CEA-LNHB computer

In this way, the PTB source is measured by both systems under the same conditions. A  $^{226}\text{Ra}$  source source was measured during a month to estimate the emanation rate.

### 5. Measurement of PTB source 2018-1441 in CEA-LNHB: result of CEA.

The way the measurements are led is presented in Sabot 2016 [2] and Sabot 2015 [3]. Due to a previous thoron measurement, the radon measurements were delicate, like we can see in Figure 6, where the thoron peaks stay with the radon peaks. The flow rate was 0.2 L/min.

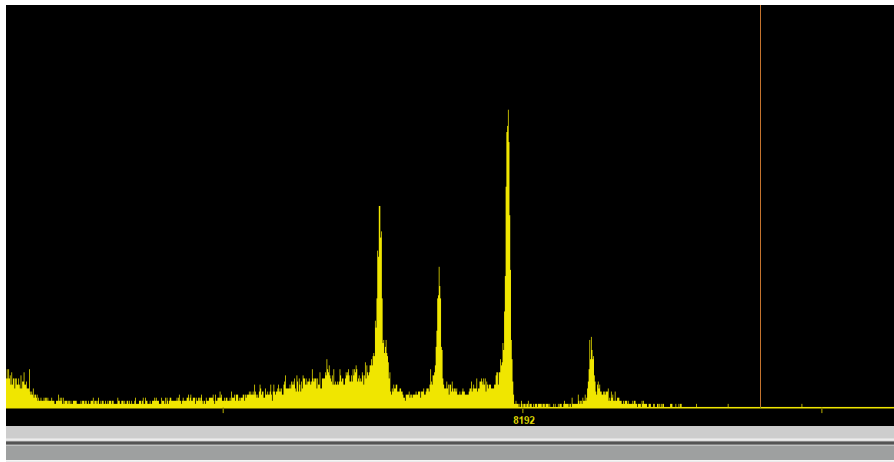


Figure 6 – Spectra obtained

In our measurement conditions, the calculations are presented in Figures 7 and 8.

Spectrum				Measurement PTHD during the spectrum acquisition :		
Date of the measurement	Ra226-2018-1441-16-12-19.lzs			Average	Standard deviation	
	06/12/2019 10:19			% RH	28,3	2,0
Legend				P (mbar)	982,5	11,5
Calculations				Flow rate Ln/min	0,200	0,000
To complete				T °C	19,95	0,2
Data				Flow rate in m³/s	3,69015E-06	1,2%
Importants results						
<b>DATA SOURCE Ra-226</b>						
Reference date	06/12/2019 12:00			<b>Ra-226</b>		
				1600	a	7
Activity of Ra-226 (Bq)	Stand. Uncert. (Bq)	Re.l Stand. Uncert. (%)		5,0491E+10	s	2,2E+08
665,5	1,9	0,3%		8,4152E+08	min	3,7E+06
Calculation of the activity concentration produced by the source :				1,4025E+07	h	6,1E+04
	Value	Stand. Uncertainty	Rel standard uncertainty	5,8439E+05	j	2,6E+03
$E = A_{Ra-226} \cdot \lambda_{Rn-222} \cdot \chi$ avec $\chi = 1$	1,3965E-03			1,6000E+03	a	7,0E+00
$Av(Rn-222)$ avec $\chi = 1$ Bq/m³	378,43	6,5	1,7%			
Calcul du volume de prélèvement entre la source et le proto thoron (m³) :				1 a =	365,2421988	j
				1 a =	31556926	s
	Value	Stand. Uncertainty	Rel standard uncertainty			
Tube 1 radius (m)	0,02	1,0E-04	0,5%			
Lenght (m)	0,2	2,0E-03	1,0%	<b>Rn-222</b>		
Total m³	2,5E-04	3,6E-06	1,4%	3,8232	j	0,0008
Radius of the cylindrical Source (m)		1,0E-04	#DIV/0!	3,3032E+05	s	6,9E+01
Lenght of the source (m)		4,0E-03	#DIV/0!	5,5054E+03	min	1,2E+00
Total m³		0,0E+00	#DIV/0!	9,1757E+01	h	1,9E-02
				3,8232E+00	j	8,0E-04
				1,0468E-02	a	2,2E-06
First radius (m)		1,0E-04	#DIV/0!			
Last radius (m)		1,0E-04	#DIV/0!			
Lenght of the cone cone (m)		4,0E-03	#DIV/0!	1 a =	365,2421988	j
Total cone source m³		0,0E+00	#DIV/0!	1 a =	31556926	s
Volume (m³)	2,51E-04	3,55E-06	1,4%			
Decay correction from ref.date	1,000	0,000	0,000%			

Figure 7 – Radon results part 1

	Value	Stand. uncert.	Rel stand. Uncert	ROI et infos
$N_{222Rn}$	6736,906241	82	0,01	2500-5996
MP ROI Rn-222	341	18	0,05	
$N_{222Rn} - MP$	3288	84	0,03	2685-6008
$N_{218Po}$	5858	77	0,01	6019-6406
MP ROI	373	19	0,05	6019-6406
$N_{218Po} - MP - Contrib, autre$	740	79	0,11	
N ROI mélange	17713	133	0,01	2665-7133
N MP Mélange	1042	32,3	0,03	
$t_{MP}$	86430	1	0,001%	MP du 5/12/19
MP avec temps mesure	10540	103	0,974%	
$N_{222Rn+218Po}$	10750			
$N_{222Rn+218Po} - MP$	210	176	84%	
$t_m (s)$	874168	1	0,000%	
$V_{det} (m^3)$	1,2440E-05	6,00E-08	0,5%	
$R_{d Rn 222}$	0,320	0,002	0,6%	
$R_{d Po 218}$	0,465	0,0100	2,2%	
$N_{214Po}$	6637	81	1,2%	
MP ROI Po214	3			
$N_{214Po} - MP$	6607			
$R_{d Po 214}$	0,474	0,010	2,2%	
	Value	Stand. uncert.	Rel stand. Uncert.	
Av (Bq.m-3)	25	21	83,9%	Inutilisable
Rn-222	946	25	2,7%	Inutilisable
Po-218	146	4	2,6%	
Po-214	1288	74	5,8%	Etrange
Mesure dispositifs commerc				
	Value	Stand. uncert.	Rel stand. Uncert.	
Alphaguard, Av (Bq.m-3)	141	15	11%	
Radon eye, Av (Bq.m-3)	191	24	12%	
Calcul taux d'émanation				
	Value	Stand. uncert.	Rel stand. Uncert.	
Emanation LNHB from peak Po-218	38,68%	1,2%	3,1%	
Emanation from Alphaguard	37,25%			

Figure 8 – Radon results part 2

The measurement made with the Alphaguard confirms our result.

## 6. Measurement of PTB source 2018-1441 in CEA-LNHB: result of PTB

It was observed, that varying humidity can impact the emanation coefficient  $\chi$  of  $^{222}Rn$  from electrodeposited  $^{226}Ra$ , where lower humidity leads to decreased emanation.

Since the magnitude of this effect can have very complex covariance on multiple different parameters, namely temperature, pressure, history of the source, plating conditions and chemical impurities, it is infeasible to correct for these dependencies by measuring all possible combinations of them. The alternative is to measure the emanation coefficient of the sources using an on-line measurement setup based on low-cost, high-resolution scintillator consisting of the inorganic crystals  $LaBr_3$ ,  $CeBr_3$  or  $SrI_2$ . PTB has investigated the application of these scintillators for this purpose by measuring the emanation coefficients of a subset of the produced

electrodeposited sources with a setup, where the sources are installed in between the respective scintillation detector and a HPGe detector.

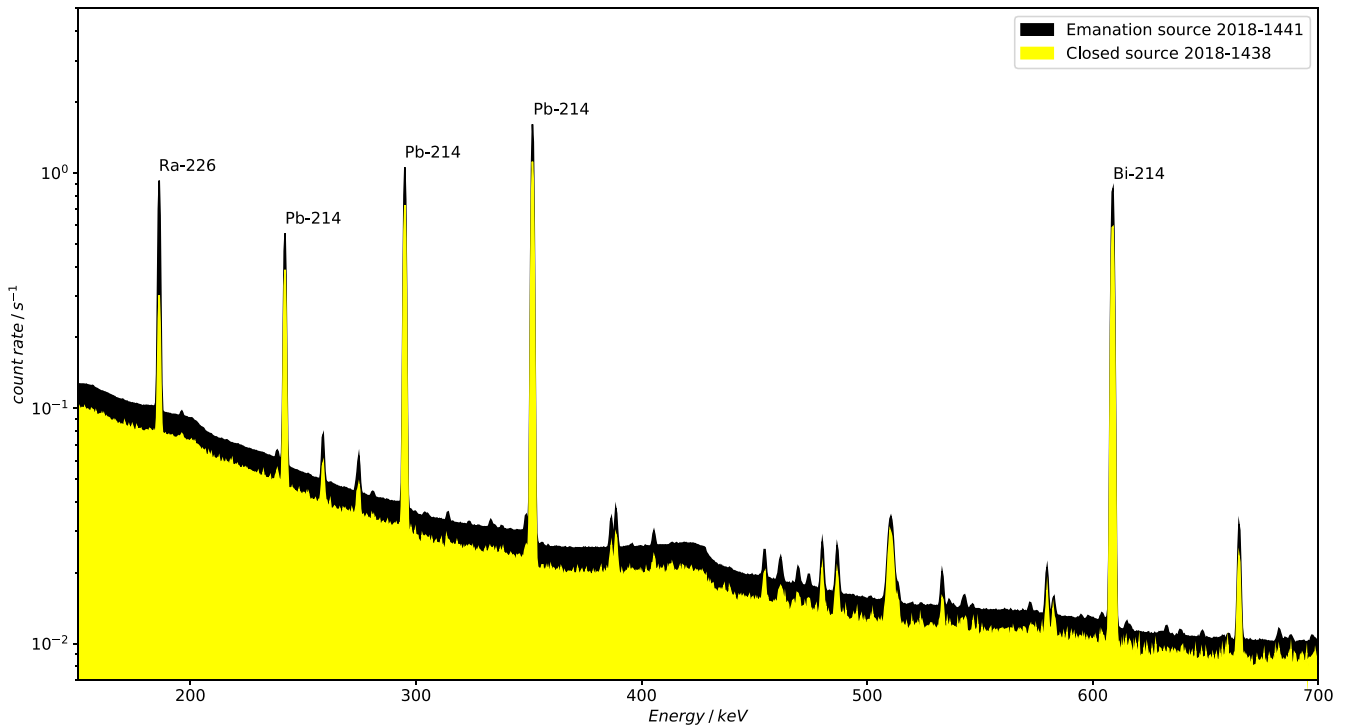


Figure 9 –  $\gamma$ -count rate spectrum versus  $\gamma$ -energy between 150 keV and 700 keV of the  $^{226}\text{Ra}$  electrodeposited emanation source 2018-1441, acquired with a HPGe detector

Thereby, it was found that the conventional approach outlined in activity report A1.1.1 is not readily applicable to these scintillators, because deviations of the thus determined  $\chi$  by over 5 % as compared to the values from the HPGe detector measurements were observed. It was shown, that this effect is due to peak overlaps in the region of the  $^{226}\text{Ra}$  peak. One possible solution to this issue is to introduce the ratio of  $^{226}\text{Ra}$  activities as introduced in equations (1). Then, the achievable uncertainty for the emanation coefficient determination by this system is limited to the uncertainty of the ratio of  $^{226}\text{Ra}$  activities achievable by DSA alpha-spectrometry. For the gamma-ray spectra of scintillation detectors, equation (1) needs to be used instead. With this adapted analysis, deviations from the values determined by HPGe detectors vanish.

$$\chi = 1 - \frac{A_{\text{Ra-226(closed)}}}{A_{\text{Ra-226(open)}}} \cdot \frac{R_{\text{Pb-214(open)}}}{R_{\text{PB-214(closed)}}} \quad (1)$$

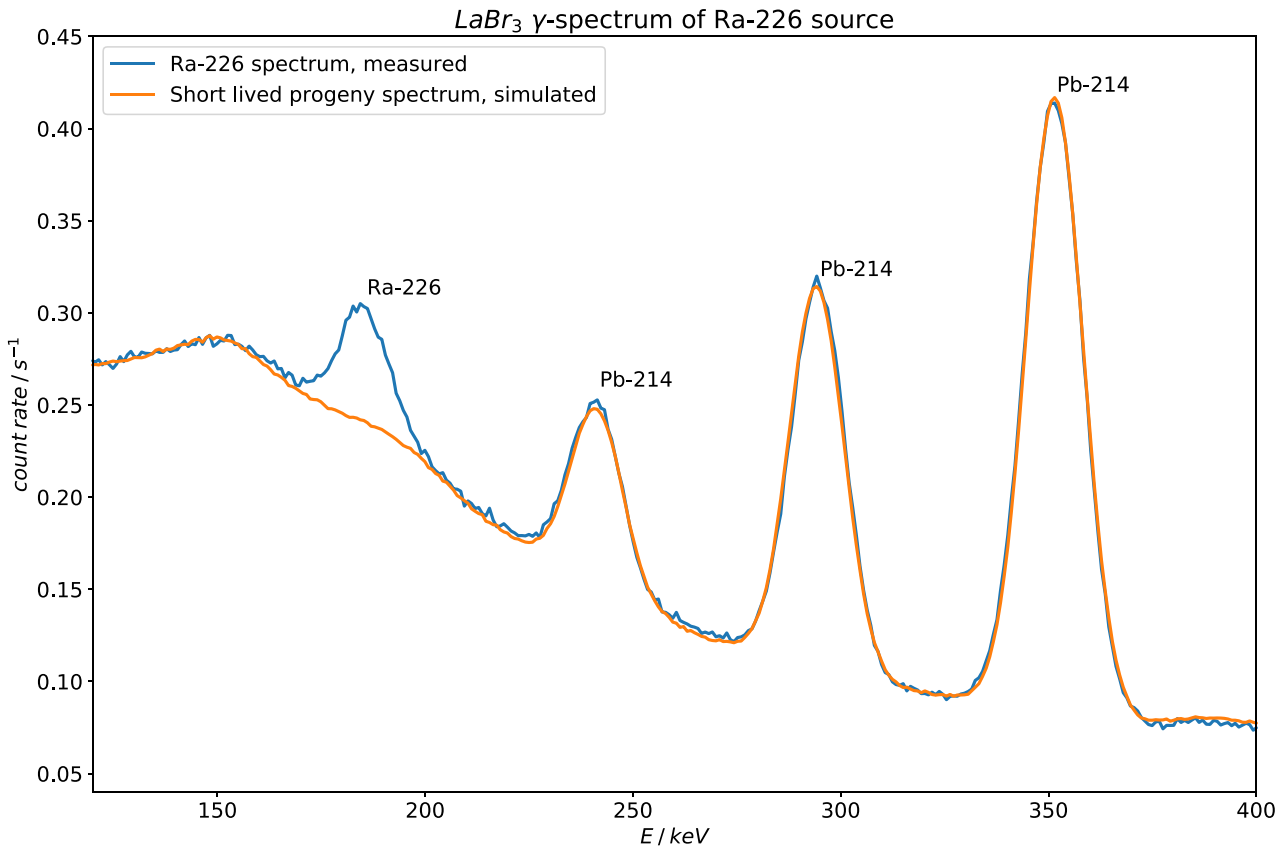


Figure 10 –  $\gamma$ -count rate spectrum versus  $\gamma$ -energy between 150 keV and 400 keV of a  $^{226}\text{Ra}$  electrodeposited emanation source 2018-1441, acquired with a  $\text{LaBr}_3$  detector

Based on these results, a portable system consisting of a 2"  $\text{LaBr}_3$  detector was implemented and used for the first time for Task 1.1.5.

The emanation coefficient during the time of the measurement as an exponential function of the time, as described in equation ((2)) and shown in Figure .

$$\chi(\Delta t) = \chi_{\infty} + (\chi_0 - \chi_{\infty})e^{\left(\frac{-\ln(2)}{t_{1/2} \cdot 86400 \text{ s}} \Delta t\right)} \quad (2)$$

The results derived from the minimisation of this function to the data of the measurement are  $\chi_0 = 0.7579(7)$  at the time of the start of the measurements and  $\chi_{\infty} = 0.5708(4)$  at the end of the measurement. The time constant of the exponential function is determined with 4.59(4) d. This is larger than the half-life of  $^{222}\text{Rn}$  (3.8232(8) d) which one would expect, gives cause to a change in emanation coefficient due to drying effect of the source.

Since the variation of the emanation coefficient has very complex reasons, as described above, stable emanation conditions and therefor stable  $^{222}\text{Rn}$  activity concentration are expected at the second half of the measurement period.

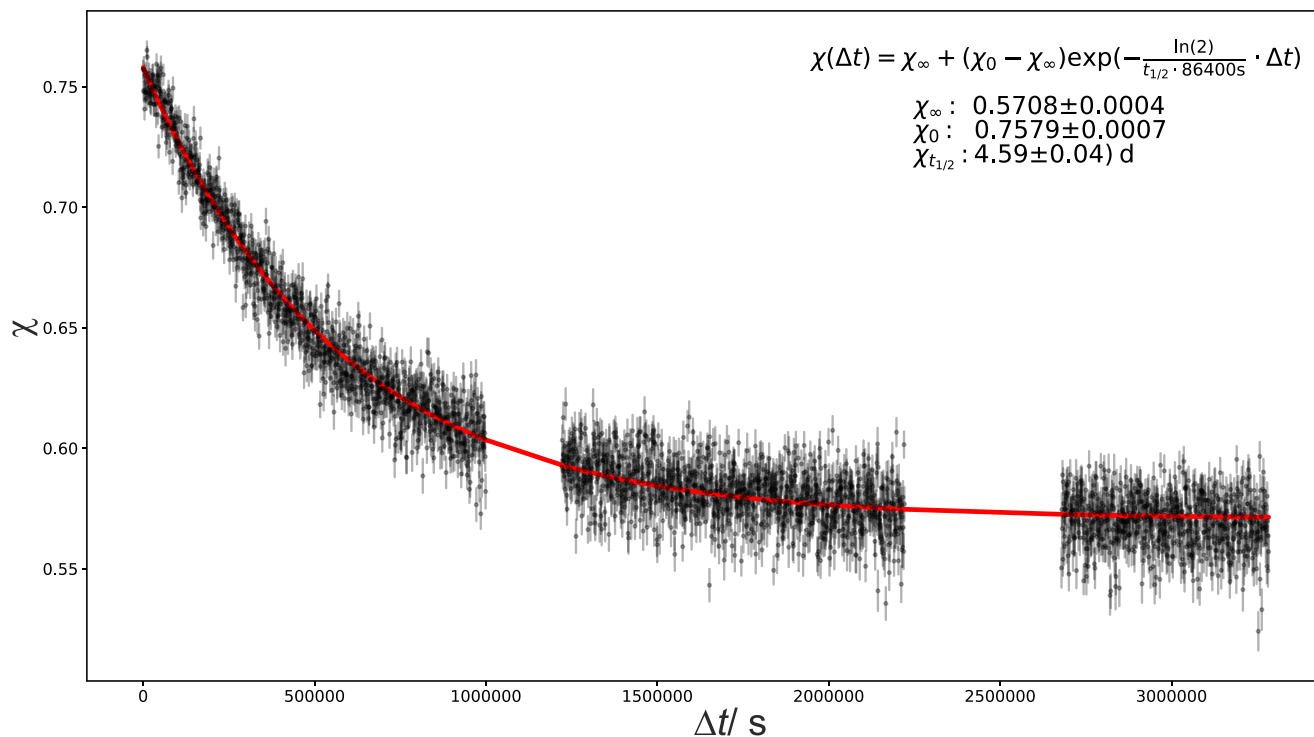


Figure 11 – Emanation power c of the electrodeposited <sup>226</sup>Ra6 source 2018-1441 as a function of time

## 7. Measurement of CMI source in CEA-LNHB

It was not possible to measure the CMI source with the PTB device, so the CMI source was introduced into the loop as shown in Figure 12.

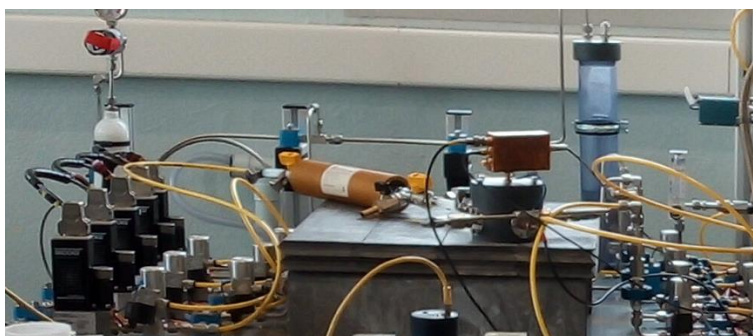


Figure 12 – CMI source

The spectra were clean (Figure 13).

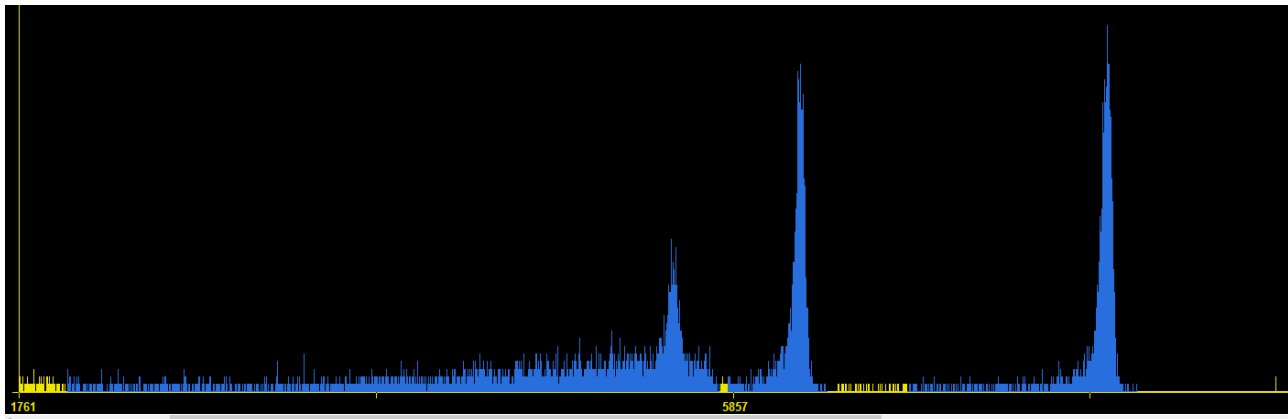


Figure 13 – CMI spectrum

We calculated the emanation with the  $^{218}\text{Po}$  peak and with the  $^{214}\text{Po}$  peak. We performed the same measurement with 3 flow rates: 0.2 L/min, 0.5 L/min and 1 L/min (Figures 14a and 14b).

DONNEES EXPERIMENTALES						
Spectre	CMI-1l/min-06-02-20				Mesures PTHD pendant l'acquisition du spectre :	
Date de mesure	30/01/2020 12:24				Moyenne	Ecart-type
					% RH	32,6
					P (mbar)	994,9
					Débit Ln/min	1,000
					T °C	21,083
Légende :						
Calculs						
A compléter						
Données						
Résultats importants					Débit corrigé en m <sup>3</sup> /s	1,82802E-05
						0,5%
DONNEES SOURCE Ra-226						
Date de référence	01/05/2018 00:00				<b>Ra-226</b>	
					1600	7
Activité Ra-226 (Bq)	Inc-type (Bq)	Inc-type rel (%)			a	
5058,0	51,0	1,0%			s	2,2E+08
Calcul activité volumique produite par la source :					min	3,7E+06
	Valeur	Inc-type	Inc-type rel.		h	6,1E+04
					j	2,6E+03
$E = A_{Ra-226} \cdot \lambda_{Rn-222} \cdot \chi$ avec $\chi = 1$	1,0614E-02				a	7,0E+00
$Av(Rn-222)$ avec $\chi = 1$ Bq/m <sup>3</sup>	580,61	7,4	1,3%			
Calcul du volume de prélèvement entre la source et le proto thoron (m <sup>3</sup> ) :					1 a =	365,2421988
					1 a =	31556926
						j
	Valeur	Inc-type	Inc-type rel.			
Rayon tube 1 (m)	0,02	1,0E-04	0,5%			
Longueur (m)	0,2	2,0E-03	1,0%			
Tota m <sup>3</sup>	2,5E-04	3,6E-06	1,4%			
					<b>Rn-222</b>	
					3,8232	0,0008
Rayon cylindre Source (m)		1,0E-04	#DIV/0!		s	6,9E+01
Longueur Source (m)		4,0E-03	#DIV/0!		min	1,2E+00
Total m <sup>3</sup>		0,0E+00	#DIV/0!		h	1,9E-02
					j	8,0E-04
Rayon début (m)		1,0E-04	#DIV/0!		a	2,2E-06
Rayon Fin (m)		1,0E-04	#DIV/0!			
Hauteur cone (m)		4,0E-03	#DIV/0!		1 a =	365,2421988
Total cone source m <sup>3</sup>		0,0E+00	#DIV/0!		1 a =	31556926
						j
						s
Volume entre source et mesure (m <sup>3</sup> )	2,51E-04	3,55E-06	1,4%			
Correction décroissance date ref	1,001	0,000	0,033%			

Figure 14a – Conditions of CMI source measurement, 1l/min

	Value	Stand. Uncert.	Rel stand. Uncert.	ROI et infos
N <sub>222Rn</sub>	3362,32	58	0,02	2031-5779
MP ROI Rn-222	359	19	0,05	
N <sub>222Rn</sub> - MP	2494	61	0,02	
N <sub>218Po</sub>	2014	45	0,02	5826-6397
MP ROI	124	11	0,09	
N <sub>218Po</sub> - MP - Contrib, autre	1714	46	0,03	
N ROI mélange	5624	75	0,01	2665-7133
N MP Mélange	484	22,0	0,05	
t <sub>MP</sub>	243314	1	0,000%	MP du 23/01/2020
MP avec temps mesure	1170	34	2,923%	
N <sub>222Rn+218Po</sub>	5624			
N <sub>222Rn+218Po</sub> - MP	4454	82	2%	
t <sub>m</sub> (s)	588373	1	0,000%	
V <sub>det</sub> (m <sup>3</sup> )	1,2440E-05	6,00E-08	0,5%	
R <sub>d Rn-222</sub>	0,320	0,002	0,6%	
R <sub>d Po-218</sub>	0,465	0,0100	2,2%	
N <sub>214Po</sub>	2219	47	2,1%	6856-8172
MP ROI Po214	127			
N <sub>214Po</sub> -MP	1912			
R <sub>d Po-214</sub>	0,474	0,010	2,2%	
	Value	Stand. Uncert.	Rel stand. Uncert.	
Av (Bq.m-3)	776	23	2,9%	Inutilisable
Rn-222	1067	27	2,6%	Inutilisable
Po-218	504	16	3,1%	
Po-214	551	17	3,1%	
<b>Mesure dispositifs commerciaux</b>				
	Value	Stand. Uncert.	Rel stand. Uncert.	
Alphaguard, Av (Bq.m-3)	570	26	5%	
<b>Calcul taux d'émanation</b>				
	Value	Stand. Uncert.	Rel stand. Uncert.	
Emanation LNHB à partir pic Po-214	94,98%	3,2%	3,4%	
Emanation Alphaguard	98,14%			

Figure 14b – Result of CMI source emanation rates, 1 L/min

The results in the 3 flow rates are given in Figure 15:

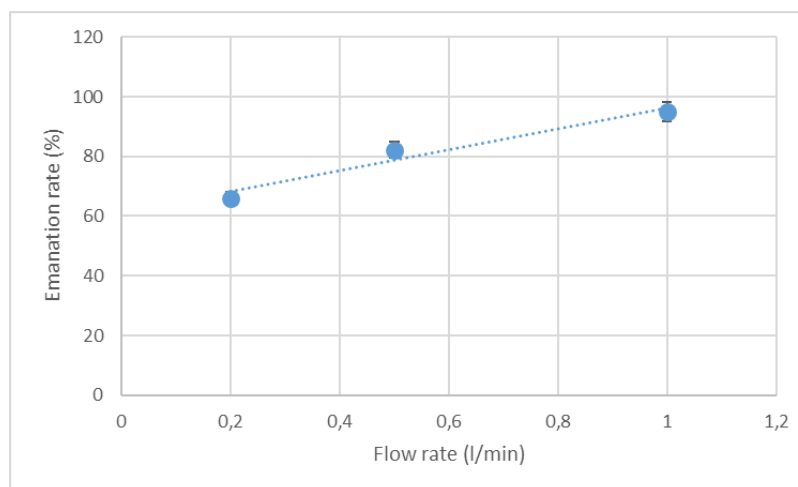


Figure 15– Result of CMI source emanation at 0.2, 0.5 and 1 L/min

## 8. References

- [1] Sabot, B., Rodrigues, M., Pierre, S., 2020. Experimental facility for the production of reference atmosphere of radioactive gases (Rn, Xe, Kr, and H isotopes). ARI 155 (2020), 108934.
- [2] Sabot, B., Pierre, S., Michielsen, N., Bondiguel, S., Cassette, P., 2016. A new thoron atmosphere reference measurement system. ARI 109 (2016), 205-209.
- [3] Sabot, B. (2015). Calibration of Thoron ( $^{220}\text{Rn}$ ) Activity Concentration Monitors. PhD thesis. NNT: 2015SACLS122, pp. 97–100.

## 9. List of Figures

Figure 1 – PTB and CEA-LNHB devices .....	3
Figure 2 – PTB and CEA-LNHB devices inside the loop .....	4
Figure 3 – PTB source .....	4
Figure 4 – PTB acquisition system .....	4
Figure 5 – CEA-LNHB computer .....	5
Figure 6 – Spectra obtained .....	5
Figure 7 – Radon results part 1 .....	6
Figure 8 – Radon results part 2 .....	7
Figure 9 – $\gamma$ -count rate spectrum versus $\gamma$ -energy between 150 keV and 700 keV of the $^{226}\text{Ra}$ electrodeposited emanation source 2018-1441, acquired with a HPGe detector .....	8
Figure 10 – $\gamma$ -count rate spectrum versus $\gamma$ -energy between 150 keV and 400 keV of a $^{226}\text{Ra}$ electrodeposited emanation source 2018-1441, acquired with a $\text{LaBr}_3$ detector .....	9
Figure 11 – Emanation power $c$ of the electrodeposited $^{226}\text{Ra}$ source 2018-1441 as a function of time .....	10
Figure 12 – CMI source .....	10
Figure 13 – CMI spectrum .....	11
Figure 14a – Conditions of CMI source measurement, 1l/min .....	11
Figure 14b – Result of CMI source emanation rates, 1l/min .....	12
Figure 15 – Result of CMI source emanation at 0.2, 0.5 and 1 l/min .....	12



# 16ENV10 MetroRADON

Activities A1.3.1 and A1.3.2

Establishment of constant and stable  $^{222}\text{Rn}$  radon activity concentrations in reference chambers and development of procedures for the calibration of radon measurement instruments at low activity concentrations

Contributors:

1. Federal Office for Radiation Protection (BfS), Germany
2. Eidgenössisches Institut für Metrologie (METAS), Switzerland
3. Horia Hulubei National Institute for Research and Development in Physics and Nuclear Engineering (IFIN-HH), Bucharest-Magurele, Romania
4. National Institute for Nuclear, Biological and Chemical Protection (SUJCHBO)
5. Budapest Főváros Kormányhivatala (BfKH), Hungary
6. Institut de Radioprotection et de Sûreté Nucléaire (IRSN), France

Due date:

Submission: 30. March 2020

**EMPIR**



The EMPIR initiative is co-funded by the European Union's Horizon 2020 research and innovation programme and the EMPIR Participating States



## Table of contents

A.	Activity Report of the German Federal Office for Radiation Protection (BfS) .....	5
A.1	Representation of the quantity radon activity concentration for accurate calibrations of radon instruments .....	5
A.1.1	Introduction.....	5
A.1.2	Equipment and components .....	6
A.1.3	Radon supply .....	6
A.1.6	Radon reference atmospheres.....	11
A.1.7	Conclusions.....	11
A.2	Calibration procedures in the activity concentration range from 100 Bq/m <sup>3</sup> to 300 Bq/m <sup>3</sup> using <sup>222</sup> Rn emanation standards .....	12
A.2.1	Introduction.....	12
A.2.2	Determination of effective air volume.....	12
A.2.3	Background of the calibration object.....	13
A.2.4	Exposures .....	14
A.2.5	Determination of the calibration factor .....	16
A.2.6	Uncertainty of the calibration factor.....	17
A.2.7	Uncertainty caused by statistical fluctuations of the measurement value.....	18
A.2.8	Conclusions.....	22
A.3	References .....	22
B.	Activity Report of the Eidgenössisches Institut für Metrologie (METAS) .....	24
B.1	Representation of the quantity radon activity concentration for accurate calibrations of radon instruments .....	24
B.1.1	Introduction.....	24
B.1.2	Equipment and components .....	24
B.1.3	Equipment and components .....	25
B.1.4	Mathematical treatment of a one-chamber system .....	25
B.1.5	Uncertainty calculations .....	27
B.1.6	Conclusion .....	27
B.2	Calibration procedures in the activity concentration of 300 Bq/m <sup>3</sup> using <sup>222</sup> Rn emanation standards .....	28
B.2.1	Introduction.....	28
B.2.2	Background of the calibration .....	28
B.2.3	Exposures.....	29
C.	Activity Report of the Horia Hulubei National Institute for Research and Development in Physics and Nuclear Engineering (IFIN-HH) .....	31
C.1	Representation of the quantity radon activity concentration for accurate calibrations of radon instruments .....	31
C.1.1	Introduction.....	31
C.1.2	The radon monitors and the new recipients used for measurements at IFIN-HH.....	32

C.1.3	The radon chamber of IFIN-HH.....	33
C.1.4	Establishment of constant and stable <sup>222</sup> Rn activity concentrations in the radon chamber .....	34
C.2	Development of a procedure for the calibration of instruments measuring the radon activity concentration in air .....	36
C.3	References .....	37
D.	Activity Report of the National Institute for Nuclear, Biological and Chemical Protection (SUJCHBO) .....	38
D.1	Representation of the quantity radon activity concentration for accurate calibration of radon instruments .....	38
D.1.1	Introduction .....	38
D.1.2	Description of the technical infrastructure .....	38
D.1.3	Mathematical treatment.....	40
D.1.4	Uncertainty in determining the radon reference level .....	41
D.2	Calibration.....	41
D.2.1	Procedures .....	41
D.2.2	Radon chamber modelling .....	44
D.3	Conclusion.....	45
E.	Activity Report of the Government Office of the Capital City Budapest (BFKH) Metrological and Technical Supervisory Department.....	46
E.1	Representation of the quantity radon activity concentration for accurate calibration of radon instruments .....	46
E.1.1	Introduction .....	46
E.1.2	Description of the measuring system .....	46
E.1.3	Radon homogeneity and the airtight closed chamber .....	48
E.1.4	Volume of the radon chamber .....	49
E.1.5	Mathematical model .....	50
E.2	Calibration procedure .....	52
E.3	References .....	52
F.	Activity Report of the Institut de Radioprotection et de Sûreté Nucléaire (IRSN) .....	53
F.1	Representation of the quantity radon activity concentration for accurate calibration of radon instruments .....	53
F.1.1	Introduction .....	53
F.1.2.	Establishment of constant and stable <sup>222</sup> Rn activity concentration in reference chambers .....	53
F.2	Calibration of radon measurement instruments at low activity concentrations .....	55
F.2.1.	Reference <sup>222</sup> Rn activity concentration and uncertainty .....	55
F.2.2.	Calibration procedure .....	56
F.2.3.	Determination of the background .....	56
F.3	Conclusion.....	57

## A. Activity Report of the German Federal Office for Radiation Protection (BfS)

### A.1 Representation of the quantity radon activity concentration for accurate calibrations of radon instruments

#### A.1.1 Introduction

As regards protection against radon exposure ( $^{222}\text{Rn}$ ) at home and at work, the transposition into national law of European Council Directive 2013/59/EURATOM requires a reliable metrological basis ensuring confidence in the measurements. The Directive follows the recommendations of the World Health Organisation and the International Commission on Radiological Protection (ICRP) and sets a value of  $300 \text{ Bq/m}^3$  as a reference level for homes and workplaces in relation to the annual average radon activity concentration above which exposure is considered inappropriate. However, so far the European metrological bodies have disseminated the quantity only for a level of  $1000 \text{ Bq/m}^3$  and above [1].

The EMPIR research project *Metrology for Radon* aims to extend traceable calibrations to areas with low radon activity concentrations and thus include the legally binding reference level. To this end, novel methods shall be developed for the traceable calibration of radon measuring instruments at activity concentrations of  $100 \text{ Bq/m}^3$  to  $300 \text{ Bq/m}^3$  with relative uncertainties  $\leq 5\%$  ( $k=1$ ). The stable radon atmospheres over time and precision are to be achieved by using emanation sources together with existing certified reference volumes.

The radon reference facility was established at the German Federal Office for Radiation Protection (BfS). Its basic components as well as its performance for the representation of radon activity concentration and the dissemination of the quantity are presented. It should be noted that the facility

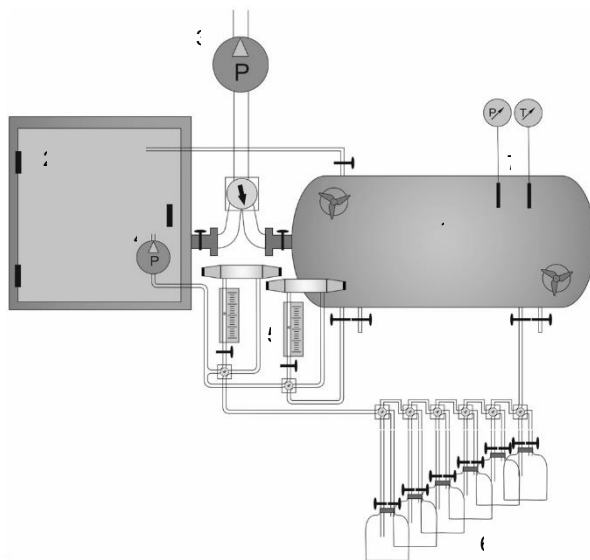


**Figure A.1.** Scheme of the facility:

- 1 Reference chamber
- 2 Secondary chamber
- 3 External pump
- 4 Internal pump
- 5 Scintillation cells (flow-through)
- 6 Sampling unit
- 7 Sensors for temperature, air pressure, humidity

outlined in this work is dedicated to the calibration of instruments measuring the radon isotope  $^{222}\text{Rn}$  in air. The adaption for calibrations of instruments measuring the isotope  $^{222}\text{Rn}$  (thoron), which is also relevant in radiation protection, will be the subject of future developments.

### A.1.2 Equipment and components

The basic component is a high vacuum chamber with a cylindrical, horizontal body made of stainless steel. The chamber has a reference volume of 168 litres with an uncertainty of 0.7 % ( $k = 2$ ). The volume is traced back directly by calibration to a standard volume provided by Physikalisch-Technische Bundesanstalt (PTB), Germany. Chamber outlets are sealed off by bellows-sealed valves.

The reference chamber is extended by a secondary chamber with cubical chamber body made of stainless steel. The secondary chamber has a volume of approx. 131 litres.

Stainless steel pipes connect both chambers. By means of an internal pump, air containing radon circulates between the two chambers. The standard flow rate of the internal circulating air is approx. 3 litres/min. Each chamber is equipped with two small ventilators in order to distribute the radon activity, and to homogenize the atmosphere.

The radon-laden air can be led through two flow-through scintillation cells to monitor the radon activity concentration inside the facility. Sensors enable monitoring of temperature, air pressure, and humidity.

The facility can be evacuated with the external pump. A sampling unit with six interfaces optionally allows the sampling of radon-laden air for other purposes (e.g. filling external scintillation cells, supply or removal of moisture). A scheme of the facility is given in Figure A.1.

The entire facility is pressure-tight to 1200 mbar and vacuum-tight to 1 mbar. The standard operating ranges in which the parameters can be kept constant over time are an air pressure between 800 mbar and 1100 mbar, a temperature between 5 °C and 35 °C and a relative humidity between 5 % and 95 %. A professional cooling unit is used to set the temperature. Temperatures below zero degrees are also possible. As the facility has no thermal insulation, the temperature can only be set and kept constant in the secondary chamber.

### A.1.3 Radon supply

#### A.1.3.1 Sources

The radon isotope 222 is generated by decay of radium-226, and has a relatively long half-life of about 3,8 days. Because of its natural occurrence and its ubiquitous presence in breathing air indoors and outdoors, radon is of utmost importance in the view of radiation protection. Therefore, the vast majority of instruments is used to measure the quantity activity concentration of radon-222. The quantity is represented for the purpose of dissemination by calibration of the instruments.

Atmospheres containing  $^{222}\text{Rn}$  can be produced by using:

1. gas standards, or
2. emanation sources.

A radon gas standard is an ampoule made of glass or stainless steel that contains a certain amount of radon activity. After transfer to a confined volume, the radon activity concentration decreases over time according to the radioactive decay of  $^{222}\text{Rn}$ .



Figure A.2. Emanation source produced by CMI

**Table A.1.** Specifications of the emanation source according to certificate [3]

Activity of $^{226}\text{Ra}$	5.058(51) kBq
Radon emanation rate	0.0106(1) Bq/s
Range of temperature at operation	0°C – 40°C
Range of relative humidity at operation	0 % – 100 %

Radon emanation sources contain radium-226 salt, which permanently releases radon into gas phase (emanation). This enables accurate and long-term stable sources with a defined generation rate for  $^{222}\text{Rn}$ . A radon emanation source provided by the Czech Metrological Institute (CMI) is used for the production of radon atmospheres (see Figure A.2) [2]. The source is enclosed in a cylindrical aluminium alloy housing with two ball valves at the ends. Radon is released from a thin polymer layer. Almost all the radon formed enters the gas phase. The activity of  $^{226}\text{Ra}$  is determined by comparison with primary standards maintained at CMI, and the emanation rate by gamma spectrometry on an HPGe detector [2]. The specifications of the emanation source according to the certificate issued by CMI are summarized in Table A.1.

The emanation source can be operated in flow-through or batch mode. In the batch mode, the radon released over time and accumulated in the gas phase of the source is immediately transferred into a confined volume. In a closed source, the accumulated radon activity approaches the activity of  $^{226}\text{Ra}$  after a time of more than 4 weeks.

In the flow-through mode, a continuous air flow through the source takes up the emanated radon, and adds it to a confined volume. The final radon activity concentration generated in the volume depends on the air flow rate. For operation in the flow-through mode, the system is equipped with a calibrated mass flow controller installed upstream of the source to ensure a constant and accurate airflow through the source into the calibration chamber. The excess air is discharged from the calibration chamber via an outlet.

To avoid interference from the radon background, the source is purged with radon-low air stored in compressed gas bottles. Radon-low air is obtained when air remains in the bottles for a few weeks after delivery before it is used. The use of radon-low air increases the accuracy of calibration measurements as background effects can be neglected.

#### A.1.3.2 Leakage test for radon

The radon activity concentration in the calibration chamber results from the equilibrium of supply, decay and release of radon. Accidental leakage releases must be negligible. Since they are not quantifiable, they affect the accuracy of calibration measurements. Great importance was attached to radon tightness during the selection of the components and the construction of the facility.

The leakage test for radon was performed by transferring radon from a gas standard into the calibration chamber. After closing the valves at the outlet ports, radon circulated between the chambers. The decrease in radon activity was measured simultaneously with two scintillation cells. The measurements of one of these scintillation cells and the results for both constants of decrease,  $\lambda_{\text{exp},1}$  and  $\lambda_{\text{exp},2}$ , respectively inferred by mathematical regression from each of the series of measurement are presented in Figure A.3. At a statistical level of 95 %, the constants of decrease derived from the measurements do not differ significantly from the value of the nominal radon decay constant authorized by BIPM. It can therefore be concluded that the facility is tight for radon. Possible small losses have no influence on the measurements and can be neglected.

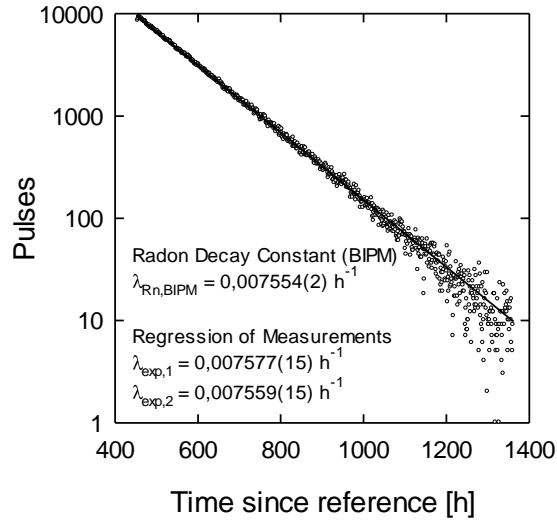


**Figure A.3.** Decrease of radon activity inside the calibration chamber after injection of radon from a gas standard, measured with scintillation cells

#### A.1.4 Mathematical treatment of the two-chamber system

The setting of radon activity concentrations in the 2-chamber calibration device is a time-dependent system which is mathematically treated by a system of two first-order linear differential equations given by

$$\begin{aligned} \frac{dC_{\text{ref}}}{dt} + \left( \lambda + \frac{\phi_i + \phi_a}{V_{\text{ref}}} \right) C_{\text{ref}} - \frac{\phi_i}{V_{\text{ref}}} C_s &= \frac{\varepsilon}{V_{\text{ref}}} \\ \frac{dC_s}{dt} + \left( \lambda + \frac{\phi_i}{V_s} \right) C_s - \frac{\phi_i}{V_s} C_{\text{ref}} &= 0 \end{aligned} \quad (\text{A-1})$$

The radon activity concentrations in the reference chamber and in the secondary chamber are denoted by  $C_{\text{ref}}$  and  $C_s$ , respectively, and accordingly the volumes of the chambers by  $V_{\text{ref}}$  and  $V_s$ . Besides the secondary chamber, the volume  $V_s$  also comprises the additional volumes of the connecting components (pipes, scintillation cells, valves, flanges), and is given by  $V_s = V_{\text{eff}} - V_{\text{ref}}$ . The internal and external flow rate are indicated by  $\phi_i$  and  $\phi_a$ , the radon decay constant by  $\lambda$ , and the radon emanation rate by  $\varepsilon$ .

The first equation of the differential equation system depicts the buildup of radon activity concentration in the reference chamber. Radon is supplied from the emanation source into the reference chamber, expressed by the source term,  $\varepsilon/V_{\text{ref}}$ . Radon loss occurs either by decay, or by transport from the reference chamber into the secondary chamber due to internal circulation, or by release from the reference chamber,  $(\lambda + (\phi_i + \phi_a)/V_{\text{ref}}) \cdot C_{\text{ref}}$ . The internal circulation conveys radon from the secondary chamber back into the reference chamber, represented by  $\phi_i \cdot C_s/V_{\text{ref}}$ . The second equation of the differential equation system depicts the buildup of radon activity concentration in the secondary chamber. The chamber is connected with the reference chamber by two pipes. Due to internal circulation, the radon is supplied through one pipe and led off by the other. The term  $\phi_i \cdot C_{\text{ref}}/V_s$  represents the radon supply, and  $(\lambda + \phi_i/V_s) \cdot C_s$  the radon loss by decay and internal circulation. The secondary chamber does not have radon sources or outlets from which radon can escape from the facility.

Using the substitutions

$$\begin{aligned} w_1 &= \lambda + \frac{\phi_i}{V_s}, & \xi_1 &= \frac{\phi_i}{V_s}, \\ w_2 &= \lambda + \frac{\phi_i + \phi_a}{V_{\text{ref}}}, & \xi_2 &= \frac{\phi_i}{V_{\text{ref}}}, \\ \tilde{\varepsilon} &= \frac{\varepsilon}{V_{\text{ref}}} \end{aligned} \quad (\text{A-2})$$

the solutions of the time dependent activity concentrations in both chambers are given by

$$\begin{aligned} C_{\text{ref}}(t) &= \frac{\tilde{\varepsilon} w_1}{w_1 w_2 - \xi_1 \xi_2} + a_1 e^{b_1 t} + a_2 e^{b_2 t} \\ C_{\text{s}}(t) &= \frac{\tilde{\varepsilon} \xi_1}{w_1 w_2 - \xi_1 \xi_2} + \frac{b_1 + w_2}{\xi_2} a_1 e^{b_1 t} + \frac{b_2 + w_2}{\xi_2} a_2 e^{b_2 t} \end{aligned} \quad (\text{A-3})$$

with the parameters

$$\begin{aligned} b_1 &= -\frac{1}{2}(w_1(1-\varphi) + w_2(1+\varphi)) \\ b_2 &= -\frac{1}{2}(w_1(1+\varphi) + w_2(1-\varphi)) \\ \varphi &= \sqrt{1 + \frac{4\xi_1 \xi_2}{(w_1 - w_2)^2}} \end{aligned} \quad (\text{A-4})$$

and

$$\begin{aligned} a_1 &= C_{\text{ref},0} \left( \frac{\varphi+1}{2\varphi} \right) + C_{\text{s},0} \left( \frac{\xi_2}{\varphi(w_1 - w_2)} \right) \\ &\quad - \frac{\tilde{\varepsilon}}{w_1 w_2 - \xi_1 \xi_2} \left( \frac{\xi_1 \xi_2}{\varphi(w_1 - w_2)} + w_1 \left( \frac{\varphi+1}{2\varphi} \right) \right) \\ a_2 &= C_{\text{ref},0} \left( \frac{\varphi-1}{2\varphi} \right) - C_{\text{s},0} \left( \frac{\xi_2}{\varphi(w_1 - w_2)} \right) \\ &\quad + \frac{\tilde{\varepsilon}}{w_1 w_2 - \xi_1 \xi_2} \left( \frac{\xi_1 \xi_2}{\varphi(w_1 - w_2)} + w_1 \left( \frac{1-\varphi}{2\varphi} \right) \right) \end{aligned} \quad (\text{A-5})$$

The variables  $C_{\text{ref},0}$  and  $C_{\text{s},0}$  denote the initial activity concentrations in the respective chambers at time  $t=0$ . The maximum radon activity concentrations,  $C_{\text{ref,max}}$  and  $C_{\text{s,max}}$ , which occurs in the stationary state, are obtained by

$$\begin{aligned} C_{\text{ref,max}} &= \frac{\varepsilon}{\lambda V_{\text{ref}} + \phi_1} \frac{\lambda(V_{\text{eff}} - V_{\text{ref}}) + \phi_a}{\lambda(V_{\text{eff}} - V_{\text{ref}}) + \phi_1} \\ C_{\text{s,max}} &= \frac{\varepsilon}{\phi_a + \lambda V_{\text{eff}} + \lambda^2(V_{\text{eff}} - V_{\text{ref}})} \frac{V_{\text{ref}}}{\phi_1} \end{aligned} \quad (\text{A-6})$$

The ratio of maxima,

$$\frac{C_{\text{ref,max}}}{C_{\text{s,max}}} = 1 + \frac{V_{\text{s}}}{\phi_1} \lambda, \quad (\text{A-7})$$

indicates that the activity concentration in the reference chamber is always slightly higher than in the secondary chamber. The difference depends on the volume of the secondary chamber and the internal flow rate used for circulation. With applying the standard values ( $V_{\text{s}} = 131$  l,  $\phi_1 = 3$  l/min) used for calibrations, a difference of about 0.5 % between the maximal values of radon activity concentration in both chambers occurs in the stationary state.

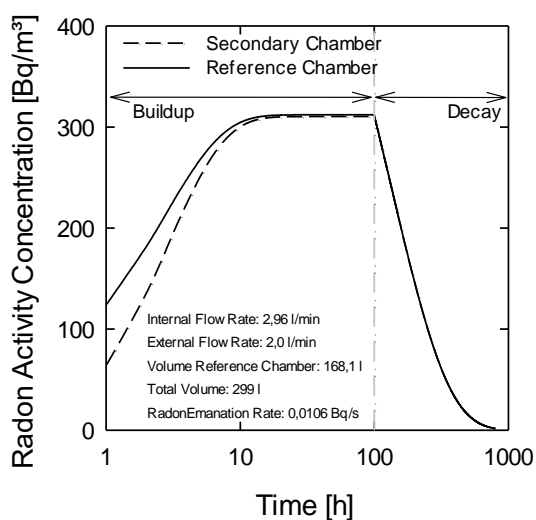


**Figure A4.** Buildup of radon activity concentration in the reference and the secondary chamber due to external radon supply (calculations were performed using standard data for the target activity concentration of about 310 Bq/m<sup>3</sup>); Times greater 100 h: external flow rate and radon supply were stopped, curves show the radioactive decay

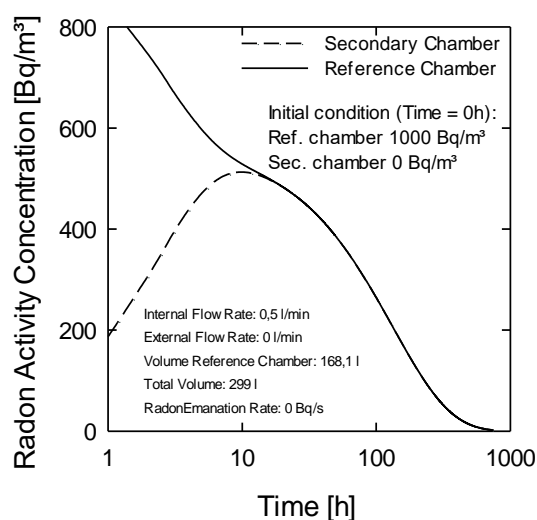


**Figure A5.** Decay and buildup of radon in the 2-chamber system for an initial injection of radon of 1000 Bq/m<sup>3</sup> in the reference chamber, the secondary chamber is radon-free at the beginning (without additional radon supply during the whole time)

**Table A.2.** Input data, traceability and uncertainty

Quantity	Value, observed	Standard uncertainty (k = 1)	Reference/Traceability
Half-life <sup>222</sup> Rn, $T_{1/2} = \ln(2)/\lambda$	3.8232 d	0.0008 d	BIPM
Internal flow rate, $\phi_i$	2.96 l/min	0.06 l/min	RvA <sup>2</sup>
External flow rate, $\phi_a$	(2–6) l/min <sup>1</sup>	0.01 l/min	RvA <sup>2</sup>
Effective volume, $V_{\text{eff}}$ (depending on calibration object, see chapter A.2.2.)	299.0 l	2.5 l	PTB <sup>3</sup>
Reference volume, $V_{\text{ref}}$	168.1 l	0.6 l	PTB
Emanation rate, $\varepsilon$	0.0106 Bq/s	0.0001 Bq/s	CMI

<sup>1</sup>depending on target activity concentration

<sup>2</sup>Dutch Accreditation Council

<sup>3</sup>according to internal calibration procedure for the effective air volume, each influence quantity is traced back to PTB

Figure A.4 represents the buildup of radon activity concentration in the reference and the secondary chamber due to external radon supply. The values used for the calculations are equal to those for standard calibrations. After commencement of radon supply, the activity concentrations rise until a maximum has reached. The activity concentration in the secondary chamber tracks that in the reference chamber. The maximum represents the stationary state in which the radon supply and loss are balanced. It is reached after a time of approx. 10 hours. At a time of 100 hours the external flow rate and radon supply were stopped. The results of the calculations show the radioactive decay in both chambers. Owing to the internal circulation of radon, the radioactive concentrations in both chambers are equivalent during decay.

Figure A.5 shows the calculation results for an initial activity concentration of 1000 Bq/m<sup>3</sup> in the reference chamber. The secondary chamber was radon-free at the beginning. The initial activity concentration decreases due to radioactive decay and the transport of radon into the secondary chamber due to internal circulation. This increases the activity concentration in the secondary chamber over time until the activity concentrations have balanced. The flow rate used for internal circulation is assumed to be 0.5 l/min. The compensation is achieved after a time of approx. 10 hours. Afterwards, the radon activity concentrations in both chambers are equivalent and decrease according to the radioactive decay.

#### **A.1.6 Radon reference atmospheres**

The facility enables the creation of stable and traceable radon reference atmospheres for calibration purposes. Long-term stable activity concentrations are achieved by using an emanation source with a constant emanation rate. The radon activity concentrations obtained in the chambers after buildup are determined by Equations A-6.

Table A.2 summarizes the quantities and their respective uncertainties used for the calculation of the radon activity concentrations according to the Equations A-6. The values of the quantities or their measurements are traced back to recognized authorities or to standards of national metrological bodies.

With applying the Equations A-6, the total uncertainties of the radon activity concentrations were determined by stochastic Monte-Carlo simulation. For the calculation to be carried out, randomly distributed values around the observed value were determined. It has been assumed that each of the distributions is rectangular with a standard uncertainty, as shown in Table A.2. Due to the assumed rectangular distribution, the respective expanded uncertainty used for the simulation is obtained from an increase with factor  $\sqrt{3}$  [4]. The resulting radon activity concentrations are again rectangular distributed with an uncertainty of 1.0 % ( $k = 1$ ). The sensitivity analysis reveals that the predominant contribution to uncertainty is caused by the external flow and the radon emanation rate of the source, while the contribution of all other quantities is marginal.

#### **A.1.7 Conclusions**

The facility, built as part of the EMPIR research project *Metrology for Radon* project, is capable of performing traceable calibrations at a high metrological level. The radon atmospheres are characterized by long-term stability and thus allow longer exposures of calibration objects. The radon activity concentration can be adjusted with uncertainties of about 1.0 % ( $k = 1$ ) in the target range between 100 Bq/m<sup>3</sup> and 300 Bq/m<sup>3</sup>. With the provision of calibrations in the low range of radon activity concentrations, the facility closes the current gap in the traceability and calibration of radon instruments.

By dissemination of the quantity radon activity concentration to external interests, the facility will contribute towards international harmonization and comparability of radon measurements.

## A.2 Calibration procedures in the activity concentration range from 100 Bq/m<sup>3</sup> to 300 Bq/m<sup>3</sup> using <sup>222</sup>Rn emanation standards

### A.2.1 Introduction

The reference facility established under Chapter A.1 is used for the calibration of devices with regard to the radon activity concentration in the range from 100 Bq/m<sup>3</sup> to 300 Bq/m<sup>3</sup>. For this purpose, suitable calibration procedures must be developed to meet the metrological requirements for precision and accuracy. The main focus is on the investigation of statistical fluctuations of the values displayed by the devices to be calibrated and thus the development of the uncertainties for longer exposures at the same activity concentration. These prolonged exposures are achieved by using emanation sources with a time-constant radon emanation rate.

A calibration of an instrument from type AlphaGUARD DF2000 was carried out [5]. This device is usually used as a reference and transfer device for the quantity radon activity concentration. This calibration was exemplarily performed to show the effects of long-term exposures to the uncertainty. Additional corrections were introduced to improve the calibrations of radon instruments. The developed procedures can also be applied analogously to other types of instruments.

### A.2.2 Determination of effective air volume

The insertion of a calibration object into the calibration chamber displaces air, which changes the available air volume in the entire system and thus the radon activity concentration at a certain activity. Therefore, the effective air volume of the entire system must be determined for accurate calibration. The effect of air displacement depends on the volume of the object to be calibrated in relation to the entire volume of the chamber. The determination of the effective air volume that includes the calibration object is carried out by isothermal pressure compensation.

The procedure for the determination is outlined exemplarily in Figure A.6: At the beginning there is a uniform air pressure of 1008 hPa in the entire system. By closing the connecting valves at the reference chamber, the entire volume is separated into two parts. Then the reference chamber is evacuated by the external pump to a final pressure of 793 hPa. By opening the connecting valves, a pressure compensation is carried out up to a final stable air pressure of 887 hPa in the entire system. Under the assumption that the procedure was carried out under isothermal conditions, the effective air volume,  $V_{\text{eff}}$ , in the entire system is calculated by

$$V_{\text{eff}} = \frac{P_0 - P_{\text{ref}}}{P_0 - P_{\text{comp}}} V_{\text{ref}} \quad (\text{A-8})$$

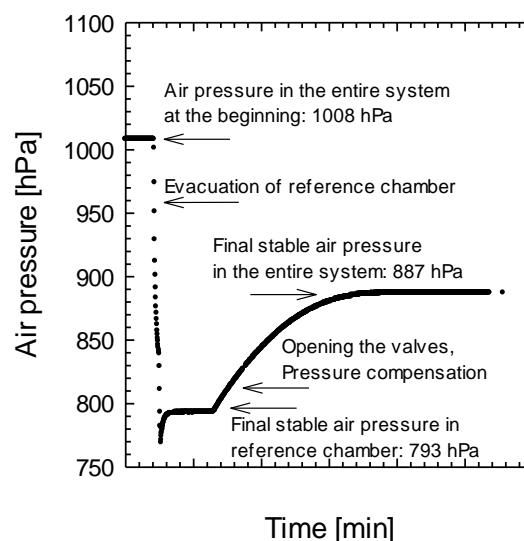


Figure A.6. Example for the determination of effective air volume

**Table A.3.** Determination of the effective air volume  $V_{\text{eff}}$

Determination	Eff. air volume $V_{\text{eff}}$	Standard Uncertainty $\Delta V_{\text{eff}} (K = 1)$
	[dm <sup>3</sup> , liter]	[dm <sup>3</sup> , liter]
1	298.1	2.3
2	297.4	2.5
3	299.7	2.4
4	299.5	2.3
Average	299.0	2.5

The variable  $p_0$  represents the pressure in the entire system at the beginning,  $p_{\text{ref}}$  is the final stable air pressure in the evacuated reference chamber,  $p_{\text{comp}}$  is the air pressure after pressure compensation, and  $V_{\text{ref}}$  is the volume of the reference chamber. The effective air volume used for calibration of the AlphaGUARD is shown in Table A.3. The effective air volume is the mean value derived from 4 determinations.

The uncertainty of the effective air volume was determined by the propagation of uncertainty considering all influencing variables according to Equation A-8. The expanded uncertainty of the effective air volume is 1.7 % ( $k = 2$ ). The estimation of uncertainty could be verified by repeated determination. In addition to the volume of the reference chamber, the measurements of pressure are also traced back by calibration to standards of PTB.

### A.2.3 Background of the calibration object

The background is the datum error for zero value of radon activity concentration. It is determined after replacing the chamber air with aged air. The thus resulting radon concentration in the chamber is considered negligible (zero). It is assumed that the background indications are normally distributed around the average. The data of the background are summarized in Table A.4, and the distribution is shown in Figure A-7.

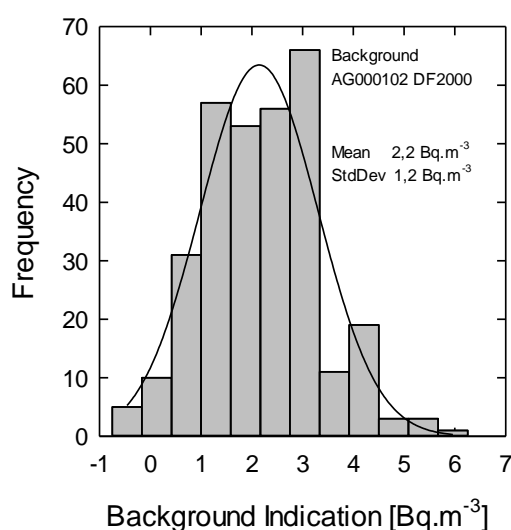


**Figure A.7.** Distribution of the background indications

**Table A.4.** Measurement of background

	Date and time		Exposure [Bq/m <sup>3</sup> ]	Indication of instrument		
	from	to		Average [Bq/m <sup>3</sup> ]	Standard deviation [Bq/m <sup>3</sup> ]	No. of meas.
Background	24.04.2019 07:00	07.05.2019 09:00	0	2.2	1.2	315

### A.2.4 Exposures

The instrument was placed in the secondary chamber of the calibration facility. The power supply and data exchange was carried out from outside via bushings. Driven by an air pump, radon circulated between the primary and secondary chambers, which were connected by pipes. The set-up made it possible to monitor the proper functioning of the instrument and read out the measurement data. The facility has gone through a number of different exposures without requiring access to the instrument or other interruptions.

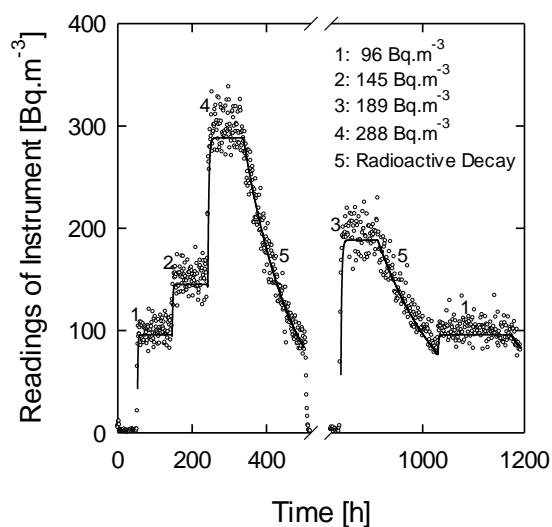


**Figure A.8.** Example for the time course of four different calibration exposures imposed on a customer instrument (AlphaGUARD) in the range between 100 Bq/m<sup>3</sup> to 300 Bq/m<sup>3</sup>; Dots indicate the readings of the instruments, and lines the results of calculation



**Figure A.9.** View of the calibration facility, the calibration object from type AlphaGUARD is placed in the secondary chamber

**Table A.3.** Exposure data and indications of the instrument

No ( <sup>a</sup> )	Date and time		Ref. radon act. conc. $C_{ref,i}$ [Bq/m <sup>3</sup> ]	Indication of instrument			No. of meas. $n_i$	(c) $T_{m,i}$ °C	(c) $rH_{m,i}$ %	(c) $p_{m,i}$ hPa
	from	to		Average ( <sup>b</sup> ) $\bar{R}_{s,i}$ [Bq/m <sup>3</sup> ]	Standard uncertainty [Bq/m <sup>3</sup> ]					
<i>i</i>	1	2	3	4	5	6	7	8	9	10
1.1	05.04.19 10:00	08.04.19 14:00	96	101	9	55	23.7	41	1008	
2	09.04.19 07:00	12.04.19 14:00	145	152	12	80	23.2	32	1018	
3	08.05.19 00:00	10.05.19 12:00	189	199	15	61	23.5	25	996	
4	13.04.19 05:00	16.04.19 14:00	288	299	16	82	22.9	27	1019	
1.2	16.05.19 00:00	21.05.19 10:00	96	102	10	131	23.8	20	1005	

<sup>a</sup> The level of 96 Bq/m<sup>3</sup> was repeated at the end of the course. The first approach is indicated by 1.1, the second by 1.2.

<sup>b</sup> Measurement values corrected for standard room conditions:  $T_s = 20^\circ\text{C}$  and  $p_s = 1013$  hPa.

<sup>c</sup> Average values of temperature, relative humidity and air pressure during measurements. Temperature and air pressure values are provided by laboratory reference instruments, relative humidity values were measured by the calibration object.

Figure A.8 shows the time course of the calibration (Alphaguard). Starting from an atmosphere without radon (measurement of the instrument background), the instrument then passes through various levels of radon activity concentrations (1-4). In addition to the approximation to the set radon values, the figure also shows the decrease in the radon activity concentration due to radioactive decay (5). The time course is interrupted between about 500 and 800 hours to reset the display of the device by exposure in a zero radon atmosphere. Exposures to radon resumed for times greater than 800 hours are used to verify the measurements and to test the repeatability of radon levels. Each of the set radon values was kept constant for about 4 days. The reference radon activity concentrations,  $C_{s,max}$ , at the constant stages were calculated from Equation A-6 using the input data from Table A.2. The data indicated by the instrument are little below the reference radon activity concentrations as ascertained for the facility.

The calibration object from type AlphaGUARD uses an pulse ionization chamber as radiation detector. The ionization produced by alpha particles emitted from radon and radon decay products in the air-filled chamber is proportional to the number of molecules of the air; that is, proportional to the density of the air. The density of atmospheric air depends on its composition, moisture content, temperature and pressure. The air above ground level is uniform in its composition. Ordinary variations in density resulting from change in composition do not affect the ionization produced in air. At standard room conditions, a change in the relative humidity of air from 20 % to 50 % changes the air density of only about 0,3 %. It is therefore assumed that air density changes are due entirely to variations in temperature and pressure [6].

With the measured value,  $R_m$ , of the radon activity concentration read from the instrument, the air density at measurement,  $\rho_m$ , and the corresponding variables for standard conditions,  $R_s$  and  $\rho_s$ , the ratio is

$$\frac{R_m}{R_s} = \frac{\rho_m}{\rho_s} \quad (\text{A-9})$$

With  $p/T \sim \rho$ , the correction for standard room conditions is

$$R_s = \frac{p_s}{p_m} \frac{T_m}{T_s} R_m. \quad (\text{A-10})$$

The temperature is used in the unit Kelvin in Equation A-10.

The average radon activity concentration as indicated by the calibration object from type AlphaGUARD were corrected for room conditions ( $T_s = 293^\circ\text{K}$  ( $20^\circ\text{C}$ ) and  $p_s = 1013$  hPa) using Equation A-10 and the temperatures and air pressures at the measurement from column 8 and 10 of Table A.3. The corrected measurement values are given in column 5 of Table A.3.

### A.2.5 Determination of the calibration factor

The calibration factor was determined from the linear regression between the indications of the instrument versus the reference values of the radon activity concentration, ( $R_{s,i}$ ,  $C_{\text{ref},i}$ ). It is assumed that for each  $C_{\text{ref},i}$  the corresponding values of  $R_{s,i}$  are normally distributed around their mean. In the classic linear model [7], the vector of parameter  $\beta = \begin{pmatrix} \beta_0 \\ \beta_1 \end{pmatrix}$  given by

$$\beta = (\mathbf{X}^T \mathbf{X})^{-1} \mathbf{X}^T \mathbf{y} \quad (\text{A-11})$$

minimizes the least square criteria  $\sum_{i=1}^n (y_i - x_i \beta_1 - \beta_0)^2$ . In Equation A-11, the vector  $\mathbf{y} = \begin{pmatrix} R_{s,1} \\ \vdots \\ R_{s,n} \end{pmatrix}$  and the

design matrix  $\mathbf{X} = \begin{pmatrix} 1 & C_{\text{ref},1} \\ \vdots & \vdots \\ 1 & C_{\text{ref},n} \end{pmatrix}$  are used.

The parameter  $\beta_1$  is interpreted as the calibration factor, which is denoted by  $k_c$  in the following. The parameter  $\beta_0$  is the intersection of the linear function with the  $R_s$ -axis. The linear function resulting from the regression between the indications of the calibration object versus the reference activity concentrations is shown in Figure A.10.

The calibration factor  $k_c = \beta_1$  and the intersection  $\beta_0$  were inferred from Equation A-11 and are given by

$$k_c = \frac{\sum_{i=1}^n (R_{s,i} C_{\text{ref},i}) - n \bar{R}_s \bar{C}_{\text{ref}}}{\sum_{i=1}^n C_{\text{ref},i}^2 - n \bar{C}_{\text{ref}}^2} \quad (\text{A-12})$$

and

$$\beta_0 = \frac{\bar{R}_s \cdot \sum_{i=1}^n C_{\text{ref},i}^2 - \bar{C}_{\text{ref}} \cdot \sum_{i=1}^n (R_{s,i} C_{\text{ref},i})}{\sum_{i=1}^n C_{\text{ref},i}^2 - n \bar{C}_{\text{ref}}^2} \quad (\text{A-13})$$

with  $n$  as the number of indications and the averages

$$\bar{R}_s = \frac{1}{n} \sum_{i=1}^n R_{s,i} \quad \text{and} \quad \bar{C}_{\text{ref}} = \frac{1}{n} \sum_{i=1}^n C_{\text{ref},i}. \quad (\text{A-14})$$

The results of the regression are summarized in Table A.4. The indications  $R_{s,i}$  are corrected for room temperature according to chapter A.2.4. A background subtraction was not performed as this has no influence on the determination of the calibration factor. The intersection with  $R_s$ -axis,  $\beta_0$ , represents a projection of the indication without the presence of radon. The value does not differ significantly from the value determined for the background of the calibration object.

**Table A.4.** Parameters derived from the regression

		Value	Uncertainty, $U(k_c)$ ( $k = 1$ )
Calibration factor	$k_c$	1.028	0.008
Intersection with $R_s$ -axis	$\beta_0$	3.5	1.4
Coefficient of regression <sup>1</sup>		0.974	

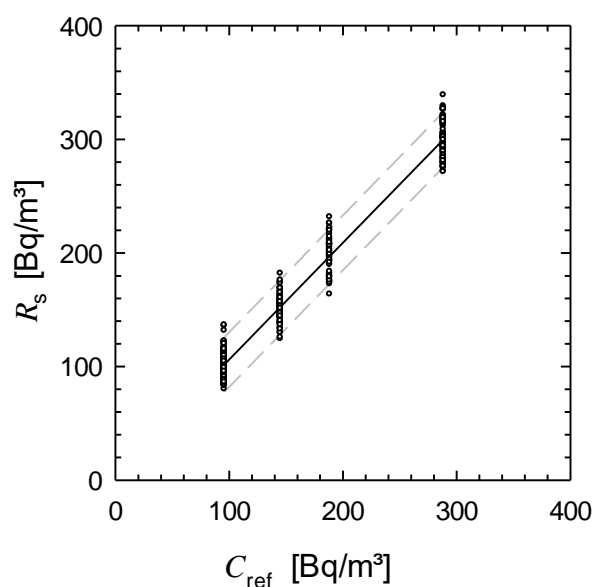


**Figure A.10.** Indications of the calibration object vs. reference activity concentration (dashed lines show the prediction interval)<sup>2</sup>

The calibration factor was determined with a relative standard uncertainty of 0,8 % ( $k = 1$ ). The method applied is in line with the objective of this EMPIR project. The dissemination of the quantity with such low uncertainty will eventually enable operators of calibration facilities to reduce the relative uncertainties with respect to their facilities below 5% ( $k = 1$ ).

#### A.2.6 Uncertainty of the calibration factor

The uncertainty of the calibration factor  $U(k_c)$  was calculated by

<sup>1</sup> The coefficient of regression is given for information only. For calculation it is referred to literature.

<sup>2</sup> The prediction interval is outlined for information only. For calculation it is referred to literature.

$$U(k_c) = \sqrt{\frac{\sum_{i=1}^n (R_{s,i} - \bar{R}_s - k_c (C_{ref,i} - \bar{C}_{ref}))^2}{(n-2) \left( \sum_{i=1}^n C_{ref,i}^2 - n \bar{C}_{ref}^2 \right)}} \quad (\text{A-15})$$

taking into account  $n-2$  degrees of freedom.

The contribution of the reference radon activity concentration,  $C_{ref}$ , to the uncertainty is low compared to the variations of the instrument indications,  $R_s$ . It is assumed that the uncertainties of  $C_{ref}$  are already contained in the variations of  $R_s$  and an explicit consideration of these is not necessary. This assumption is justified by the Berkson Model [8], as for each measurement the corresponding value of  $C_{ref}$  is set at an assigned value calculated from Equation A-6. The reference radon activity concentration,  $C_{ref}$ , is thus a controlled quantity with a well-known nominal value. The actual value of  $C_{ref}$  might deviate from the nominal value due to statistical variations in the adjustments, the influences of temperature, air pressure etc. However, the contribution to the uncertainty from these variations is statistically independent of  $C_{ref}$ , since the causes for the variations occur independent from the nominal value  $C_{ref}$ . The scatter around the fitted straight line provides a measure for the variance of  $R_s$  and  $C_{ref}$ , rather than for  $R_s$  alone. From the Berkson Model thus it follows that the uncertainty in the response of  $R_s$  is composed by two parts: the uncertainty of measurement and an uncertainty induced in  $R_s$  as a result of the failure of the actual value of  $C_{ref}$  to be identical with its nominal value.

In opposite to the Berkson Model, the classical approach should be applied if  $C_{ref}$  is determined by a direct measurement with uncertainties. Then the assumption of the statistical independency of  $C_{ref}$  from the uncertainties is no longer valid.

### A.2.7 Uncertainty caused by statistical fluctuations of the measurement value

The measurement of the quantity radon activity concentration is based on the registration of the radioactive decay in a confined volume. The instrument from type AlphaGUARD uses a pulse ionization chamber with a volume of 0.62 liters as the measurement unit [9]. It registers the ionizations of air caused by alpha particles emitted from radon and its short-lived radon decay products.

In an atmosphere with a radon activity concentration of 100 Bq/m<sup>3</sup>, the radon-222 nuclides emit 100 alpha particles per second in a cubic meter. When radon-222 is in equilibrium with its short-lived decay products, each of the alpha-emitting decay products <sup>218</sup>Po and <sup>214</sup>Po releases the same rate of alpha particles. Under this assumption, a total of 300 alpha particles per second are released in one cubic meter. If the same considerations are applied to the pulse ionization chamber of the AlphaGUARD with a volume of 0.62 liters, only about 11.2 events are caused by alpha particles in one minute. The assumption of equilibrium between Rn-222 and its decay products is not completely fulfilled even in the pulsed ionization chamber, because deposits of decay products occur on walls and surfaces, which lead to emissions of alpha particles that do not or not fully contribute to the ionization of the air. Other causes such as the recombination of ionized air particles, inhomogeneities of the electric field in the ionization chamber and other physical and electrical effects also influence the measuring sensitivity. For this reason, the counts recorded by the instrument in the time interval under consideration are below the total number of all alpha particles released in the volume of the ionization chamber. The manufacturer specifies a sensitivity of the AlphaGUARD of 5 counts per minute at a radon activity concentration of 100 Bq/m<sup>3</sup> [9]. This is about 45% of all alpha particles that are theoretically released in the volume of the pulse ionization chamber.

The radon activity concentration,  $C_m$ , taken from a measurement using an instrument from type AlphaGUARD is calculated by

$$C_m = k_c f (R_m - R_0), \quad (\text{A-16})$$

where  $k_c$  denotes the calibration factor,  $R_m$  the radon activity concentration as indicated by the instrument, and  $R_0$  the instrument's background. The factor  $f$  represents an optional correction for environmental conditions, e.g. for temperature and air pressure in relation to standard room conditions. The manufacturer of

the device provides little information on signal processing, except for the sensitivity,  $s$ , which is given in counts per time interval per radon activity concentration.

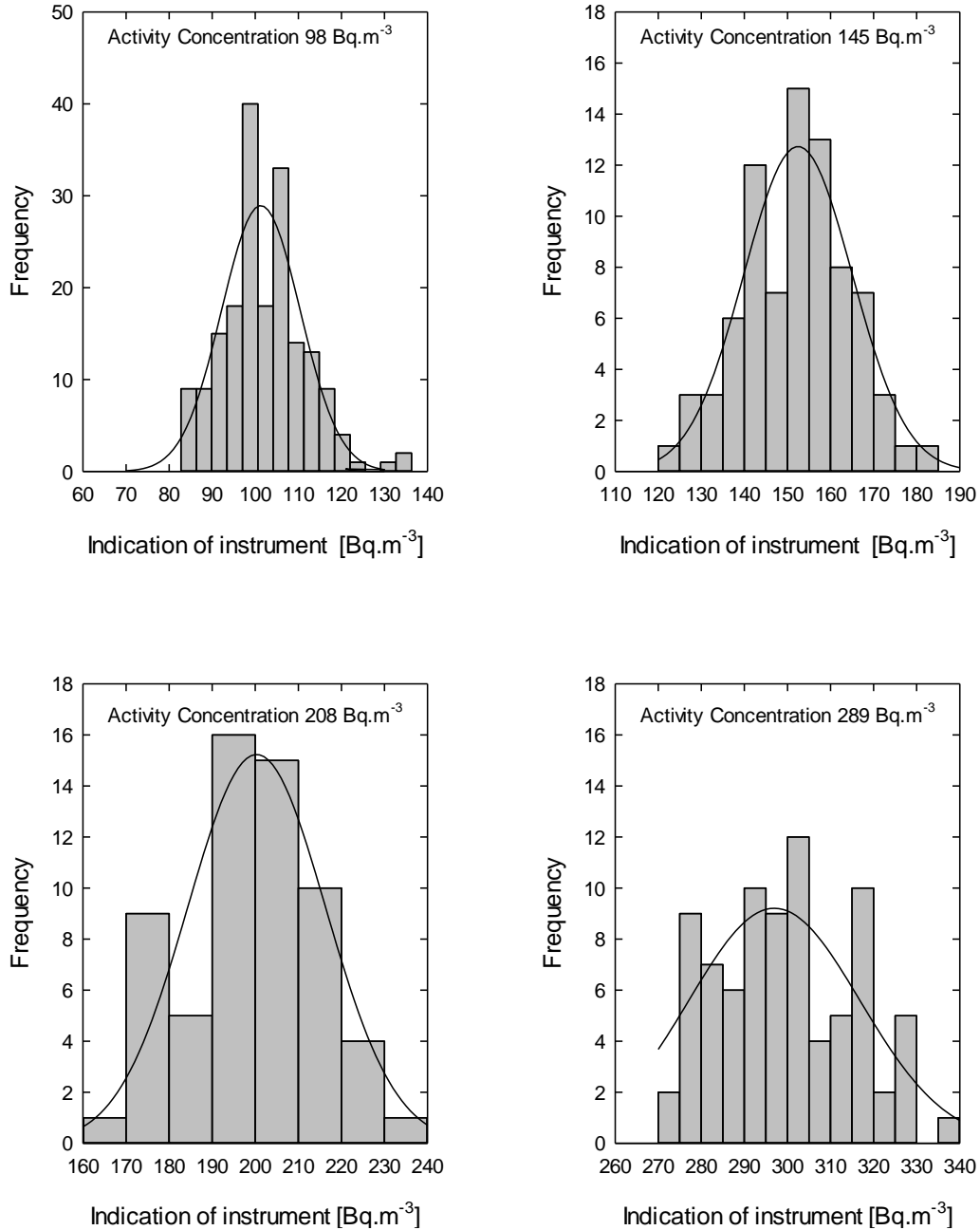


**Figure A.11.** Frequency distribution of measurements taken with an AlphaGUARD for different radon activity concentrations in the range between 100 Bq/m<sup>3</sup> and 300 Bq/m<sup>3</sup>

In a calibration scenario, the calibration factor,  $k_c$ , is determined from the ratio of the known reference activity concentration,  $C_{ref}$ , to the indication of the instrument, including the necessary corrections,

$$k_c = \frac{C_{ref}}{f(R_m - R_0)}. \quad (A-17)$$

The indication,  $R_m$ , can also be written as

$$R_m = \frac{\dot{I}_m}{s} = \frac{P_m}{st}, \quad \text{A-18)}$$

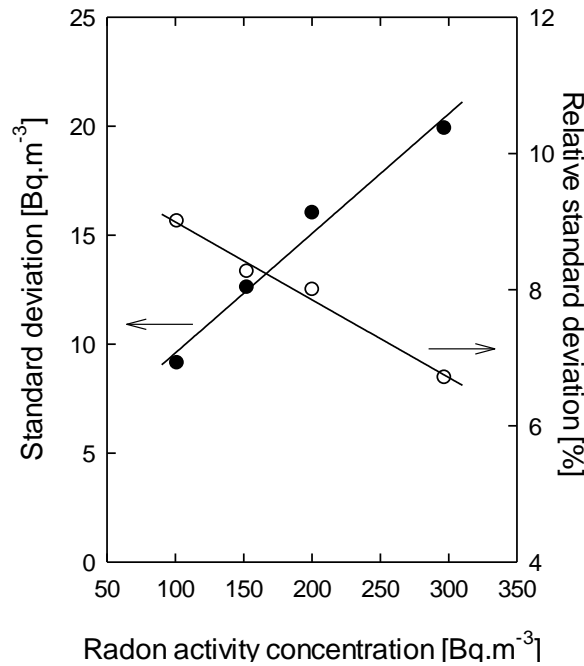


**Figure A.12.** Standard deviation and relative standard deviation of the distribution of measurements taken with an AlphaGUARD for different radon activity concentrations in the range between 100 Bq/m<sup>3</sup> and 300 Bq/m<sup>3</sup>, compiled from the results represented in Figure A.11

where  $\dot{I}_m$  denotes the intrinsic pulse rate measured by the instrument given by  $\dot{I}_m = P_m/t$  with  $P_m$  as the number of pulses registered in the time interval  $t$ . An analogous equation can be written for the background, by inserting the respective values for the background:  $R_0, \dot{I}_0, P_0$ . Assuming that the registered intrinsic pulses are Poisson distributed, the uncertainty of the number of pulses is  $\Delta P_m = \sqrt{P_m}$  or  $\Delta P_0 = \sqrt{P_0}$ .

Taking into account these considerations, the relative standard uncertainty of the calibration factor is inferred from Equation A-17 with [10]

$$\frac{\Delta k_c}{k_c} = \sqrt{\left(\frac{\Delta C_{\text{ref}}}{C_{\text{ref}}}\right)^2 + \left(\frac{\Delta f}{f}\right)^2 + \frac{1}{st} \cdot \frac{k_c f}{C_{\text{ref}}} \left(1 + 2R_0 \frac{k_c f}{C_{\text{ref}}}\right)}. \quad \text{(A-19)}$$

Unlike Equation A-15, which represents the uncertainty as derived from linear regression analysis at different reference activity concentrations, Equation A-19 is the uncertainty from a single determination using error propagation. The main contribution to the relative standard uncertainty results from the third term under the root, which quantifies the contribution by statistical fluctuations of the measurement values. From this term, the calibration conditions for limiting the uncertainties due to statistical fluctuations can be derived:

1. The relative uncertainty of the calibration factor is proportional to  $\sim 1/\sqrt{t}$ .

The greater the time interval of exposure, the smaller the uncertainty. An extension of the exposure time has a greater influence on the uncertainty for short periods. The longer the exposure time is already, the smaller is the influence of a further extension. The extension of the exposure time can be seen as an increase in sensitivity.

2. Calibrations shall be performed at sufficiently high radon activity concentrations to minimize the influence of the background,  $C_{\text{ref}} \gg k_c f R_0$ .

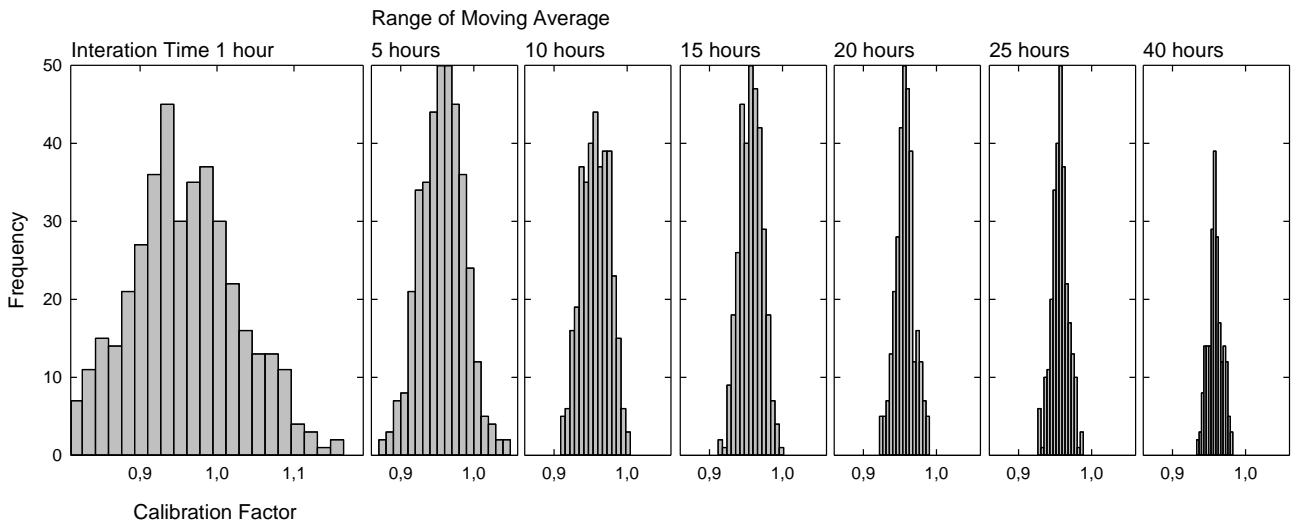


**Figure A.13.** Distributions of the calibration factor determined from measurements taken with an AlphaGUARD due to the extension of the time interval (integration time) of the exposure in a reference atmosphere (simulated by a moving average)

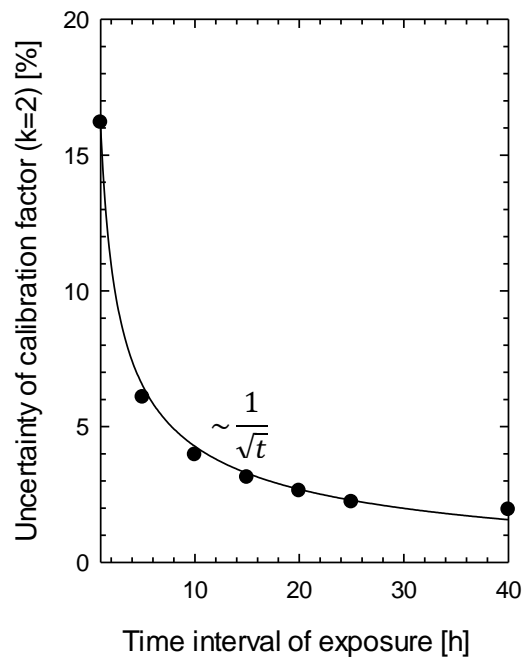


**Figure A.14.** Uncertainties of the calibration factor determined from the standard deviations of the distributions shown in Figure A.13.

3. The relative uncertainty of the calibration factor is proportional to  $\sim \frac{1}{\sqrt{C_{\text{ref}}}}$ .

It follows that the greater the reference activity concentration, the smaller the uncertainty. The influence on the uncertainty by further increase is the smaller, the higher the activity concentration is.

The fluctuations in the indication of the instrument are shown in the figures. The frequency distributions of measurements taken with an AlphaGUARD for different radon activity concentrations in the range between 100 Bq/m<sup>3</sup> and 300 Bq/m<sup>3</sup> are presented in Figure A.11. The measurements were taken for a time interval of  $t = 1$  hour. The results are distributed around the mean value and can be well approximated by Gaussian

distributions. The development of the standard deviation and the relative standard deviation of these Gaussian distributions are shown in Figure A.12. Although the standard deviations increase for increasing the radon activity concentration, the relative standard deviations decrease. The relative standard deviation of the measurements is about 9% for a radon activity concentration of about 100 Bq/m<sup>3</sup>; for a 300 Bq/m<sup>3</sup> it is reduced to 6,5%.

Figure A.13 shows the distribution of the calibration factor according to its determination from the measurements. The distributions are given for different time intervals of the exposure. The time intervals range from 1 hour to 40 hours. The distributions for time intervals greater than 1 hour represent the dispersion of the moving average calculated for the respective time interval. The dispersions can be well approximated by Gaussian distributions. It is shown that the standard deviations are reduced for longer time intervals of exposure. The uncertainties represented by the standard deviations of the calibration factors are summarized for the different time intervals in Figure A.14. The decrease in uncertainty is inversely proportional to the square root of the time interval  $t$ , thus fulfilling the theoretically predicted correlation according to Equation A-19.

### A.2.8 Conclusions

New calibration procedures in the range of radon activity concentrations between 100 Bq/m<sup>3</sup> and 300 Bq/m<sup>3</sup> were developed on the basis of a calibration exemplarily carried out for an instrument from type AlphaGUARD DF2000. The instrument was exposed in atmospheres with long-term constant radon activity concentrations provided by a radon-222 emanation source. Corrections for the effective volume in the atmosphere as well as corrections of the measurements for standard room conditions, and a method for the precise determination of the instruments background were implemented.

The calibration factor for the instrument was inferred from the linear regression of the instrument's indication versus the respective reference radon activity concentrations established in the atmosphere. The calibration factor was determined with a relative uncertainty of 0.8% ( $k = 1$ ). This uncertainty fulfills the target relative uncertainty for calibrations at low activity concentrations of  $\leq 5\%$  ( $k = 1$ ), and is the basis for the dissemination of the quantity to other reference laboratories in Europe.

The study examined in detail the statistical fluctuations of the measurements, which predominantly contribute to the uncertainty at low activity concentrations. The effects of extending the time interval of exposure and increasing the reference activity concentration on the uncertainty of the resulting calibration factor could be investigated. The results show that there are limitations with regard to minimizing the uncertainty. For example, the extension of the time interval of exposure is limited for practical reasons and because of the increasingly smaller impact on the uncertainty. Besides increased exposure times, the uncertainty can also be reduced by calibrations in atmospheres with higher radon activity concentrations. The lowest activity concentration for the calibrations carried out in this study was about 100 Bq/m<sup>3</sup>. A further reduction of the reference activity concentration is limited due to the increasing contribution of the instrument background to uncertainty.

The study provides practical advice and recommendations on how to optimise calibration procedures in order to obtain accurate and consistent results of radon measurements and thus build confidence in radiation protection measures.

## A.3 References

- [1] BIPM key comparison database, <https://www.bipm.org/>
- [2] Czech Metrology Institute, Radionuclide calibration standards 2017, <http://www.eurostandard.cz/Euro-standard-catalog-2011.pdf>
- [3] Czech Metrology Institute, Certificate of the measurement standard of activity, Certificate No. 1035-SE-40254-18
- [4] BIPM, JCGM 101, 2008

- [5] Bundesamt für Strahlenschutz: Calibration Certificate: Calibration of a reference instrument in the framework of the EMPIR research project Metrology for Radon. R-19-02, Berlin 2019
- [6] Taylor, L.S., Singer, G.: Air density corrections for X-ray ionization chambers. [https://nvlpubs.nist.gov/nistpubs/jres/8/jresv8n3p385\\_a2b.pdf](https://nvlpubs.nist.gov/nistpubs/jres/8/jresv8n3p385_a2b.pdf)
- [7] Fahrmeir, L., Kneib, T., Lang, S.: Regression. Modelle, Methoden und Anwendungen. Springer-Verlag, Berlin, Heidelberg 2009
- [8] Hartung, J.: Statistik. Lehr-und Handbuch der angewandten Statistik. München, Wien, Oldenburg 1986
- [9] [www.bertin-instruments.com/product/radon-professional-monitoring/radon-alphaguard/](http://www.bertin-instruments.com/product/radon-professional-monitoring/radon-alphaguard/)
- [10] ISO 11929:2010, Determination of characteristic limits (detection threshold, detection limit and limits of the confidence interval) for measurements of ionizing radiation – Fundamentals and application

## B. Activity Report of the Eidgenössisches Institut für Metrologie (METAS)

### B.1 Representation of the quantity radon activity concentration for accurate calibrations of radon instruments

#### B.1.1 Introduction

The Swiss radon reference test site was established at the Federal Institute of Metrology (METAS). It is designed for the calibration of instruments measuring the radon isotope  $^{222}\text{Rn}$  in air. The upgrade for measuring  $^{220}\text{Rn}$  (thoron) will be the subject of future developments.

#### B.1.2 Equipment and components

The basic component is a cylindrical vacuum chamber made of stainless steel. The chamber has a reference volume of  $0.13\text{ m}^3$  (130 litres) with an uncertainty of 1 % ( $k = 1$ ). The volume is traced back by calibration to a standard volume provided by METAS, Switzerland.

Four ISO-K DN63 we equipped with connectors and valves for gas inlet and outlet. A combined sensor is installed inside the chamber for monitoring temperature, pressure and humidity. The radon activity concentration can be measured with one diffusion scintillation cell (Lucas cell) inside the chamber. Inside the chamber a 60 mm ventilator is installed to distribute the radon activity, and to homogenize the atmosphere. Furthermore, the chamber is equipped with different electrical connection lines to power supply and read-out measurement instruments inside. Therefore three ISO-K DN160 flanges are welded on the chamber wall.

The standard operating ranges of pressure and temperature is depending on environmental conditions of the laboratory. Therefore the air pressure is  $950 \pm 20\text{ mbar}$  and the temperature  $22 \pm 2\text{ }^\circ\text{C}$ . The chamber is vacuum-tight to 0.01 mbar and pressure-tight to 2000 mbar.

A block diagram of the test site is given in Figure B.1.

#### METAS $^{222}\text{Rn}$ test site

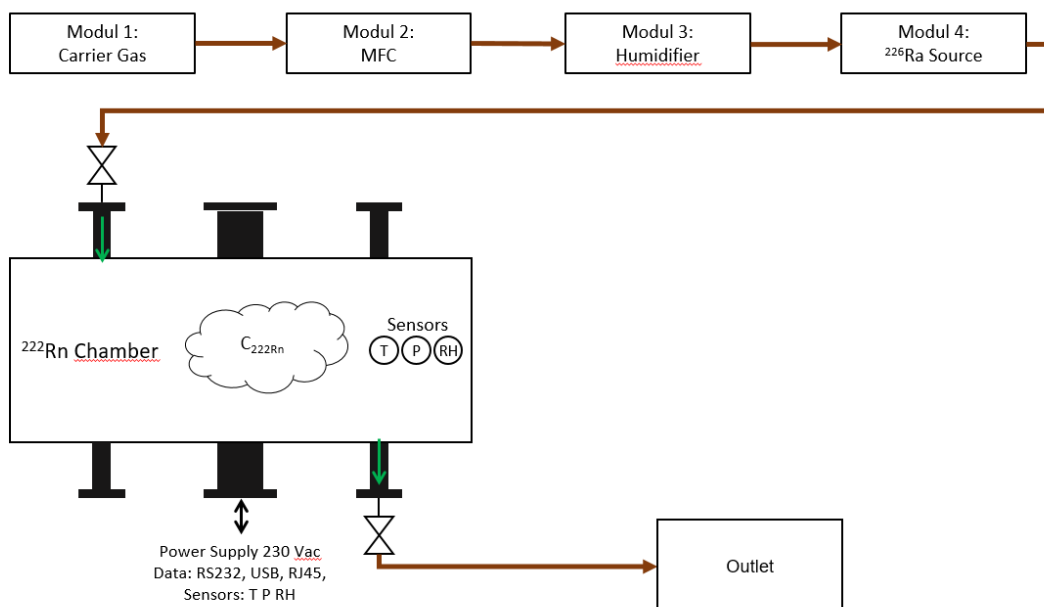


Figure B.1. Block diagram test site

### B.1.3 Equipment and components

The isotope  $^{222}\text{Rn}$  is generated by the decay of  $^{226}\text{Ra}$ . For producing a  $^{222}\text{Rn}$  atmosphere inside the chamber a  $^{222}\text{Rn}$  emanation source based on  $^{226}\text{Ra}$  salt is used. METAS did use two different  $^{222}\text{Rn}$  emanation sources provided by EUROSTANDARD CZ and certificated by Czech Metrological Institute (CMI) to create a defined  $^{222}\text{Rn}$  atmosphere inside the chamber. Table B.1 summarized the specifications of the emanation sources of the test site.

**Table B.1.** Specifications  $^{222}\text{Rn}$  sources

Parameter		RF20 source	RF200 source
$^{226}\text{Ra}$ activity	$A_0$	20.80 kBq	199.9 kBq
$^{222}\text{Rn}$ emanation power	$\chi$	0.995	0.998
Temperature range	T	0 ... 40 °C	0 ... 40 °C
Humidity range	rH	0 ... 100 %	0 ... 100 %

The  $^{222}\text{Rn}$  emanation source is operated in flow-through mode. A continuous air flow rate through the  $^{222}\text{Rn}$  source takes up the emanated  $^{222}\text{Rn}$  gas inside the source and transport it into the volume of the chamber. The final  $^{222}\text{Rn}$  activity concentration generated inside the chamber volume depends mainly on the air flow rate through the  $^{222}\text{Rn}$  source. The test site is equipped with two calibrated mass-flow-controllers (MFC) to ensure a constant, adjustable, air flow rate through the  $^{222}\text{Rn}$  source and the connected chamber volume of the test site. The excess gas of the chamber is piped outside the laboratory.

As carrier gas, compressed air in bottles is used. To ensure that the carrier gas has a very low  $^{222}\text{Rn}$  concentration, the bottles are stored for a few weeks after delivery.

### B.1.4 Mathematical treatment of a one-chamber system

The final  $^{222}\text{Rn}$  activity concentrations inside the chamber is time-dependent and mathematically describable by following equation:

$$C_{\text{Rn-222}} = C_0 + \frac{E}{\lambda_{\text{Rn-222}} \cdot V + Q_V}$$

With:

- (1)  $E = A_{\text{Ra-226}} \cdot \lambda_{\text{Rn-222}} \cdot \chi$   $^{222}\text{Rn}$  Emanation rate [Bq/s], with:
- (1.1)  $A_{\text{Ra-226}} = A_{0 \text{ Ra-226}} \cdot k_D$   $^{226}\text{Ra}$  Activity [Bq] of the source at time t, with:
- (1.1.1)  $A_{0 \text{ Ra-226}}$   $^{226}\text{Ra}$  Reference Activity [Bq] of the source at reference date  $t_0$  (given by the certificate of the source)
- (1.1.2)  $k_D = e^{\left(\frac{\ln(2)}{T_{1/2 \text{ Ra-226}}}(t-t_0)\right)}$  Decay factor [1]  $^{226}\text{Ra}$  Activity of the Source at time t
- (1.1.2.1)  $T_{1/2 \text{ Ra-226}}$   $^{226}\text{Ra-226}$  Half-live time [d] (BIPM:  $584388 \pm 2557$  d)
- (1.1.2.2)  $t$  Date / Time of measurement
- (1.1.2.3)  $t_0$  Reference Date / Time of the Activity  $A_{0 \text{ Ra-226}}$  of the source
- (1.2)  $\lambda_{\text{Rn-222}} = \frac{\ln(2)}{T_{1/2 \text{ Rn-222}}}$   $^{222}\text{Rn}$  decay constantant [1/s]
- (1.2.1)  $T_{1/2 \text{ Rn-222}}$   $^{222}\text{Rn}$  Half-live time [d] (BIPM  $3.8232 \pm 0.0008$  d)
- (1.3)  $\chi$  Emanation power / coefficient [1] of the source (given by the certificate of the source)
- (3)  $C_0$   $^{222}\text{Rn}$  concentration of carrier gas [Bq]
- (4)  $V$  Volume [ $\text{m}^3$ ] of the chamber
- (4)  $Q_V = Q_{n,c} \cdot k_{PT}$  Flow rate of the MFC at environmental condition
- (4.1)  $Q_{n,c} = Q_n \cdot k_Q$  Calibrated flow rate of the MFC
- (4.1.1)  $Q_n$  Flow rate of the MFC [Ln/min]
- (4.1.2)  $k_Q = \frac{1}{1+\Delta_{r,q}}$  Correction factor of the MFC flow rate
- (4.1.2.1)  $\Delta_{r,q}$  Relative flow rate deviation of the calibrated MFC

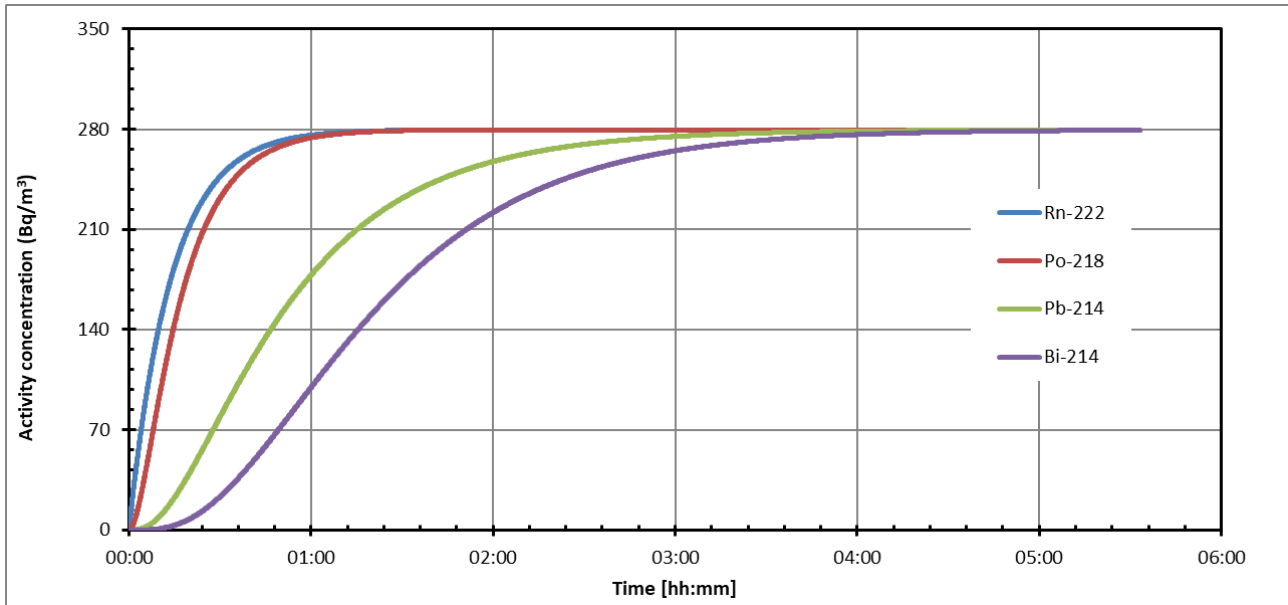


Figure B.2. Calculated build-up of  $^{222}\text{Rn}$  activity concentration and its decay products ( $^{218}\text{Po}$ ,  $^{214}\text{Pb}$ ,  $^{214}\text{Bi}$ ) inside the chamber

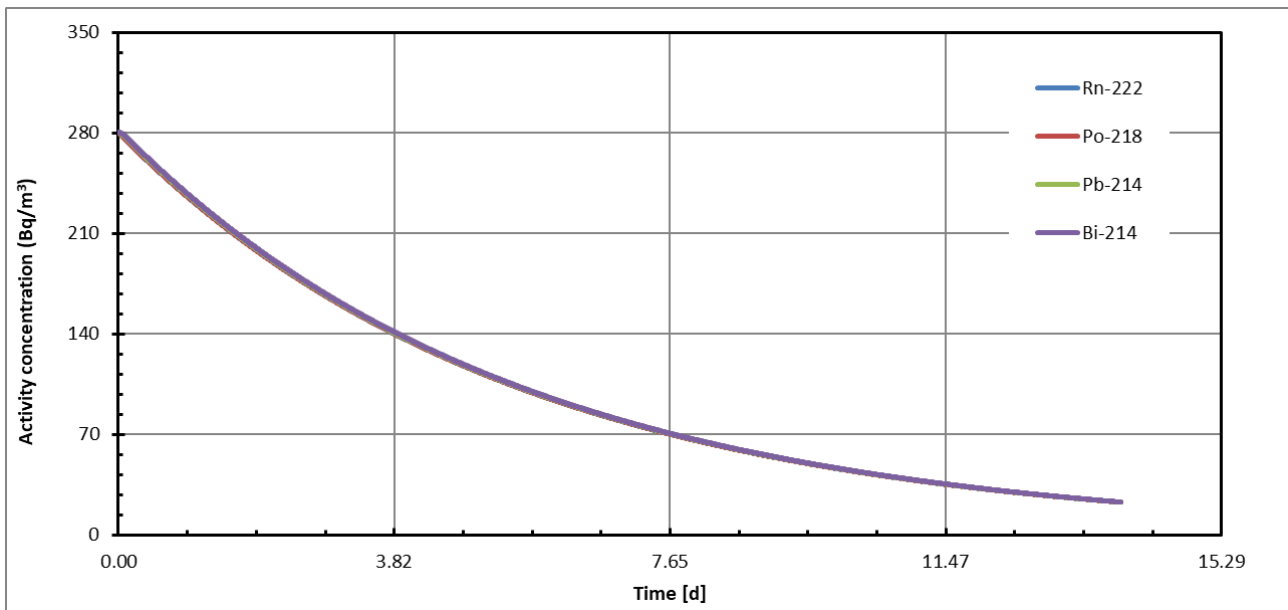


Figure B.3. Calculated decay of  $^{222}\text{Rn}$  activity concentration and its decay products ( $^{218}\text{Po}$ ,  $^{214}\text{Pb}$ ,  $^{214}\text{Bi}$ ) inside the chamber

(4.2)	$k_{PT} = \frac{p_0}{p_c} \cdot \frac{T_c + T_0}{T_0}$	Correction factor for pressure-temperature of the flow rate
(4.2.1)	$p_0 = 1013.25 \text{ hPa}$	Standard pressure according DIN 1343
	$T_0 = 273.15 \text{ K}$	Standard temperature according DIN 1343
	$p_c = p \cdot k_p + k_{offset}$	Corrected pressure
	$T_c = T \cdot k_T + T_{offset}$	Corrected temperature

Figure B.2 shows the calculated build-up of  $^{222}\text{Rn}$  activity concentration inside the chamber, including the build-up of the decay products  $^{218}\text{Po}$ ,  $^{214}\text{Pb}$  and  $^{214}\text{Bi}$ , due to an external  $^{222}\text{Rn}$  supply by a flow-through source. The target activity concentration of  $^{222}\text{Rn}$  is  $280 \text{ Bq/m}^3$ . The stabilisation time  $T_{99\%}$  of  $^{222}\text{Rn}$  concentration is reached after 1 h 4 min, the secular equilibrium is reached after 4 h 8 min.

Figure B.3 shows the calculation results according a radioactive decay for an initial activity concentration of 280 Bq/m<sup>3</sup> inside the chamber.

### B.1.5 Uncertainty calculations

Based on the equation:

$$C_{Rn-222} = C_0 \cdot \frac{E}{\lambda_{Rn-222} \cdot V + Q_V} = C_0 \cdot \frac{A_{0\ Ra-226} \cdot k_D \cdot \lambda_{Rn-222} \cdot \chi}{\lambda_{Rn-222} \cdot V + Q_V}$$

with  $C_0 = 0$ , the combined uncertainty becomes:

$$(U1) \quad u(C_{Rn-222}) = \sqrt{\left(\frac{\partial C}{\partial A}\right) \cdot u^2(A) + \left(\frac{\partial C}{\partial k}\right) \cdot u^2(k) + \left(\frac{\partial C}{\partial \lambda}\right) \cdot u^2(\lambda) + \left(\frac{\partial C}{\partial \chi}\right) \cdot u^2(\chi) + \left(\frac{\partial C}{\partial V}\right) \cdot u^2(V) + \left(\frac{\partial C}{\partial Q}\right) \cdot u^2(Q)}.$$

**Table B.2.** Input data and uncertainty

Uncertainty	Abs. uncertainty (k=1)	Rel. uncertainty (k=1)	Reference
$u(A_{0\ Ra-226})$	RF20: 0.31 kBq RF200: 3.0 kBq	RF20: 1.49 % RF200: 1.50 %	Certificate <sup>222</sup> Rn source
$u(\chi)$	RF20: 0.015 RF200: 0.015	RF20: 1.51% RF200: 1.50%	Certificate <sup>222</sup> Rn source
$u(Q_n)$	Depending on flow	0.1%	Certificate calibration MFC
$u(p)$	0.1 hPa	0.01%	Certificate calibration pressure meter
$u(T)$	0.05 °C	0.02%	Certificate calibration temperature meter
$u(T_{1/2\ Ra-226})$	2557 d	0.44%	Monographie BIPM-5, Vol 2
$u(T_{1/2\ Rn-222})$	0.0008 d	0.02%	Monographie BIPM-5, Vol 4
$u(V)$	1.3 l	1.0%	Certificate calibration chamber volume

Table B.2 summarizes the quantities and their uncertainties used for the calculation of the radon activity concentrations.

For the METAS <sup>222</sup>Rn test site the relative uncertainty for the <sup>222</sup>Rn activity concentration is  $u_r(C_{Rn-222}) = 1.52\%$  (k=1). The predominant contribution to uncertainty is caused by the emanation power of the <sup>222</sup>Rn source. The impact of all other quantities is marginal.

### B.1.6 Conclusion

The Swiss radon reference test site is built-on and operable at METAS. The calculation results for the activity concentration are comparable with the measurement results. An estimation for the combined uncertainty were done, the result of the uncertainty is within the project goals.

## B.2 Calibration procedures in the activity concentration of 300 Bq/m<sup>3</sup> using <sup>222</sup>Rn emanation standards

### B.2.1 Introduction

With the actual METAS <sup>222</sup>Rn test site an activity concentration in the range of 270 Bq/m<sup>3</sup> until 150 KBq/m<sup>3</sup> can be achieved.

### B.2.2 Background of the calibration

After flushing the chamber with ten times the volume of aged air, the resulting <sup>222</sup>Rn activity concentration inside the chamber is nearly zero. The data of background measurements inside the METAS <sup>222</sup>Rn test site is shown in Table B.3. In 07/2018 as well as 01/2020 the whole ionisation chamber inside the <sup>222</sup>Rn measurement instrument AlphaGuard PQ2000 Pro, S/N EF2142, was replaced due to high contamination of <sup>222</sup>Rn decay products. The distribution of background measurement BGR-2020-01 is shown in Figure B.4.

**Table B.3.** Background measurement with AlphaGuard PQ2000 Pro, S/N EF2142

Measurement	Start date time	End date time	C <sub>Average</sub> [Bq/m <sup>3</sup> ]	Std. dev. [Bq/m <sup>3</sup> ]	No. of measurement points (Δt = 10 min)
BGR-2020-01	13.02.2020 08:00	14.02.2020 14:30	3.75*	3.41	184
BGR-2019-02	17.09.2019 20:30	18.09.2019 00:20	6.4	4.5	24
BGR-2019-01	14.05.2019 12:30	14.05.2019 16:20	9.6	4.6	24
BGR-2018-02	19.11.2018 19:30	20.11.2018 17:40	8.2	4.6	133
BGR-2018-01	18.07.2018 18:50	20.07.2018 18:10	1.8*	2.37	284

\*New ionization chamber

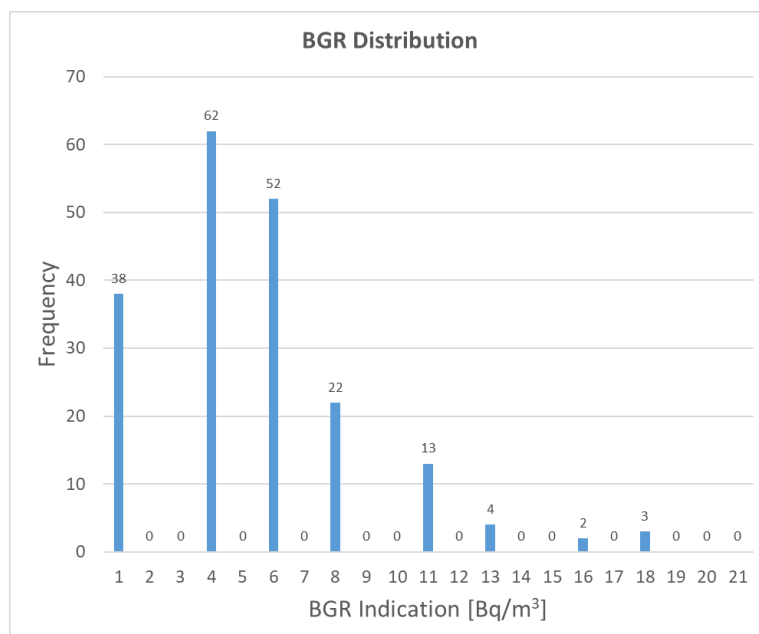


**Figure B.1.** Distribution of Background indications.

### B.2.3 Exposures

The  $^{222}\text{Rn}$  measurement instrument AlphaGuard PQ2000 Pro, S/N EF2142, was placed inside the chamber. After a background measurement the test site was set to a  $^{222}\text{Rn}$  activity concentration of  $303.4 \text{ Bq/m}^3$ . After a stabilisation time of 4 h, due to reach the secular equilibrium of  $^{222}\text{Rn}$  and his daughter products, a weighting interval of 4 h at  $303.4 \text{ Bq/m}^3$  was performed for ten times. Figure B.5 is showing the performed exposure in general and Table B.4 shows the single results for ten different measurements. The combined uncertainty of the reference concentration can give with  $u_r(C_{\text{Ref}}) = 1.5\%$  ( $k = 1$ ) and for the measured concentration with  $u_r(C_{\text{meas}}) = 2.8\%$  ( $k = 1$ ).

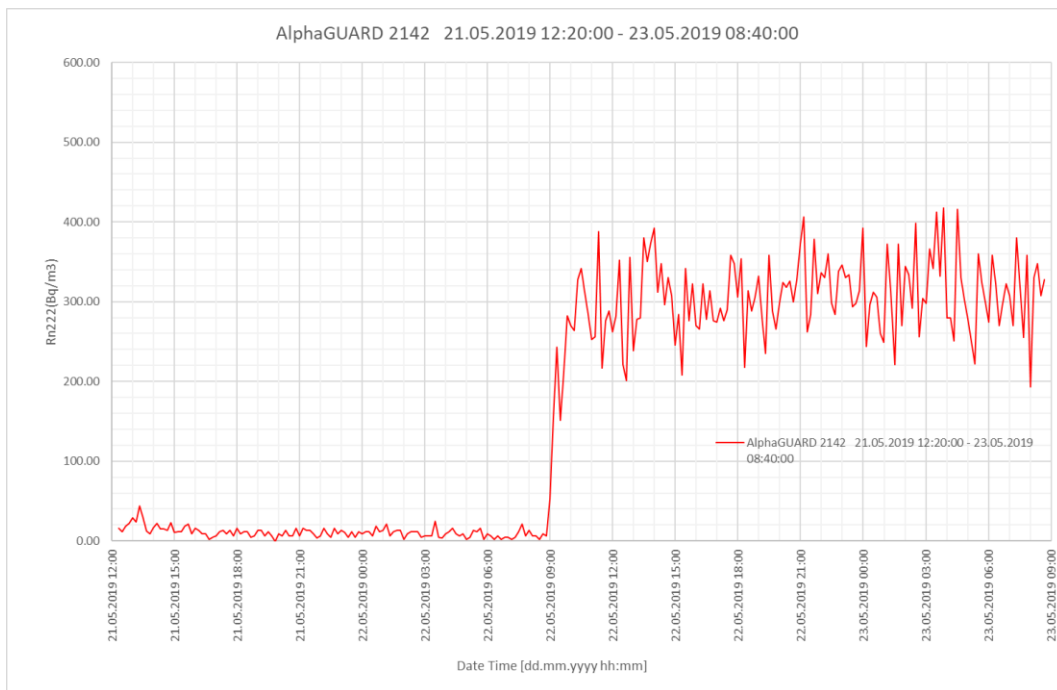
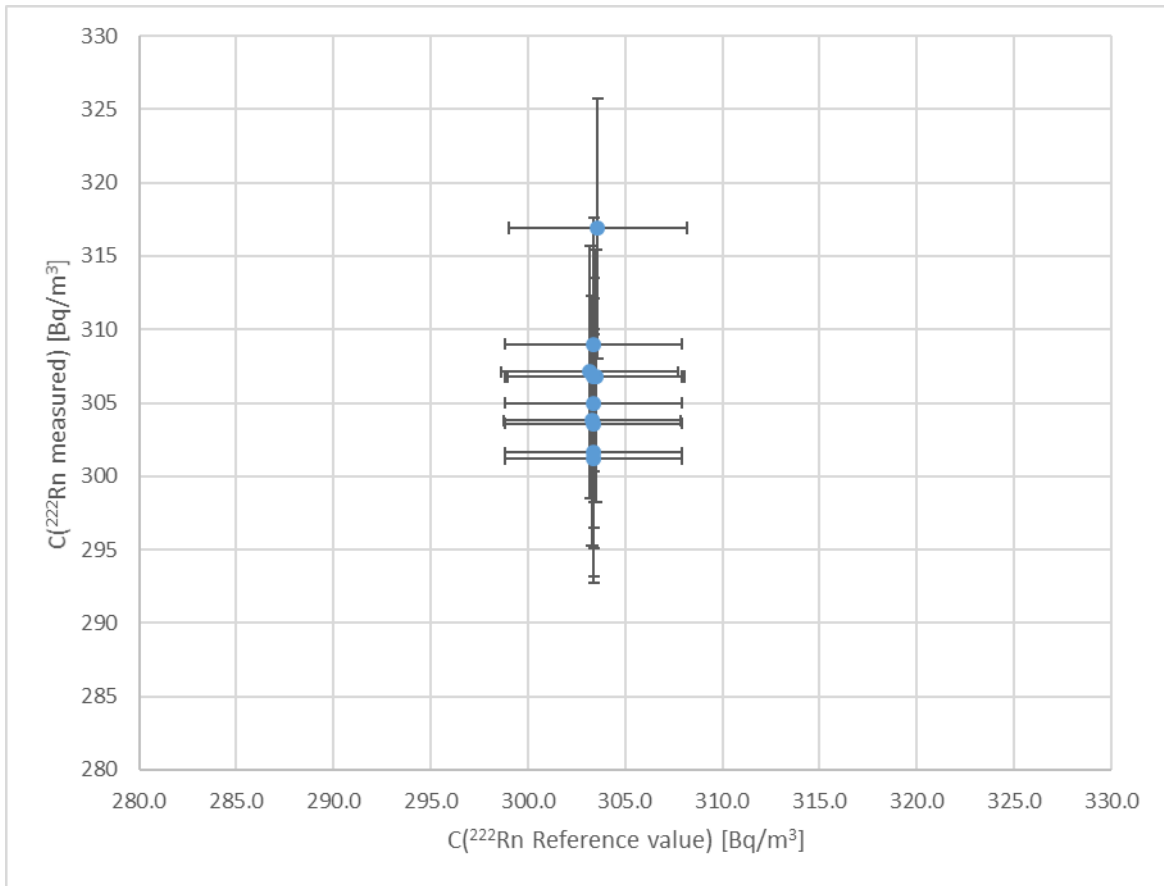


Figure B.5. Exposition Background and  $300 \text{ Bq/m}^3$

Table B.4. Measurement at  $300 \text{ Bq/m}^3$  with AlphaGuard PQ2000 Pro, S/N EF2142

No.	Date [dd.mm.yyyy]	$^{222}\text{Rn}$ Ref.Conc. (CALC) $C_{\text{Ref}}$ [ $\text{Bq/m}^3$ ]	$^{222}\text{Rn}$ Meas.Conc. (AVG) $C_{\text{meas}}$ [ $\text{Bq/m}^3$ ]	Std.Dev. (AVG) $\sigma(C_{\text{meas}})$ [ $\text{Bq/m}^3$ ]	No. of measurement points ( $\Delta t = 10 \text{ min}$ )
1	14.05.2019	303.3	303.8	37.3	24
2	22.05.2019	303.2	307.1	46.8	24
3	13.06.2019	303.4	309.0	52.7	24
4	19.06.2019	303.4	301.2	56.3	24
5	23.07.2019	303.4	306.8	42.8	24
6	07.08.2019	303.6	316.9	49.3	24
7	14.08.2019	303.4	301.6	43.3	24
8	03.09.2019	303.4	305.0	44.2	24
9	11.09.2019	303.5	306.8	59.1	24
10	18.09.2019	303.4	303.6	40.5	24



**Figure B.6.** Comparison of <sup>222</sup>Rn concentration measurements

## C. Activity Report of the Horia Hulubei National Institute for Research and Development in Physics and Nuclear Engineering (IFIN-HH)

### C.1 Representation of the quantity radon activity concentration for accurate calibrations of radon instruments

#### C.1.1 Introduction

At IFIN-HH, the measurement of the  $^{222}\text{Rn}$  radon and its progeny has a long tradition: activity of the radon in air or dissolved in solutions contained in sealed vials, dosimetry, monitoring of the radon activity concentration indoor and outdoor (emanations from the soil), <http://meteo.nipne.ro/>.

Within the former Radionuclide Metrology Laboratory (now, the Ionizing Radiation Metrology Laboratory - LMRI) from IFIN-HH, an original method for the primary activity standardization of  $^{222}\text{Rn}$  was developed about 10 years ago. It is based on the Liquid Scintillation Counting – Triple to Double Coincidence Ratio (LSC-TDCR) method [1][2][3].

A radon standard system was established at IFIN-HH, [2]. It uses a  $^{226}\text{Ra}$  (250 kBq) standard source of Pylon RN-1025 type to generate  $^{222}\text{Rn}$ , which is transferred in different types of ampoules and vials (in vacuum), Figure C.1. The system allows also the radon transfer from one vial to an ampoule filled with liquid scintillator solution (LS), Figure C.2.



Figure C.1. The radon standard system at IFIN-HH (left); glass vial with radon (right)



Figure C.2. The sealing of an ampoule with liquid scintillator after the radon transfer in the solution.

Then, the activity of the radon dissolved in solution (LS) can be primary standardized using the LSC-TDCR installation from the Ionizing Radiation Metrology Laboratory (LMRI) of IFIN-HH. Using this method, radon activity uncertainties of about 1.2 % were obtained (for a coverage factor  $k = 1$ ).

Based on the primary standard of radon activity, two installations for relative activity measurements were calibrated at IFIN-HH: a gamma-ray spectrometry system with a high resolution semiconductor detector (HPGe type) and a  $4\pi\gamma$  ionization chamber (Centronic IG12/20A). These secondary standardization systems are measuring the gamma-ray emissions of the  $^{222}\text{Rn}$  daughters ( $^{214}\text{Pb}$ ,  $^{214}\text{Bi}$ ). After the establishment of the secular equilibrium between  $^{222}\text{Rn}$  and its daughters mentioned above, the two secondary installations can be used successfully for the radon activity standardization (gas contained in different types of recipients, including ampoules with LS solution). The half-life of  $^{222}\text{Rn}$  is  $T_{1/2} = (3.8232 \pm 0.0008)$  days, with the uncertainty corresponding to a coverage factor  $k = 1$ , [4]. The secondary methods allow an easier and faster way to standardize the radon activity, but with a higher uncertainty (usually about 5 %,  $k = 1$ ).

The results obtained at IFIN-HH were validated by the successful participation of the laboratory in two international comparisons of radon ( $^{222}\text{Rn}$ ) activity measurements, as shown by the draft B reports of these comparisons: CCRI(II)-K2.Rn-222 (in 2015) and the EURAMET project no. 1475 –EURAMET.RI(II)-S8.Rn-222N (in 2019, included in the current 16ENV10 MetroRADON project, task 1.2).

### C.1.2 The radon monitors and the new recipients used for measurements at IFIN-HH

Two radon monitors are currently available in the LMRI laboratory from IFIN-HH: a Radon Scout from SARAD GmbH (Germany), bought in 2008 and an AlphaE hand-held monitor from Saphymo GmbH (Germany). The Radon Scout monitor was recently re-calibrated by the manufacturer (2019), using a reference instrument calibrated annually by BfS from Germany (standards metrological traceable to PTB). According to the Calibration Certificate no. CC\_RSC2\_00189\_2019-05-23, the radon activity concentration was in the range (1148 – 2048) Bq/m<sup>3</sup> at an average temperature of 24.9 °C, relative humidity 46 %. The sensitivity was 1.65 m<sup>3</sup>/(min·kBq), statistical error (relative uncertainty) of 4.4 % ( $k=2$ ).

Since 2017, two attempts were made to buy an AlphaGuard DF2000 for professional multiparameter analysis, but because of some problems related to the public acquisition procedures, the monitor was not purchased. Such a high-quality radon monitor would be used as reference instrument for the calibration of different radon monitors and other devices used by customers for the measurement of radon activity concentration in air.

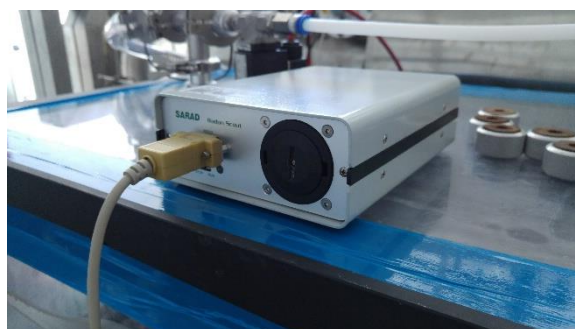


**Figure C.3.** The Radon Scout monitor

Despite its limitations and lower metrological quality of the measurements, in the absence of an AlphaGUARD monitor, the Radon Scout monitor (Figure C.3) was used by the LMRI laboratory within the current project, in order to measure the radon activity concentration in air inside the radon chamber of IFIN-HH. The AlphaE hand-held device was used only to monitor the radon activity concentration in air, in the radon laboratory, in order to assure the radiation protection of the staff.

Four new stainless steel recipients were purchased in order to be used for the radon transfer from the standard system, radon storage and transfer into the radon chamber for calibrations and different experiments. The volume of each recipient is about 105 cm<sup>3</sup>; it has two outputs with taps allowing to open/close the recipient (Figure C.4, below, shows a recipient connected to the radon standard system). It is safer to use these metallic recipients than the glass vials/ampoules; they are easier to connect to the radon chamber.



**Figure C.4.** A stainless steel recipient used for radon extraction, storage and transfer

### C.1.3 The radon chamber of IFIN-HH

The implementation of the European Union Council Directive no. 2013/59/EURATOM requires facilities to assure reliable and accurate calibration of the instruments measuring the radon concentration in air, in all the EU countries.

In the frame of the Romanian national research project “Realization of a radon chamber – Calibration stand for the equipment used in the measurement of radon and daughter products concentration in air” (CARSTEAM), <http://proiecte.nipne.ro/pn2/141-projects.html>, a radon chamber was designed, constructed and installed at IFIN-HH, in the Radionuclide Metrology Laboratory (LMR), with the participation of the scientific partners from ICSI Rm. Valcea and the University of Bucharest. The chamber was designed in order to obtain a System for Test Atmospheres with Radon, according to the standard IEC 61577-4 (Radiation Protection Instrumentation – Radon and radon decay product measuring instruments). The radon chamber is a large metallic vessel, tight, with walls made of stainless steel (4 mm thick), cylindrical shaped, with a door; the inner volume is 1 m<sup>3</sup> (Figure C.5). In order to achieve the control of the main environmental parameters during the calibration procedures (temperature, humidity and pressure), using air-conditioning equipment, the radon chamber is placed inside a larger, external chamber with thin double steel walls containing polyurethane foam in between (thermal insulator of 150 mm thick). Two alternative inputs for radon gas were foreseen: one - from an external recipient (like the one in Figure C.4) containing a certified activity of radon (standard source), and another one – from a small pipe transporting a continuous radon flux emanated from the <sup>226</sup>Ra source (Pylon type). The second system for radon transfer into the radon chamber is not yet implemented.

Temperature, pressure and humidity sensors are mounted inside the radon chamber and transmit the recorded data on a desktop computer. Two small fans are used to homogenize the radon inside the chamber. Electrical power supply is available for the radon measurement instruments to be calibrated in the chamber; the data signal is transferred to the same computer through air tight serial connectors type RS232. Input/output pipes with electrical valves can introduce pressurized air of high purity (99.99%), respectively evacuate the mixture of air with radon and its daughters in the building special ventilation system. A vacuum pump can be connected to the inner volume of the radon chamber.

Recently, the first version of a calibration procedure for the instruments measuring the radon activity concentration in air was established and included in the LMRI quality management system, ISO 17025:2017 compliant. The calibration is based on the use of a high quality reference instrument for the measurement of the  $^{222}\text{Rn}$  activity concentration in air (now – the Radon Scout monitor, and in the near future, hopefully, an AlphaGuard monitor). Only radon ( $^{222}\text{Rn}$ ) decaying standard sources are used for the instruments calibration. In the future, it is intended to develop the calibration procedure, by using also radon emanation sources (with certified emanation rate).

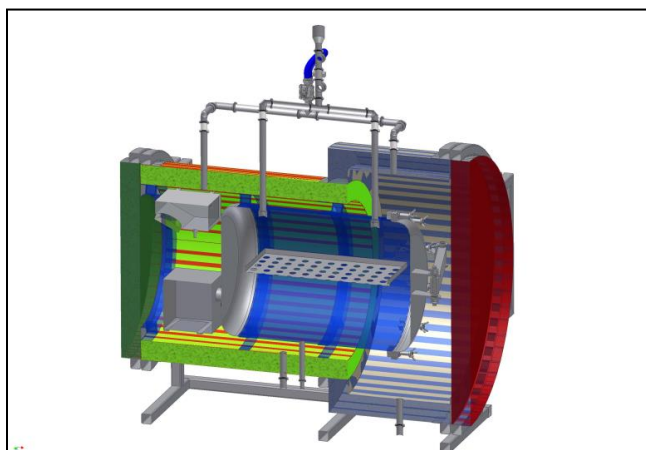


**Figure C.5.** The radon chamber from IFIN-HH: 3D concept design (left), photo (right)

#### C.1.4 Establishment of constant and stable $^{222}\text{Rn}$ activity concentrations in the radon chamber

In the IFIN-HH radon chamber three radon reference atmospheres were recently established, by transferring radon from the stainless steel recipients. The radon ( $^{222}\text{Rn}$ ) activity was measured by gamma-ray spectrometry, with a high resolution semiconductor detector of HPGe type (secondary standard installation), calibrated using the primary radon activity standard from IFIN-HH and a correction derived from the reference value of the radon activity comparison (2019), performed in the frame of the same project – MetroRADON, Task 1.2.1.

The radon activity values at the reference times, measured for each steel recipient, are presented below, in Table C.1.

**Table C.1.** Radon activity values extracted in the steel recipients

Recipient no.	$^{222}\text{Rn}$ activity (Bq)	Relative Uncertainty (%), for $k = 1$	Reference time (local time, GMT+2h)
1	211731	5.3	17 January 2020, 10:29
2	7845	5.9	21 January 2020, 8:40
4	3633	5.5	6 February 2020, 10:13

Following the measurements, after several days, the radon from the three recipients was transferred, successively, into the radon chamber. This was done by flushing high purity air from a pressurized bottle (with very low radon content) through the recipient connected to the radon chamber (about 1 liter/minute). After 10 minutes, the connection with the air bottle was closed. The stability of the radon atmospheres and the climate parameters were monitored for periods between 25 hours to 52 hours. The temperature varied from 21 °C to 26 °C, the relative humidity was in the range (18-29) % and the air pressure was 101.5 kPa.

The radon activity concentration was measured using the Radon Scout monitor. The average values were in good agreement with the values measured by gamma-ray spectrometry (see Table C.1), computed at the new reference times and considering 1 m<sup>3</sup> (±5 %, k=1) as an estimation of the radon chamber air volume (this will be precisely calibrated in the future).

Table C.2 presents the obtained results (average values of the radon activity concentration) for the three radon reference atmospheres. The values from the Table C.2 include the radon background due to the air from the radon chamber, measured by the radon monitor: 61 Bq/m<sup>3</sup> (± 41 %) for recipients 1 and 2, and 42 Bq/m<sup>3</sup> (± 50 %) for recipient 4.

**Table C.2.** Radon activity concentrations obtained in the radon chamber.

Recipient no.	Results – Radon Scout monitor		Reference time (local time, GMT+2h)	<sup>222</sup> Rn activity concentration (Bq/m <sup>3</sup> ) and relative uncertainty (k=1) - estimation
	<sup>222</sup> Rn activity concentration (Bq/m <sup>3</sup> )	Relative Uncertainty, for k=1		
1	7916	4 %	4-Feb-2020, 13:38	7971 (7.3 %)
2	438	15 %	6-Feb-2020, 17:20	465 (9.0 %)
4	1093	10 %	12-Feb-2020, 13:20	1238 (7.5 %)

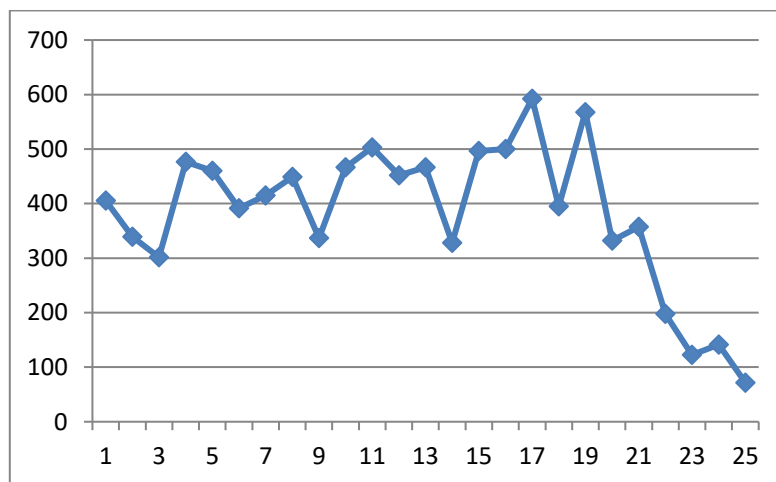


**Figure C.6.** Radon activity concentration (Bq/m<sup>3</sup>) in the radon chamber versus time (25 hours exposure)

As an example of the stability of the radon activity concentration obtained, measured with the Radon Scout monitor, Figure C.6 presents the radon exposure after connecting the recipient no. 2 to the radon chamber at

IFIN-HH. This corresponds to the lowest radon activity concentration obtained in the radon chamber (all the values are computed at the reference time (6<sup>th</sup> of February 2020, 17:20 local time (GMT+2h)). During the last 5 hours, the radon chamber valves were open and the air with radon was pushed out from the chamber (and outside the building, through the chimney), using an air compressor (this explains the drop of the activity concentration down to the background values).

These are the first results obtained with the radon chamber from IFIN-HH. In the future, it is foreseen to improve the stability of the radon reference atmospheres from the radon chamber by using electroplated <sup>226</sup>Ra low activity sources with constant and stable radon emanation and also air flow-through <sup>226</sup>Ra standard sources with a metering flow controller and dispenser, such as the sources developed within the MetroRADON project, work package 1, task 1.1.

## C.2 Development of a procedure for the calibration of instruments measuring the radon activity concentration in air

A procedure for the calibration of the instruments measuring the radon activity concentration in air was recently developed at IFIN-HH, in the LMRI laboratory. The radon chamber of 1 m<sup>3</sup> is used for this purpose. It is based on the use of radon decaying activity standards (produced at the radon standard system), together with a high quality reference instrument (a Radon Scout monitor - now, to be replaced by an AlphaGUARD monitor in the future). The radon activity standards were produced in a wide range of activities: from 220 kBq down to 400 Bq. For the potential customers, there is an interest to calibrate their instruments at low radon activity (below 1000 Bq/m<sup>3</sup>). In fact, for the implementation of the EU Council Directive no. 2013/59/EURATOM, reliable and accurate measurements even below 300 Bq/m<sup>3</sup> are necessary. The main steps of the procedure are:

- the check of the installation natural background (the background is measured in a background chamber, using “radon free” air from a pressurized bottle);
- the reference radon monitor and the customer’s device are introduced in the radon chamber; radon gas is transferred in a controlled way into the sealed radon chamber, then the radon activity concentration in air (Bq/m<sup>3</sup>) is measured with both instruments (at least 5 measurements in a radon reference atmosphere);
- the experimental data are processed and corrected (for background, radioactive decay, standard temperature and pressure conditions); three types of data can be recorded: instantaneous radon activity concentration at given times, average radon activity concentration on a given time period of exposure (e.g. one hour) or radon activity concentration integrated on a long time period (days, weeks etc.).

The combined uncertainty (coverage factor  $k=1$ ) will be computed, too. For example, in the case of a radon monitor measuring the average radon activity concentration ( $\bar{A}$ ) in air, exposed for a time period of  $\Delta t$ , starting at  $t_1$ :

$$\bar{A} = A(t_1) \frac{1 - e^{-\lambda \cdot \Delta t}}{\lambda \cdot \Delta t}, \quad (\text{C-1})$$

With the combined uncertainty:

$$u_c(\bar{A}) = \bar{A} \sqrt{\frac{u_c^2(A(t_1))}{A^2(t_1)} + \frac{[\lambda \cdot \Delta t \cdot e^{-\lambda \cdot \Delta t} + e^{-\lambda \cdot \Delta t} - 1]^2 \left[ \frac{u_c^2(\lambda)}{\lambda^2} + \frac{u_c^2(\Delta t)}{\Delta t^2} \right]}{(1 - e^{-\lambda \cdot \Delta t})^2}}, \quad (\text{C-2})$$

where  $\lambda = \ln(2)/T_{1/2}$  is the decay constant for <sup>222</sup>Rn.

The relative difference between the average radon activity concentration measured with the customer’s installation and the true conventional value measured by the reference instrument of LMRI, at the same reference time, is calculated. If the relative difference is lower than 10 %, then it is compared with the combined uncertainty of the customer instrument, according to the technical specifications of the manufacturer. For relative differences higher than 10 %, a multiplicative correction factor will be calculated and mentioned in the calibration certificate issued for the customer’s instrument.

Optionally, a linearity check of the customer's installation can be performed. The radon activity concentration can be measured at different time intervals (5 ... 20 times), covering a period when the radon activity decays up to an order of magnitude (about two weeks). The measured values will be compared with those calculated from the activity decay curve (a relative difference of up to 10 % is accepted).

Following the IFIN-HH / LMRI participation to the MetroRADON project, several improvements to the calibration procedure will be possible, especially for the calibration in the range of low level radon activity concentrations (from 100 Bq/m<sup>3</sup> to 300 Bq/m<sup>3</sup>) and for other devices, such as alpha-track detectors or electrets.

### C.3 References

- [1] Cassette, P., Sahagia, M., Grigorescu, L., Lepy, M.C., Picolo J.L. 2006. Standardization of Rn-222 by LSC and comparison with alpha and gamma spectrometry. *Appl. Radiat. Isot.* 64, 10-11, 1465-1470.
- [2] Sahagia, M., Stanga, D., Waetjen, A.C. Luca, A., Cassette, P., Ivan, C., Antohe, A. 2010. The Rn-222 standard system established at IFIN-HH, Romania. *Appl. Radiat. Isot.* 68, 1503 -1506.
- [3] Sahagia, M., Luca, A., Watjen, A. C., Antohe, A., Ivan, C. Varlam, C., I. Faurescu, I., P. Cassette, P., 2011. Establishment of the Rn-222 traceability chain with the Romanian Standard System. *Nuclear Instrum. and Meth. in Phys. Res. A*, 631, 73-79.
- [4] Bé, M.-M., Chisté, V., Dulieu, C., Browne, E., Chechev, V., Kuzmenko, N., Kondev, F., Luca, A., Galán, M., Pearce, A., Huang, X., 2008. Monographie BIPM-5: Table of Radionuclides (Vol. 4 – A = 133 to 252), Bureau International des Poids et Mesures, Sèvres, France, ISBN 92-822-2230-6.

## D. Activity Report of the National Institute for Nuclear, Biological and Chemical Protection (SUJCHBO)

### D.1 Representation of the quantity radon activity concentration for accurate calibration of radon instruments

#### D.1.1 Introduction

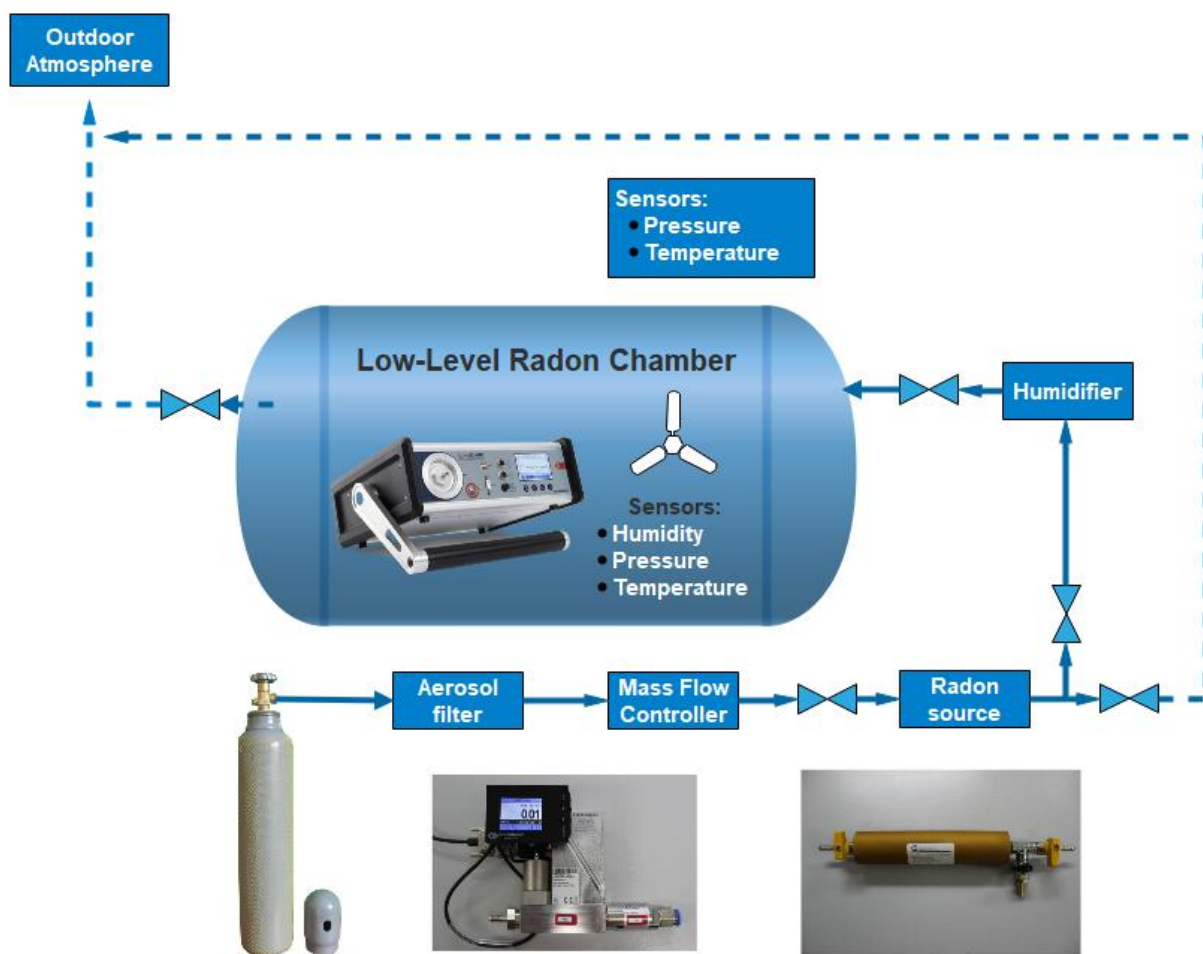
The National Institute for Nuclear, Biological, and Chemical Protection, under the European project 16ENV10 MetroRADON (the European metrology program for innovation and research, EMPIR), has developed unique equipment for the testing of measuring devices at low-level radon activity concentrations (Figure D.1). The construction of the equipment allows the time-stable radon activity concentration to be maintained at a precise level for several days. Radon concentration values can be arbitrarily and continuously set in the range from  $100 \text{ Bq}\cdot\text{m}^{-3}$  to  $300 \text{ Bq}\cdot\text{m}^{-3}$ . The equipment will be used for the testing of measuring devices for radon.



Figure D.1 The SUJCHBO Low-Level Radon Chamber

#### D.1.2 Description of the technical infrastructure

The equipment consists particularly of an airtight Low-Level Radon Chamber (LLRCH) with an inner volume of 324 liters; a  $^{222}\text{Rn}$  type RF 5 flow-through source with a  $^{226}\text{Ra}$  activity of 4.955 kBq developed by Czech Metrological Institute, regional inspectorate Prague within the above-mentioned project; and a pressure vessel as a radon-free air source. The mass flow controller of the Bronkhorst EL-Flow type is a part of the apparatus and ensures the requested airflow through the radon source—partialized if necessary—through the chamber. The homogeneity of the atmosphere in the chamber is ensured by means of a continuously regulated fan



**Figure D.2** Scheme of the equipment construction

(airflows in the range of  $0.1 - 3.5 \text{ m}\cdot\text{s}^{-1}$  can be established). Another important chamber component is the measuring device of climatic conditions, since temperature, air pressure, and relative humidity must be determined. Figure D.2 represents a simplified scheme of the equipment construction.

In order to achieve a low-level radon activity concentration in the chamber, it is necessary to ensure a constant supply of radon and provide defined ventilation of the chamber. At a low-level radon concentration, it is difficult to obtain sufficiently "clean" air free from radon for ensuring a ventilation. Radon concentration in outdoor air in the area of SUJCHBO, v.v.i. Kamenna can reach from tens to hundreds  $\text{Bq}\cdot\text{m}^{-3}$ . Therefore, the device uses enough "old" air coming from the pressure vessel. The air passes through the protective aerosol filter and calibrated mass flow gas controller into the source of radon. The radon atmosphere is prepared by a flow source of radon. The air-radon mixture is further passed through a humidifier. The main part of the device is a gas-tight chamber LLRCh (Low-Level Radon Chamber) which is made from steel and painted by a special color. The atmosphere homogeneity inside the radon chamber is ensured with the help of a continually regulated ventilator. Sensors for the measurement of climatic conditions are placed inside the LLRCh (measuring of humidity, air pressure and temperature) and two sensors are placed also outside of the chamber (measuring of air pressure and temperature).

The Low-level radon source was developed by Czech Metrological Institute, regional inspectorate in Prague. An emulsion of salts of fatty acids in silicone rubber was formed from the weighed standard solution. The emulsion was polymerize in a steel tray with the following dimensions:  $70 \times 30 \text{ mm}$ . The activity of the standard as determined by the weight of the  $^{226}\text{Ra}$  solution, the weight of the resulting emulsion and the losses ( $<0.1\%$ ). The whole process was controlled by weighing and gamma spectrometry on an HPGe detector. The 185 keV gamma-ray emission intensity was measured with the use of the standard solution, which confirmed excellent conformity with the tabulated value. Figure D.3 shows the scheme of the low-level radon source. The source

was constructed as a stainless-steel cylindrical case, supplied on the ends with ball valves and two aerosol filters connected on the output aperture of the valves. The steel tray with  $^{226}\text{Ra}$  was placed in the middle of this cylindrical case, and radon was released from this thin layer.

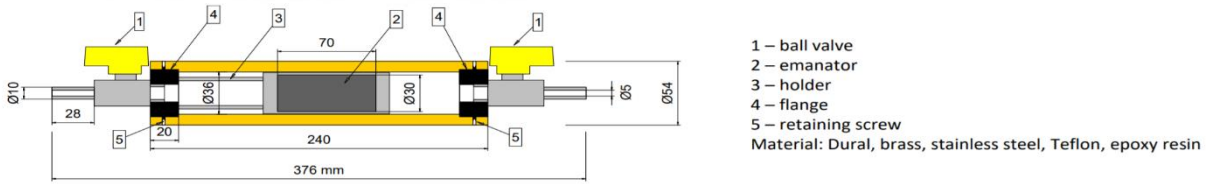


Figure D.3 Scheme of the low-level radon source by the CMI

The emanation coefficient of the source was determined by measuring the activity of the  $^{222}\text{Rn}$  daughter products ( $^{214}\text{Pb} / ^{214}\text{Bi}$ ) and the activity of  $^{226}\text{Ra}$  and was almost equal to 1 (0.99). The detection efficiency of the gamma photons was calculated by the MCNP code (Monte Carlo N-Particle Transport). Figure D.4 shows the real photo of the radon source developed by the CMI with an original label.



Figure D.4 The flow-through low-level radon source developed by the CMI.

### D.1.3 Mathematical treatment

For designing of the device, a model of constant radon input and constant ventilation was applied:

$$a(t) = a_o \cdot e^{-(\lambda_{\text{Rn}}+k) \cdot t} + \frac{R}{V(k+\lambda_{\text{Rn}})} (1 - e^{-(\lambda_{\text{Rn}}+k) \cdot t}), \quad (\text{D-1})$$

- $a(t)$  radon activity concentration at time  $t$  ( $\text{Bq} \cdot \text{m}^{-3}$ )
- $a_o$  radon activity concentration at time 0 ( $\text{Bq} \cdot \text{m}^{-3}$ )
- $\lambda_{\text{Rn}}$  radon decay constant ( $\text{h}^{-1}$ )
- $k$  air exchange intensity ( $\text{h}^{-1}$ )
- $t$  time (h)
- $R$  radon input rate ( $\text{Bq} \cdot \text{h}^{-1}$ )
- $V$  volume of radon chamber ( $\text{m}^3$ )

For the steady state ( $t = \infty$ ) at a constant air exchange intensity and constant radon input rate, the following applies:

$$a_{\text{V,Rn}} = R_{\text{Rn}} / ( Q_{\text{settled}} \cdot \frac{M \cdot p \text{ at Q calibration}}{R \cdot T \text{ at Q calibration}} / \frac{M \cdot p \text{ at confrontation}}{R \cdot T \text{ at confrontation}} + \lambda_{\text{Rn}} \cdot V), \quad (\text{D-2})$$

- $a_{\text{V,Rn}}$  radon activity concentration ( $\text{Bq} \cdot \text{m}^{-3}$ )
- $Q_{\text{settled}}$  flow rate ( $\text{m}^3 \cdot \text{h}^{-1}$ )

**M** molar mass ( $\text{kg}\cdot\text{mol}^{-1}$ )  
**p<sub>at Q calibration</sub>** air pressure 1013,25 (hPa)  
**R** molar gas constant ( $\text{J}\cdot\text{mol}^{-1}\cdot\text{K}^{-1}$ )  
**T<sub>at Q calibration</sub>** temperature 273,16 (K)  
**p<sub>at Rn confrontation</sub>** air pressure (Pa)  
**T<sub>at Rn confrontation</sub>** temperature (K)  
 **$\lambda_{\text{Rn}}$**  radon decay constant ( $\text{h}^{-1}$ )  
**V** volume of radon chamber ( $\text{m}^3$ )  
**R<sub>Rn</sub>** radon emanation power ( $\text{Bq}\cdot\text{h}^{-1}$ )

#### D.1.4 Uncertainty in determining the radon reference level

The required value of radon activity concentration is  $100 \text{ Bq}\cdot\text{m}^{-3}$ , volume of the chamber is  $0.324 \text{ m}^3$  and flow rate  $0.3252 \text{ m}^3/\text{h}$ . The following applies to the calculation of radon activity concentration:

$$a_{V,Rn} = R_{Rn} / ( Q_{\text{settled}} \cdot \frac{M \cdot p_{\text{at Q calibration}}}{R \cdot T_{\text{at Q calibration}}} / \frac{M \cdot p_{\text{at confrontation}}}{R \cdot T_{\text{at confrontation}}} + \lambda_{\text{Rn}} \cdot V ) \quad (\text{D-3})$$

**Table D.1.** Budget of uncertainty

Quantity $X_i$	Estimate $x_i$	Reliability $u(x_i)$	Sensitivity coefficient $c_i$	uncertainty contribution $u_i(y)$
$R_{Rn}$	$37.44 \text{ Bq}\cdot\text{h}^{-1}$	$0.72 \text{ Bq}\cdot\text{h}^{-1}$	$2,67 \text{ h}\cdot\text{m}^{-3}$	$1.9 \text{ Bq}\cdot\text{m}^{-3}$
$Q_{\text{settled}}$	$0.3252 \text{ m}^3\cdot\text{h}^{-1}$	$0.0010 \text{ m}^3\cdot\text{h}^{-1}$	$267 \text{ h}\cdot\text{Bq}\cdot\text{m}^{-6}$	$0,7 \text{ Bq}\cdot\text{m}^{-3}$
<b>M</b>	$0.02895 \text{ kg}\cdot\text{mol}^{-1}$	$2\cdot 10^{-5} \text{ kg}\cdot\text{mol}^{-1}$	$3333 \text{ Bq}\cdot\text{mol}/(\text{kg}\cdot\text{m}^3)$	$0.06 \text{ Bq}\cdot\text{m}^{-3}$
<b>p<sub>at Q calibration</sub></b>	101.3325 kPa	0.4 kPa	$0.9869 \text{ Bq}/(\text{kPa}\cdot\text{m}^3)$	$0.4 \text{ Bq}\cdot\text{m}^{-3}$
<b>R</b>	$8.314 \text{ J}\cdot\text{mol}^{-1}\cdot\text{K}^{-1}$	$10^{-9} \text{ J}\cdot\text{mol}^{-1}\cdot\text{K}^{-1}$	$12.03 \text{ Bq}\cdot\text{K}\cdot\text{mol}/(\text{J}\cdot\text{m}^3)$	negligible
<b>T<sub>at Q calibration</sub></b>	273.16 K	0.60 K	$0.366 \text{ Bq}/(\text{K}\cdot\text{m}^3)$	$0.22 \text{ Bq}\cdot\text{m}^{-3}$
<b>p<sub>at Rn confrontation</sub></b>	96.290 kPa	0.4 kPa	$1.0385 \text{ Bq}/(\text{kPa}\cdot\text{m}^3)$	$0.42 \text{ Bq}\cdot\text{m}^{-3}$
<b>T<sub>at Rn confrontation</sub></b>	296.95 K	0.58 K	$0.3368 \text{ Bq}/(\text{K}\cdot\text{m}^3)$	$0.20 \text{ Bq}\cdot\text{m}^{-3}$
<b><math>\lambda_{\text{Rn}}</math></b>	$0.007554 \text{ h}^{-1}$	$0.000003 \text{ h}^{-1}$	$86.5 \text{ h}\cdot\text{Bq}\cdot\text{m}^{-3}$	$2.6\cdot 10^{-4} \text{ Bq}\cdot\text{m}^{-3}$
<b>V</b>	$0.324 \text{ m}^3$	$0.002 \text{ m}^3$	$2.017 \text{ Bq}\cdot\text{m}^{-6}$	$0.004 \text{ Bq}\cdot\text{m}^{-3}$
<b><math>a_{V,Rn}</math></b>	$100 \text{ Bq}\cdot\text{m}^{-3}$			$2.0 \text{ Bq}\cdot\text{m}^{-3} (2,0\%)$

The table shows an expanded uncertainty - the product of the standard measurement uncertainty and the expansion coefficient  $k = 2$  (which corresponds to a coverage probability of about 95% for normal distribution) in accordance with EA 04/02.

## D.2 Calibration

### D.2.1 Procedures

Two reference measuring devices—AlphaGuard DF 2000 and AlfaGuard PQ 2000—were used for the determination of radon activity concentration. Both devices are owned by SUJCHBO, v.v.i. and they were calibrated in BfS Berlin, Germany. During all experiments, the system was connected as shown in Figure D.2. The

flow-through source of  $^{222}\text{Rn}$  type RF 5 with an emanation coefficient of 0.99 was used. Changes in the setting of the required level of radon activity concentrations were controlled by modifications of the flow rate through the radon source. Figures D.5 – D.8 show the results of different settings of flow rates, the final required levels of radon activity concentrations in the LLRCH and the various times of radon activity concentration stabilizations.

The graph on Figure D.5 shows results of the experiment in which the source of radon was not connected to the system. Only air free from radon was sent into the chamber. The goal of this experiment was to verify the air-tightness of the chamber and compare the background of measuring devices with data taken from calibration

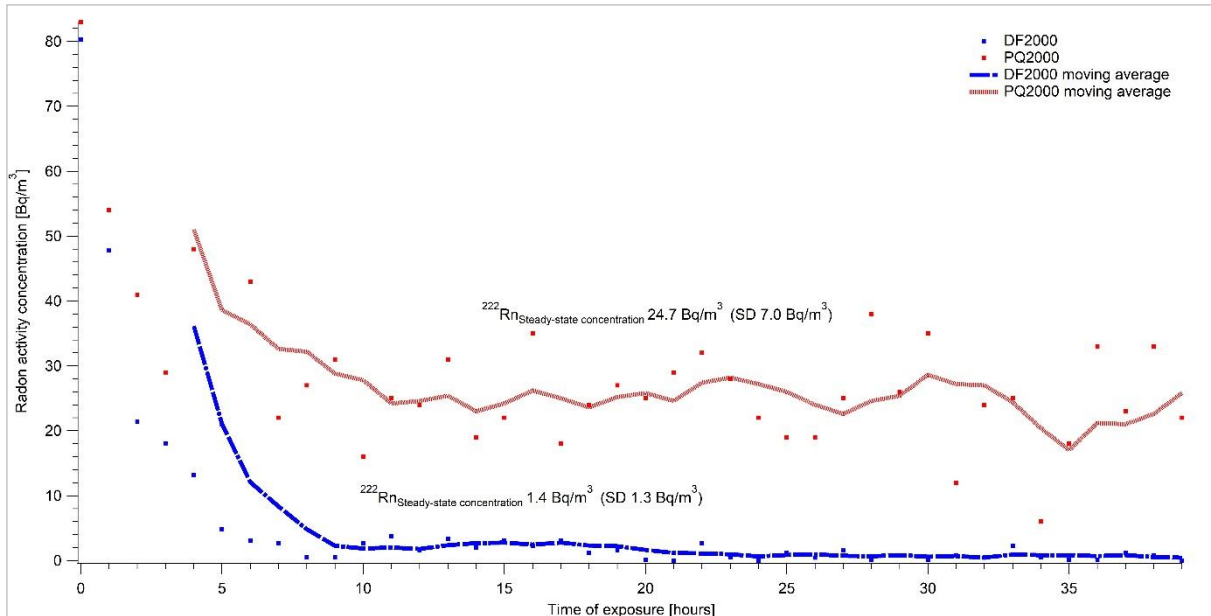


**Figure D.5** A stable radon-free atmosphere was set in approximately eight hours. Individual points show the real measured data and curves represent a moving average of measured results.

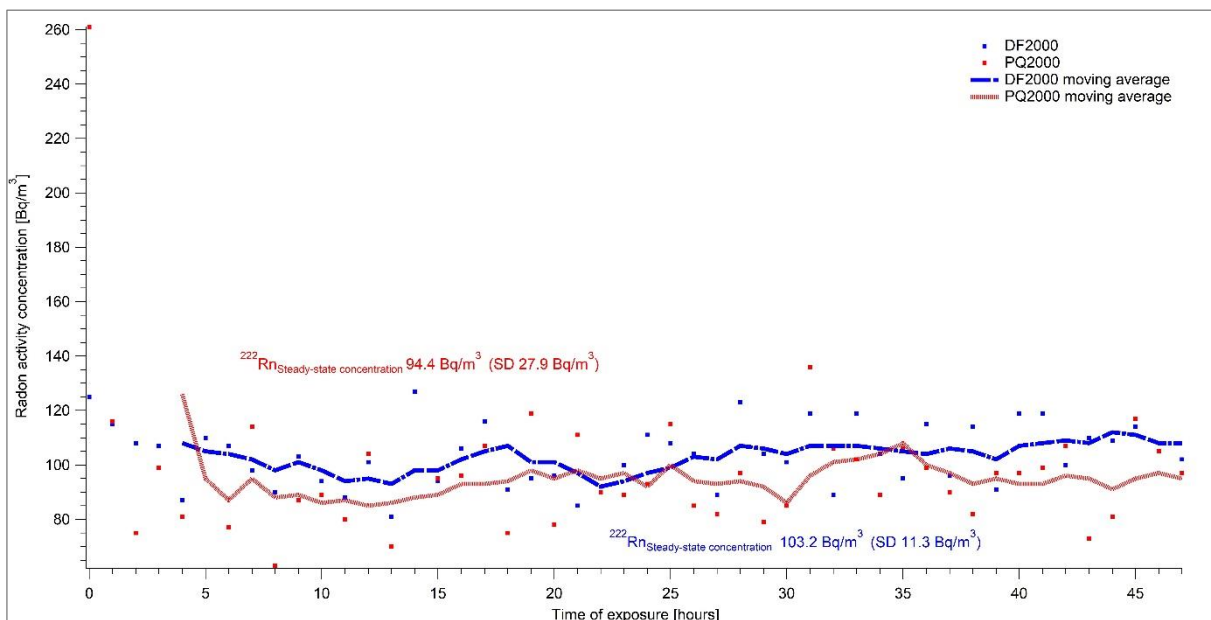


**Figure D.6** At the beginning of the experiment, the radon activity concentration in the laboratory was about  $120 \text{ Bq}\cdot\text{m}^{-3}$ . The flow rate was set to  $6.20 \text{ l}\cdot\text{min}^{-1}$ . The stable radon atmosphere at the level of  $100 \text{ Bq}\cdot\text{m}^{-3}$  was set in approximately 6 hours. Individual points show the real measured data and curves represent a moving average of measured results.

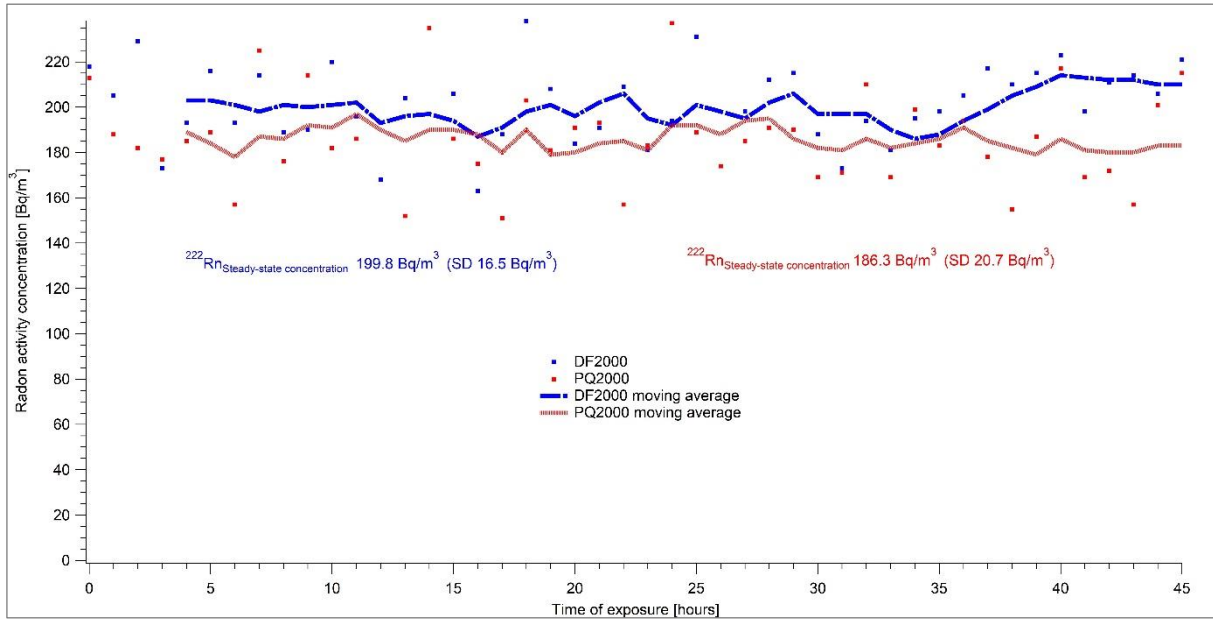


**Figure D.7** At the beginning of the experiment, at the required radon activity concentration of  $200 \text{ Bq}\cdot\text{m}^{-3}$ , the radon activity concentration in the laboratory was at a similar level. The flow rate was set to  $3.08 \text{ l}\cdot\text{min}^{-1}$ . The stable radon atmosphere was set almost immediately. Individual points show the real measured data and curves represent a moving average of measured results.

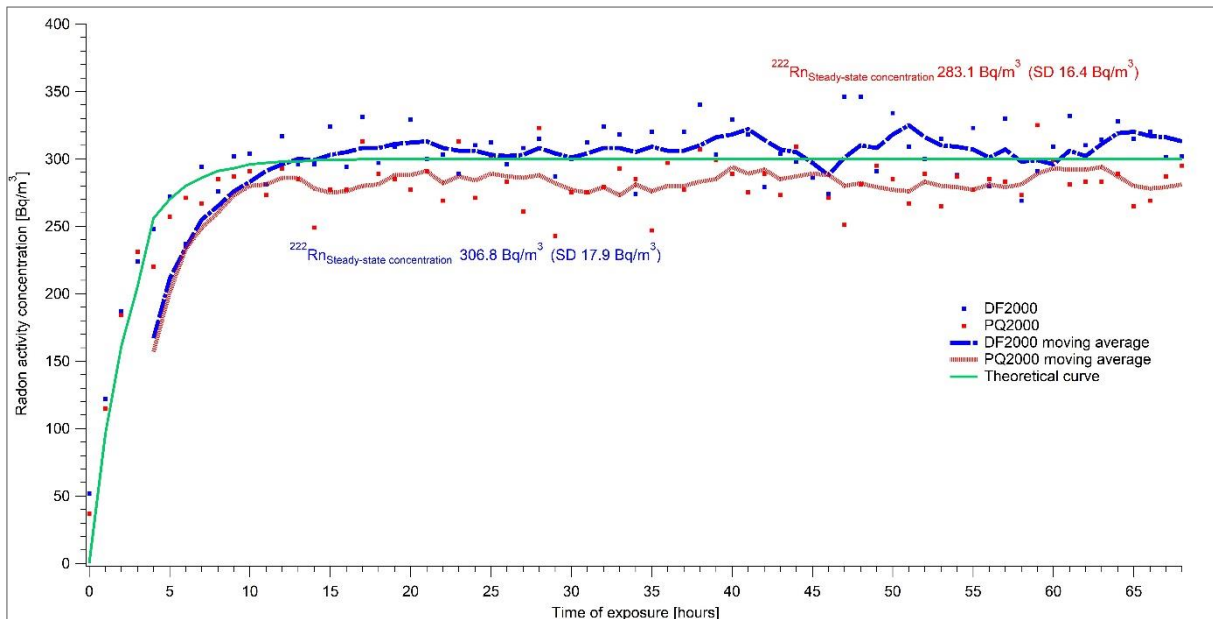


**Figure D.8** The flow rate in the experiment was set to  $2.04 \text{ l}\cdot\text{min}^{-1}$ . The stable radon activity concentration of  $300 \text{ Bq}\cdot\text{m}^{-3}$  was set in approximately 10 hours. Individual points show the real measured data and curves represent a moving average of measured results. The continuous green line shows the theoretical radon activity trend obtained by applying Equation 2. The results of both measuring devices approximate the theoretical curve.

sheets. According to the Calibration sheets of both AlphaGuards, their backgrounds are  $2.2 \pm 1.2 \text{ Bq}\cdot\text{m}^{-3}$  for the DF 2000 model and  $29.0 \pm 7.0 \text{ Bq}\cdot\text{m}^{-3}$  for the PQ 2000 model. The measured average radon activity concentrations during the first experiment were  $1.4 \pm 1.3 \text{ Bq}\cdot\text{m}^{-3}$  with AlphaGuard DF 2000 and  $24.7 \pm 7.0 \text{ Bq}\cdot\text{m}^{-3}$  with AlphaGuard PQ 2000. The results of the experiment testify that zero radon activity concentration was maintained in the LLRCH for more than 30 hours.

A set of experimental measurements was taken, demonstrating both the air-tightness of the Low-Level Radon Chamber and the capability of establishing and stably maintaining different radon concentrations. Radon reference atmospheres of 100, 200 and 300  $\text{Bq}\cdot\text{m}^{-3}$  (Figures D.6 – D.8) were adjusted. The required radon activity concentrations were stabilized within hours, depending on the required radon activity concentration and related intensity of air exchange. The results were more than satisfying: for AlphaGuard DF 2000, the average radon activity concentrations were  $103.2 \pm 11.3 \text{ Bq}\cdot\text{m}^{-3}$ ,  $199.8 \pm 16.5 \text{ Bq}\cdot\text{m}^{-3}$  and  $306.8 \pm 17.9 \text{ Bq}\cdot\text{m}^{-3}$ ; for AlphaGuard PQ 2000, the average radon activity concentrations were  $94.4 \pm 27.9 \text{ Bq}\cdot\text{m}^{-3}$ ,  $186.3 \pm 20.7 \text{ Bq}\cdot\text{m}^{-3}$  and  $283.1 \pm 16.4 \text{ Bq}\cdot\text{m}^{-3}$ . All results are presented after subtracting AlphaGuard’s background (according to the calibration sheets) and the calibration factor was used. Calibration factors for both AlphaGuards were determined in the framework of a unit traceability with the Czech Metrological Institute’s (CMI) primary standard of  $^{226}\text{Ra}$  with the declared activity of  $^{226}\text{Ra}$ .

The radon activity concentrations could be steadily maintained for several days depending on the amount of radon-free air available in the pressure vessel.

### D.2.2 Radon chamber modelling

The developed general system architecture can be applied to a different radon chamber size. The radon activity concentration set in different chambers depends on the emanation power of a radon source and the flow rate of the air free from radon coming from a vessel to the radon source and then to the chamber, as in Equations (1) and (2). The time of radon activity concentration stabilization strongly depends on the volume of the chamber. Figure D.9 shows the radon activity concentration trends obtained according to Equation (2) by modelling the radon chambers in use at the Federal Office of Metrology and Surveying (BEV, Austria), the Federal Office for Radiation Protection (BfS, Germany), the Radiation and Nuclear Safety Authority (STUK, Finland), and the Slovak Office of Standards, Metrology and Testing (Slovak Institute of Metrology, Slovak Republic).

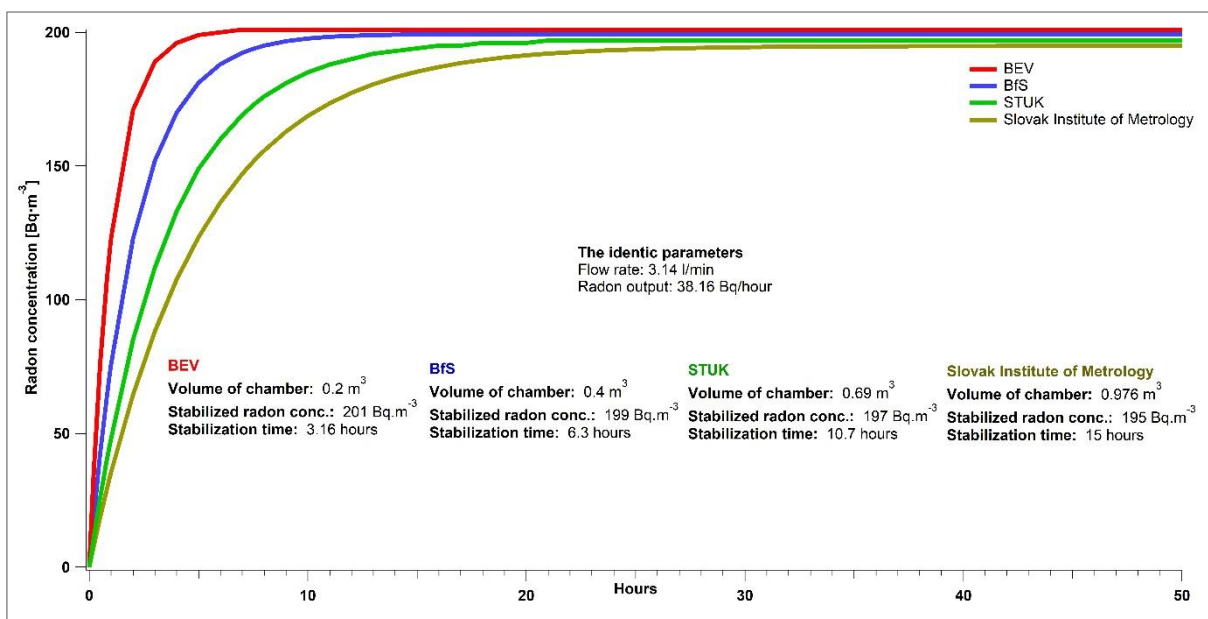


Figure D.9 Theoretical radon activity concentration trend for a few selected existing radon chambers around the world.

### D.3 Conclusion

The Low-Level Radon Chamber of SUJCHBO, v.v.i. is a specific device developed for the calibration of measuring devices at a low-level radon activity concentration in the range of  $100 \text{ Bq}\cdot\text{m}^{-3}$  to  $300 \text{ Bq}\cdot\text{m}^{-3}$ . Many tests have validated the air-tightness of the chamber and the possibility of adjusting a stable radon activity concentration to a required level for several days. A stable radon activity concentration is reached in several hours, depending on the required level of radon activity concentration and related intensity of air exchange. Generally, a higher required value of radon activity concentration means a lower intensity of air exchange and a much longer required time for stabilizing the radon atmosphere inside the chamber.

The level of radon activity concentration in the LLRCH can be changed continuously during the experiment by an operator. The climatic parameters are continuously monitored by the sensors placed inside the chamber.

The low-level radon source of the CMI (Czech Metrological Institute, Prague) can be used for different radon chambers with a volume between 200 and 1000 liters.

## E. Activity Report of the Government Office of the Capital City Budapest (BFKH) Metrological and Technical Supervisory Department

### E.1 Representation of the quantity radon activity concentration for accurate calibration of radon instruments

#### E.1.1 Introduction

The Government Office of the Capital City Budapest (BFKH) Metrological and Technical Supervisory Department (MMFF), in frame of the European project 16ENV10 MetroRADON (the European metrology program for innovation and research, EMPIR), has improved its radon chamber for the testing of measuring devices at low-level radon activity concentrations (Figure E.1). The radon chamber allows to set up and maintain any radon concentration from 100 Bq/m<sup>3</sup> to 5 kBq/m<sup>3</sup>. This equipment is suitable for type testing of radon measuring devices.



Front-view



Back part with radon source and buffer

Figure E.1 The radon chamber with the radon source

#### E.1.2 Description of the measuring system

The equipment consists of an airtight stainless steel chamber, a radon-222 source (type RF 500 from Czech Metrological Institute), a leakproof gas pump (Alpha Pump, rate flows 0.3, 0.5 and 1 L/min), a nitrogen gas-cylinder, a controller unit with computer and an environmental parameters (temperature, air pressure and relative humidity) measuring units. The volume of the chamber is 840 liter. The activity of the radium source is 630.4 kBq with a very high emanation factor (99 %). The homogeneity of the radon gas in the chamber is ensured by two continuously running fans. The radon chamber's specialty is the two gas circuits which have a common branch. The common branch consists of the radon generator and the pump. Figure E.2 shows the scheme of the measuring system. In the figure, the blue lines indicate the gas paths and the red one the electrical control lines.

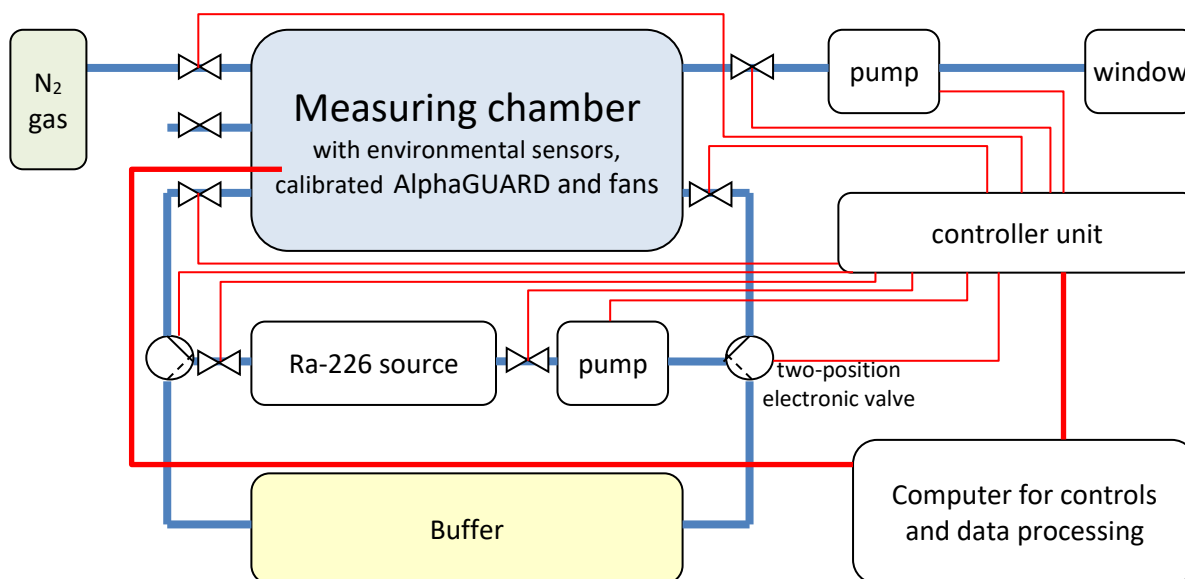


**Figure E.2** Scheme of the measuring system.

From the radium source, the radon gas is transferred by a pump to either the buffer or the measuring chamber. The buffer volume (including the radon generator) is 120 liters. The flow branch (buffer or chamber) is determined by the state of the two-position electronic gas valves. All valves in the radon chamber are electronic and can be controlled from a computer. The desired activity concentration in the radon chamber can be set by opening the two-way valves for  $t_1$  second towards to the chamber and  $t_2$  second towards to the buffer. The definitions of  $t_1$  and  $t_2$  are given in the following ( $t_1 - t_2 = \Delta t$ ) section. After the defined radon activity concentration is reached, the valves are open to the measuring chamber only until the number of decayed radon atoms replenish.

In order to keep the background of the radon meters in the chamber as low as possible, after the door is closed the air should be removed. For this aim the chamber is flushing with nitrogen gas ( $N_2$ ). After the calibration the radon gas transfer to the open air using a pipe across the window.

The Figure E.3 shows the environmental parameter collector and its specifications.

Specifications:

sensors	range	uncertainty
2 pieces temperature	15-60 °C	$\pm(0.01-0.03)$ °C
air pressure	90-110 kPa	$\pm 30$ Pa
relative humidity	20%-80%	$\pm 2$ %



**Figure E.3** The environmental parameters collector.

The Figure E.4 shows the radon generator and its specifications.

Specifications:

type:	RF-500
$^{226}\text{Ra}$ activity	630.4 kBq
$^{220}\text{Rn}$ emanation factor	$0.998 \pm 0.001$
reference date	01.02.1998
manufacturer	Czech Metrological Institute



**Figure E.4** The radon generator.

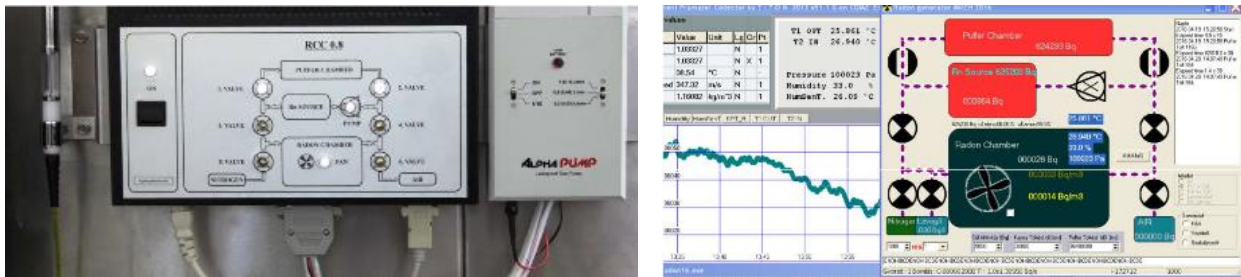


Figure E.5 The controller unit and the software.

Finally in the Figure E.5 visible the controller unit and the software.

### E.1.3 Radon homogeneity and the airtight closed chamber

Radon distribution within the chamber was investigated using solid-state track detectors. The Figure E.6 shows the track detectors in the chamber. The track detectors were located at various important places in the chamber (center, corner, etc...).



Figure E.6 The track detectors in the chamber.

The result of the evaluation after detector etching is illustrated in the Figure E.7. The mean value and its standard deviation ( $k = 1$ ) are also visible on the graph.

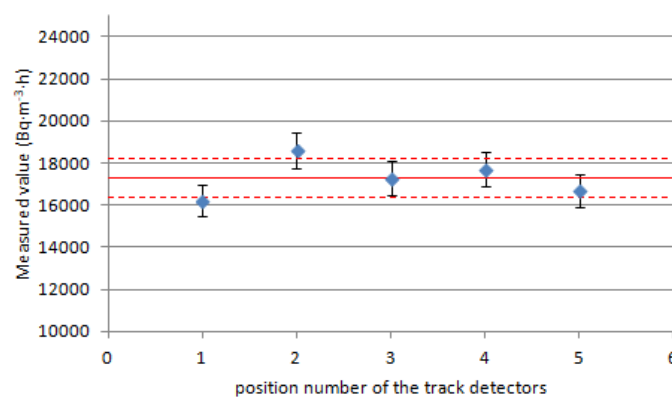
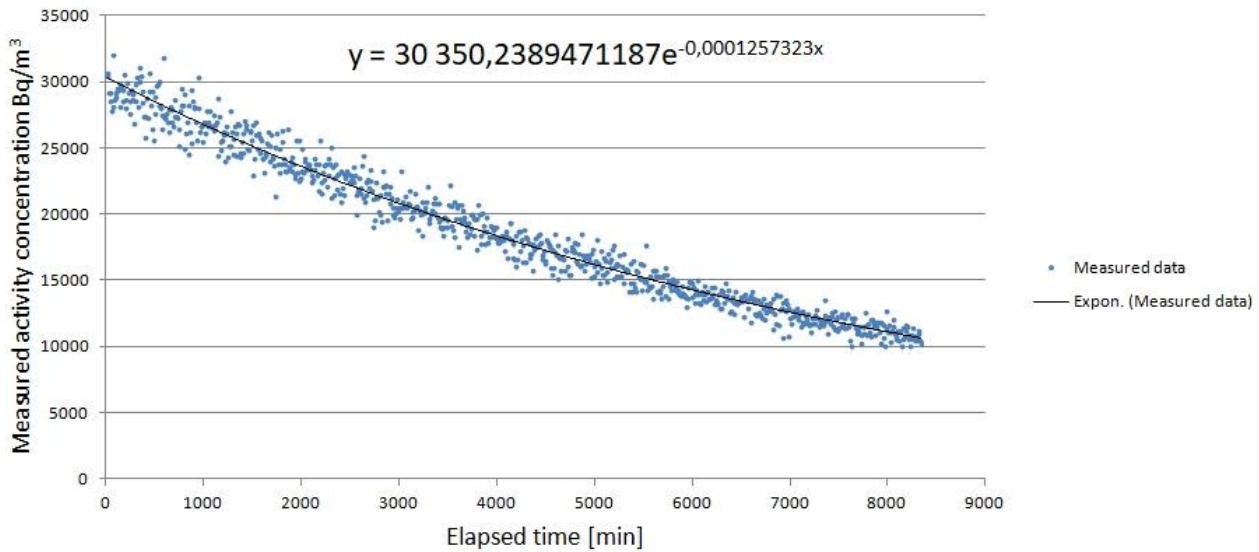


Figure E.7 The homogeneity results.

In addition to the homogeneous distribution of radon gas, airtight sealing of the chamber is also important. The leakage test was investigated by the radon gas decay. After the measuring chamber was filled with radon gas all valves were closed and flow was stopped. An AlphaGUARD continuously measured the radon concentration in the chamber (Figure E.8)



**Figure E.8** Decay of the closed radon gas

An exponential function fit was made to the measured points. The value of the parameter in the exponent:

$$\lambda = 0.0001257323 = \ln(2)/T_{1/2} \tag{E-1}$$

From the (E-1) relation  $T_{1/2} = 3.828$  days. The radon half-life from the literature is  $3.8232 \pm 0.0008$  days [1]. The two half-life values are within 0.2% which indicates that the chamber is really airtight.

#### E.1.4 Volume of the radon chamber

A very important parameter is the volume of the radon chamber. AlphaGUARD measures the radon concentration and if have to measure the total activity the volume is also required. This was also in case the 1.2.1 radon comparison measurement.

It is not easy to determine the volume, since the value calculated from the side edges may be different from the actual one (side swell, etc ...). The radon chamber volume was determined by CO concentration measurement. The advantage of this method is that the walls of the chamber do not deform under high or low pressure. A well-known amount of CO was introduced into the chamber and circulated through a CO concentration meter. Using the universal gas law:

$$pV = nRT \tag{E-2}$$

where p: pressure,  
V: volume,  
n: amount of chemical substance (mol),  
R: the universal gas constant,  
T: temperature.

From the expression (E-2) the volume can be determined. The measured volume of the measuring chamber is:

$$V_{chamber} = (844.9 \pm 5.9) \text{ litre} \tag{E-3}$$

Of course the minimum and the maximum volume have been determined from the side edges as well. The measured edges parameters are in the Figure E.9.

parameter	length (cm)
a	79.6
b	87.4
c	80.4
d	88.3
e	119.1
f	119.6
g	119.6
h	119.6
i	79.6
j	87.4
k	79.9
l	87.6

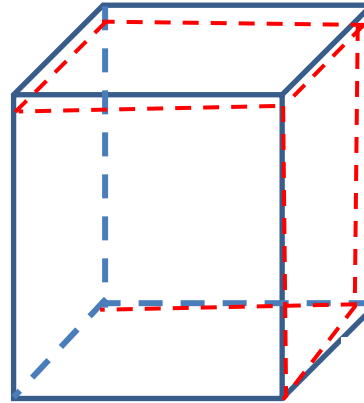


**Figure E.9** Chamber volume from edge lengths.

The calculated minimum volume is 828.6 litre and the maximum volume is 849.1 litre. The volume determined by CO concentration measurement is within the minimum-maximum range. It has been accepted as the volume value.

### E.1.5 Mathematical model

First the system be open toward to the buffer (valves allow radon gas flows across the buffer). The amount of radon formed in the buffer is given by (E-4) expression:

$$\frac{dN_{Rn}}{dt} = \eta \cdot \lambda_{Ra} \cdot N_{Ra} - \lambda_{Rn} \cdot N_{Rn} \quad (E-4)$$

- $N_{Rn}$  number of radon-222 atoms,
- $N_{Ra}$  number of radium-226 atoms,
- $\lambda_{Ra}$  decay constant of radium-226,
- $\lambda_{Rn}$  decay constant of radon-222,
- $\eta$  emanation factor

Solution of the differential equation:

$$N_{Rn}(t) = N_{Ra}(0) \cdot \frac{\eta \cdot \lambda_{Ra}}{\lambda_{Rn} - \lambda_{Ra}} \cdot (e^{-\lambda_{Ra} \cdot t} - e^{-\lambda_{Rn} \cdot t}) + N_{Rn}(0) \cdot e^{-\lambda_{Rn} \cdot t} \quad (E-5)$$

- $N_{Rn}(0)$  number of radon-222 atoms at t=0,
- $N_{Ra}(0)$  number of radium-226 atoms at t=0

Change in radon-222 activity:

$$A_{Rn}(t) = \lambda_{Rn} \cdot N_{Rn}(t) = A_{Ra}(0) \cdot \frac{\eta \cdot \lambda_{Rn}}{\lambda_{Rn} - \lambda_{Ra}} \cdot (e^{-\lambda_{Ra} \cdot t} - e^{-\lambda_{Rn} \cdot t}) + A_{Rn}(0) \cdot e^{-\lambda_{Rn} \cdot t} \quad (E-6)$$

Activity concentration in the buffer branch:

$$c_{Rn}(t) = \frac{A_{Ra}(0)}{V} \cdot \frac{\eta \cdot \lambda_{Rn}}{\lambda_{Rn} - \lambda_{Ra}} \cdot (e^{-\lambda_{Ra} \cdot t} - e^{-\lambda_{Rn} \cdot t}) + c_{Rn}(0) \cdot e^{-\lambda_{Rn} \cdot t}$$

$$c_{Rn}(t) = \frac{A_{Ra}(0)}{V} \cdot \frac{\eta \cdot \lambda_{Rn}}{\lambda_{Rn} - \lambda_{Ra}} \cdot e^{-\lambda_{Ra} \cdot t} - \left( \frac{A_{Ra}(0)}{V} \cdot \frac{\eta \cdot \lambda_{Rn}}{\lambda_{Rn} - \lambda_{Ra}} - c_{Rn}(0) \right) \cdot e^{-\lambda_{Rn} \cdot t} \quad (E-7)$$

Because the half-life of radium is much longer than the radon half-life and  $c_{Rn}(0) = 0$ , the first member of the equation will be dominant and gives the radon concentration in the buffer.

The next step is to fill the radon chamber measuring volume with radon gas. The equation describing the radon concentration in the radon chamber over unit time is:

$$c_1 = \frac{c_0 \cdot V_C + c_{B0} \cdot V_L - c_0 \cdot V_L}{V_C} = c_0 + (c_{B0} - c_0) \cdot \frac{V_L}{V_C} \quad (E-8)$$

- $c_0$  a radon concentration in the chamber before the filling,
- $c_1$  a radon concentration in the chamber after the filling,
- $V_C$  volume of the chamber,
- $c_{B0}$  a radon concentration in the buffer before the filling,
- $V_L$  volume of the filled gas.

The  $V_L$  depends from the flow rate and the filling time. The radon concentration in the buffer circuit:

$$c_{B1} = \frac{c_{B0} \cdot V - c_{B0} \cdot V_L + c_0 \cdot V_L}{V} = c_{B0} - (c_{B0} - c_0) \cdot \frac{V_L}{V} \quad (E-9)$$

- $V$  volume of the buffer

After  $\Delta t$  time to fill a newer  $V_L$  radon gas into the chamber. Before filling the radon gas into the chamber the activity concentration is:

$$c'_1 = c_1 \cdot e^{-\lambda_{Rn} \cdot \Delta t} \quad (E-10)$$

Radon concentration in the buffer:

$$c'_{B1} = \frac{A_{Ra}(0)}{V} \cdot \frac{\eta \cdot \lambda_{Rn}}{\lambda_{Rn} - \lambda_{Ra}} \cdot (e^{-\lambda_{Ra} \cdot \Delta t} - e^{-\lambda_{Rn} \cdot \Delta t}) + c_{B1} \cdot e^{-\lambda_{Rn} \cdot \Delta t} \quad (E-11)$$

After the filling the new activity concentrations:

$$c_2 = c'_1 + (c'_{B1} - c'_1) \cdot \frac{V_L}{V_C} \quad (E-12)$$

$$c_{B2} = c'_{B1} - (c'_{B1} - c'_1) \cdot \frac{V_L}{V}$$

With this iteration the desired radon concentration can be achieved.

The third step is to maintain the level of achieved activity concentration. This means that always have to replace the decayed radon atoms. Introducing the notation below

$$K := \frac{A_{Ra}(0)}{V} \cdot \frac{\eta \cdot \lambda_{Rn}}{\lambda_{Rn} - \lambda_{Ra}} \quad (E-13)$$

The  $c_2$  radon concentration:

$$c_2 = c_1 \cdot e^{-\lambda_{Rn} \cdot \Delta t} + \left( K \cdot (e^{-\lambda_{Ra} \cdot \Delta t} - e^{-\lambda_{Rn} \cdot \Delta t}) + (c_{B1} - c_1) \cdot e^{-\lambda_{Rn} \cdot \Delta t} \right) \cdot \frac{V_L}{V_C} \quad (E-14)$$

It follows from the condition  $c_2 = c_1$  that:

$$\left( c_1 + (c_{B1} - c_1 - K) \cdot \frac{V_L}{V_C} \right) \cdot e^{-\lambda_{Rn} \cdot \Delta t} = c_1 - K \cdot \frac{V_L}{V_C} \cdot e^{-\lambda_{Ra} \cdot \Delta t} \quad (E-15)$$

Knowing the  $V_L$  (volume of radon transport per unit time) value the  $\Delta t$  time may be adjusted so that the radon concentration in the chamber does not change.

## E.2 Calibration procedure

The reference measuring device is a GENITRON AlphaGUARD PQ 2000 (serial number is 1150). It was calibrated in PTB, the number of calibration certificate is PTB-6.13-38-4046931.

During calibration, the measuring device to be calibrated and the reference instrument are in the radon chamber together. Data is collected from the reference AlphaGUARD by the computer. If a computer connection to the instrument to be calibrated is not possible readings are taken with a camera. After the chamber is closed, the chamber is flushed with nitrogen gas. The radon concentration corresponding to the calibration points is adjusted in ascending order. After each calibration point has been reached have to keep a one hour stabilization period.

After the last calibration point has been recorded the radon gas in the chamber is flushed out by a pump to the open air.

## E.3 References

[1] Monographie BIPM-5. Vol. 4, 2008.

## **F. Activity Report of the Institut de Radioprotection et de Sûreté Nucléaire (IRSN)**

### **F.1 Representation of the quantity radon activity concentration for accurate calibration of radon instruments**

#### **F.1.1 Introduction**

This work is done in the frame of the EMPIR project 16ENV10 MetroRADON: “Metrology for radon monitoring”, it is a part of the working package 1 (Development of novel procedures for the traceable calibration of radon ( $^{222}\text{Rn}$ ) measurement instruments at low activity concentrations (100 Bq/m<sup>3</sup> to 300 Bq/m<sup>3</sup>) with relative uncertainties below 5 % ( $k = 1$ )); and task 1.3 (Establishment of constant and stable  $^{222}\text{Rn}$  activity concentration in reference chambers and development of procedures for the calibration of radon measurement instruments at low activity concentrations).

IRSN investigated the stability and the reproducibility of low activity radon concentration for long-term operation in its reference radon chamber BACCARA. Because we could not get the standard emanation sources, developed in this project, on time, a  $^{226}\text{Ra}$  emanation source from Pylon ( $^{222}\text{Rn}$  flow-through sources, Pylon Electronic, Inc.) was used to create a low radon activity concentration atmosphere. For this Pylon source only the  $^{226}\text{Ra}$  activity is certified and not the emanation of radon. Then, the traceability of the radon activity concentration to a radon standard needs to be done with another instrument. For this purpose, we used an alphaGUARD which has been calibrated with a radon gas standard (traceable to LNHB) to determine the radon activity concentration reference value.

#### **F.1.2. Establishment of constant and stable $^{222}\text{Rn}$ activity concentration in reference chambers**

The constant and stable  $^{222}\text{Rn}$  activity concentration atmosphere was created in the IRSN reference radon chamber called BACCARA. The basic components and modules consist of a radon chamber or volume where instruments can be placed, a  $^{226}\text{Ra}$  emanation sources, a carrier and dilution gas with mass flow controllers, a fan and an exhaust pipe (Figure F.1).

The radon chamber consists of a one cubic meter stainless steel cylinder in which instruments to be calibrated can be placed together (Figure F.2). This volume is connected to a  $^{222}\text{Rn}$  flow-through source (Pylon Electronic, Inc.) with a certified  $^{226}\text{Ra}$  activity concentration and a constant emanation. Dry and clean compressed air is used to carry the radon gas from the radon source to the radon chamber. Air go through the Pylon source at a standard flow rate of one liter per minute, then the radon rich air is mixed and diluted with dry and clean compressed air and directed to the bottom end of the cylinder (the radon chamber). The exhaust is placed on the other end at the top. The same quantity of radon rich air enters and leaves the chamber, the flow rate can vary from 3 m<sup>3</sup>.h<sup>-1</sup> to 10 m<sup>3</sup>.h<sup>-1</sup> depending on the radon concentration that needs to be set-up. Homogeneity of radon concentration inside the container is obtained by turbulences generated by the flow rate entering the chamber and a fan. In this configuration, the steady state and radon activity concentration plateau inside the chamber is reached after three air exchanges of its volume, which corresponds to 30 min to one hour. Activity concentration of  $^{222}\text{Rn}$  and climatic parameters, temperature, pressure and relative humidity are measured continuously inside the chamber.

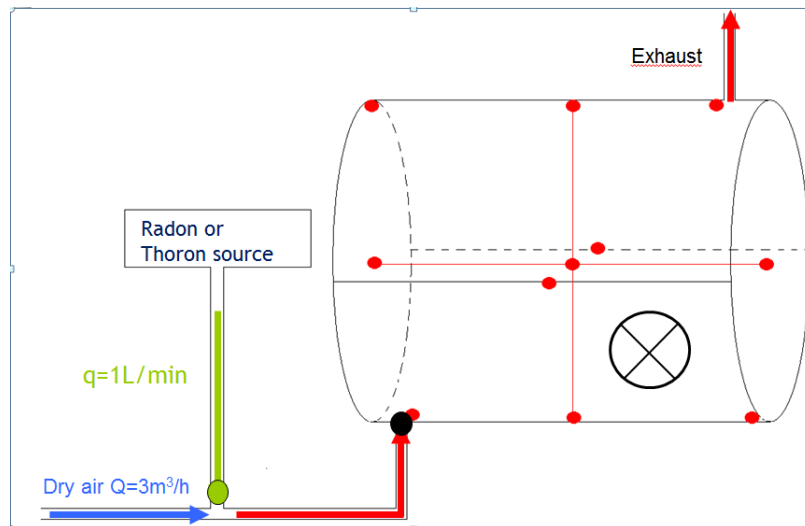


**Figure F.1** Schematic diagram of BACCARA

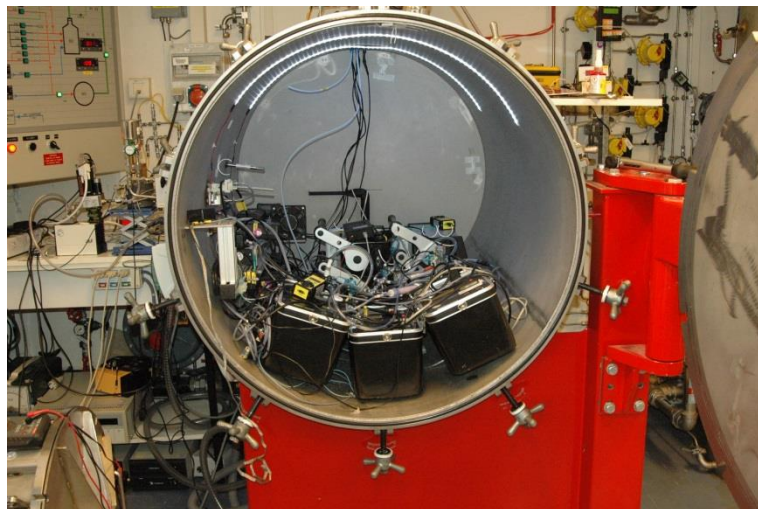


**Figure F.2** Photo of instruments placed inside BACCARA

An example of the reading of two different instruments (an alphaGUARD and a RAD7) showing the stability of the plateau over 30 days' time period is given in Figure F.3.

The establishment of this constant and stable  $^{222}\text{Rn}$  activity concentration was used in A.1.3.3 to test long term integrated radon measurement systems.

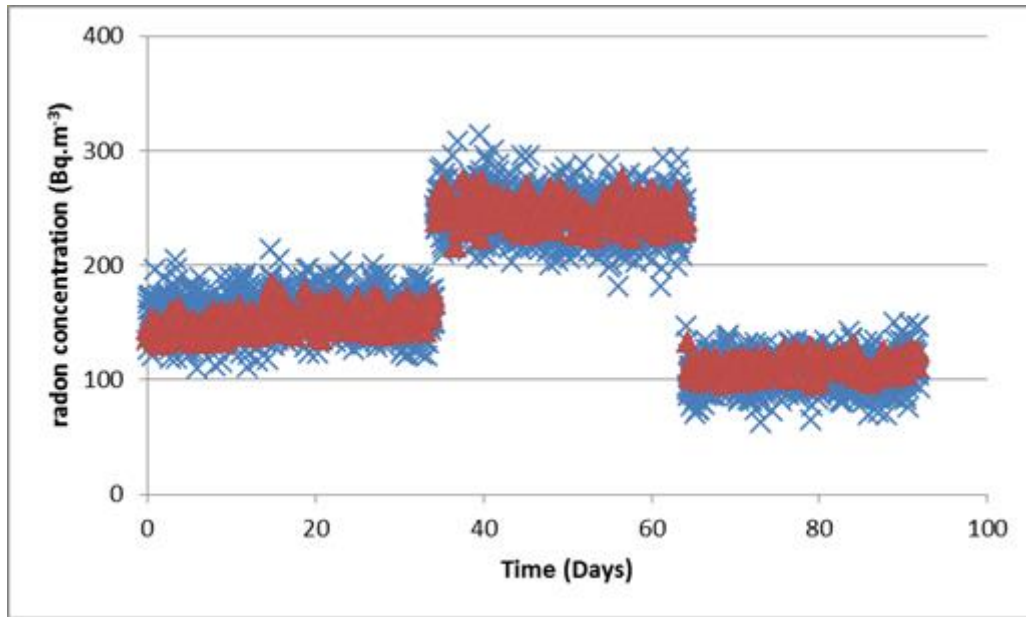


Figure F.3 Data measurement of two instruments for long period of time at low radon activity concentration

## F.2 Calibration of radon measurement instruments at low activity concentrations

### F.2.1. Reference $^{222}\text{Rn}$ activity concentration and uncertainty

The reference activity concentration was determined with an alphaGUARD previously calibrated with a  $^{222}\text{Rn}$  gas standard, traceable to LNHB (certificate number LNHB-222Rn-IRSN-07-2017), using the IRSN calibration procedure DSU/SERAC/LPMA/BACCARA/MOP-02. This calibration covers a large activity range (Michielsen and al. 1999, Picolo and al. 1999) from  $40 \text{ Bq.m}^{-3}$  to  $40 \text{ kBq.m}^{-3}$ . The reference  $^{222}\text{Rn}$  activity concentration is determined as follow:

$$A_{ref} = \frac{(A_{mean} - BCG_{mean})}{R_{dev}} \quad (\text{F-1})$$

where  $A_{mean}$  is the average of  $n$  hourly measurements of the radon activity concentration of the reference alphaGuard and  $BCG_{mean}$  is the background of the apparatus in  $\text{Bq. m}^{-3}$ .  $R_{dev}$  is the calibration factor of the device traceable to LNHB radon gas standard. In order to have a good statistic, the number of measurement used to calculate the mean is chosen to be higher than twenty.

The combined uncertainty of  $A_{ref}$  is calculated as follow:

$$U(A_{ref}) = A_{ref} \sqrt{\frac{\sigma(A_{mean}) + \sigma(BCG_{mean})}{((A_{mean}) - (BCG_{mean}))^2} + \left(\frac{U(R_{dev})}{R_{dev}}\right)^2} \quad (\text{F-2})$$

where  $U(R_{dev})$  is the combined uncertainty of  $R_{dev}$ ,  $\sigma(A_{mean})$  is the standard deviation of the mean of  $n$  measurement and  $\sigma(BCG_{mean})$  is the standard deviation of  $BCG_{mean}$ .

The relative uncertainty on  $R_{dev}$  is 2% at  $k = 2$ .

The relative uncertainty obtained on the  $^{222}\text{Rn}$  activity concentration were under 5% at  $k = 1$ , i.e. 1.7 % at  $230 \text{ Bq.m}^{-3}$  and 2.4 % at  $153 \text{ Bq.m}^{-3}$ .

### F.2.2. Calibration procedure

The aim of the calibration is to compare the measurement of the instrument to be calibrated to the reference instrument. For this purpose the ratio,  $r_{dev}$ , is determined as follow:

$$r_{dev} = \frac{(A_{dev} - BCG_{mean})}{A_{ref}} \quad (\text{F-3})$$

where  $A_{dev}$  is the average of  $n$  hourly measurements of the radon activity concentration of the device to be calibrated and  $BCG_{mean}$  its background.  $A_{ref}$  is the reference  $^{222}\text{Rn}$  activity concentration. All values are expressed in  $\text{Bq. m}^{-3}$ .

The combined uncertainty on  $r_{dev}$  is calculated as follow:

$$U(r_{dev}) = r_{dev} \sqrt{\frac{\sigma(A_{dev}) + \sigma(BCG_{mean})}{(A_{dev} - BCG_{mean})^2} + \left(\frac{U(A_{ref})}{A_{ref}}\right)^2} \quad (\text{F-4})$$

where  $\sigma(A_{dev})$  and  $\sigma(BCG_{mean})$  are the standard deviation of the means  $A_{dev}$  and  $BCG_{mean}$  respectively.

Examples of calibration factor determined at low  $^{222}\text{Rn}$  activity concentration are given in Table F.1.

**Table F.1** Instruments calibration results

Instrument	n	$A_{ref}$ in $\text{Bq.m}^{-3}$	$U(A_{ref})$ in $\text{Bq.m}^{-3}$	$r_{dev}$	$U(r_{dev})$
EF0521	31	229.5	3.9	0.98	0.02
EF0947	31	229.5	3.9	1.01	0.02
RAD7 517	22	152.9	3.6	0.88	0.04
RAD7 2644	22	152.9	3.6	0.94	0.04

### F.2.3. Determination of the background

Background of all apparatus (reference instrument and instruments to be calibrated) is determined using the IRSN background procedure DSU/SERAC/LPMA/BACCARA/MOP-03. It consists of placing the devices in a rectangular box where free radon air circulate for one or two days. The free radon air is obtained by ageing synthetic air pressurized bottles for at least 2 months in order to let the radon decay. In addition an almost zero background instrument, i.e. a RAD7, is also placed inside the box in order to verify the absence of radon.

A number of  $n$  hourly measurements are recorded in the free radon atmosphere, then the arithmetic mean value of the background and the standard deviation of this mean,  $BCG_{mean}$  and  $\sigma(BCG_{mean})$ , are calculated as follow:

$$BCG_{mean} = \frac{1}{n} \sum_{i=1}^n m_i \quad (\text{F-5})$$

with  $m_i$ , the measurement result for one hour;

$$\sigma(BCG_{mean}) = \sqrt{\frac{\sum_{i=1}^n (m_i - BCG_{mean})^2}{n(n-1)}} \quad (\text{F-6})$$

Table F.2 shows some examples of background data obtained for different types of apparatus.

**Table F.2** Examples of background results

Instrument	n	BCG <sub>mean</sub> in Bq.m <sup>-3</sup>	σ(BCG <sub>mean</sub> ) in Bq.m <sup>-3</sup>
EF0521	45	0.2	0.3
EF0947	45	2.1	0.3
EF1549	42	- 10	1
EF0520	42	22	1
RAD7 517	52	0.7	0.1
RAD7 2644	52	2.0	0.3

Even though the background of some instruments can be considered negligible, the value of some of them can reach 10% or 20% of the reference value.

### F.3 Conclusion

IRSN investigated the stability and the reproducibility of low activity radon concentration for long-term operation in its reference radon chamber BACCARA. A <sup>226</sup>Ra emanation source (<sup>222</sup>Rn flow-through sources, Pylon Electronic, Inc.) was used to create a low radon activity concentration atmosphere in the radon chamber BACCARA. For the traceability of the radon activity concentration to a radon standard, a reference alphaGUARD which has been calibrated with a radon gas standard (traceable to LNHB) was used.

Stable radon activity concentrations between 100 Bq.m<sup>-3</sup> and 300 Bq.m<sup>-3</sup> have been reached in less than one hour and stay for more than a month with a combined standard uncertainty of the order of 2 %, below the required level of the project (5%).

Calibration of instrument and dedicated procedure has been developed in the framework of MetroRADON. Because background of the instruments, in the case of low radon activity concentration calibration, cannot be considered negligible, the background value and its uncertainty was taken into account to determine the calibration,  $r_{dev}$ , of the instruments. A combined standard uncertainty of 4 % has been reached on this calibration factor for a radon activity concentration of 153 Bq.m<sup>-3</sup>.



# 16ENV10 MetroRADON

Activity A1.3.3

Accuracy of commonly used integrated radon measurement instruments

Institut de Radioprotection et de Sûreté Nucléaire (IRSN)

Due date: December 2019  
Submission: February 2020

**EMPIR**



The EMPIR initiative is co-funded by the European Union's Horizon 2020 research and innovation programme and the EMPIR Participating States

## Table of contents

1. Object.....	3
2. Participants.....	3
3. Radon exposure principal .....	3
4. Instruments tested .....	5
5. Radon Exposure results .....	5
6. Instrument results .....	7
7. Conclusion.....	11
Annex 1 .....	12
Annex 2 .....	13

## 1. Object

This work is done in the frame of the EMPIR project 16ENV10 MetroRADON: “Metrology for radon monitoring”, it is a part of the working package 1 (Development of novel procedures for the traceable calibration of radon ( $^{222}\text{Rn}$ ) measurement instruments at low activity concentrations (100 Bq/m<sup>3</sup> to 300 Bq/m<sup>3</sup>) with relative uncertainties below 5 % ( $k = 1$ )); and task 1.3 (Establishment of constant and stable  $^{222}\text{Rn}$  activity concentration in reference chambers and development of procedures for the calibration of radon measurement instruments at low activity concentrations).

The aim of the activity 1.3.3. is to determine the accuracy of cheaper instruments (alpha track detectors) at low radon concentration. Alpha-track detectors are the most commonly used radon devices in the world and the most often used for regulation purposes; hence the aim of this activity is to investigate the accuracy of those devices using reference chambers with a radon activity concentration traceable to a radon standard. This will improve the traceability of this type of instruments.

In this activity, each partner investigates the instruments available in their laboratory or their country using their radon reference chamber.

## 2. Participants

The exercise was proposed to the laboratories involved in the task 1.3 who developed low radon activity concentration procedures in their radon reference chamber with traceability to a radon primary standard. The list of participants who send their results is shown in table 1.

Table 1 - Participants by alphabetic order

Acronym	Name	Country
BfS	Bundesamt für Strahlenschutz	Germany
IRSN	Institut de Radioprotection et de Sûreté Nucléaire	France
METAS	Eidgenössisches Institut für Metrologie	Switzerland

## 3. Radon exposure principal

To limit the radon risk to individuals, a reference level for the annual average activity concentration in air of 100 Bq.m<sup>-3</sup> is recommended by the World Health Organization. The maximum limit set by the European Council Directive 2013/59/EURATOM is an annual average activity concentration in air of 300 Bq.m<sup>-3</sup>. In order to estimate the annual exposure in buildings, long term measurements are carried out. ISO 11665-8 and most of the national standards had chosen a time duration for the measurement of at least two months, the commonly periods being two or three months. Meanwhile, in some country, shorter periods of measurement (one or two weeks) are advised, in dwellings for example before the transaction.

The determination of the public radon exposure is usually carried out using a long term integrated measurement. The commonly used integrated measurement systems accumulate a physical quantity (etched tracks, electric charges, etc.) on a suitable sensor over the sampling period (for example one week or some months). This cumulated quantity is related to the radon exposure expressed in  $\text{kBq}\cdot\text{m}^{-3}\cdot\text{h}$ . In the case of instruments using alpha track detector or electret, one can assume that fading of the accumulated quantity is not a problem. Therefore, long term exposure with low concentration is equivalent to shorter exposure with a higher concentration. Figure 1 shows the values of radon exposure in  $\text{kBq}\cdot\text{m}^{-3}\cdot\text{h}$  for different time duration of exposure and two levels of radon average activity concentration:  $100 \text{ Bq}\cdot\text{m}^{-3}$  and  $300 \text{ Bq}\cdot\text{m}^{-3}$ . For example, a measurement instrument exposed for three months in an average radon concentration of  $300 \text{ Bq}\cdot\text{m}^{-3}$  has a radon exposure of  $662 \text{ kBq}\cdot\text{m}^{-3}\cdot\text{h}$ . If the exposure is kept 2 months at an average radon concentration of  $100 \text{ Bq}\cdot\text{m}^{-3}$  then the radon exposure is  $146 \text{ kBq}\cdot\text{m}^{-3}\cdot\text{h}$ , while shorter period of measurement or exposure, one week for example at  $300 \text{ Bq}\cdot\text{m}^{-3}$ , yields to a radon exposure of  $50 \text{ kBq}\cdot\text{m}^{-3}\cdot\text{h}$ .

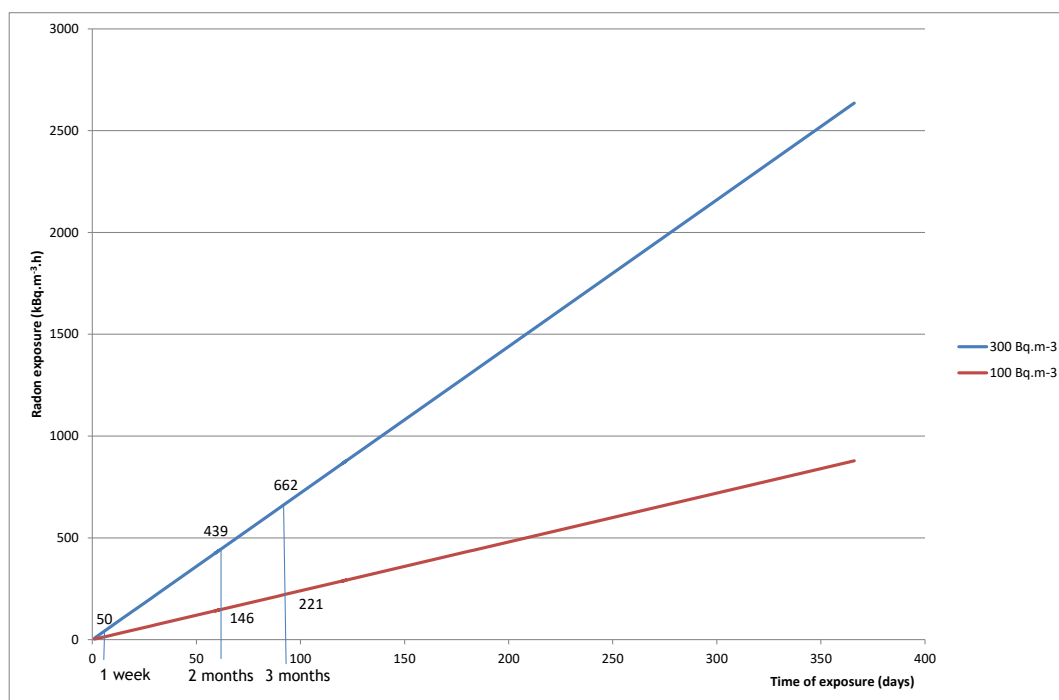


Figure 1 - Radon exposure versus duration of the exposure for two activity concentrations

For this exercise a time exposure above one week and a radon exposure below  $650 \text{ kBq}\cdot\text{m}^{-3}\cdot\text{h}$  were required. The integrated measurement systems were exposed in a radon reference atmosphere and tested with the procedures developed in A1.3.1 and A1.3.2 or in agreement with previous procedure of the participant laboratory. The radon activity concentration of the reference atmosphere was traceable to a radon primary standard.

The following exposures were asked:

- two levels of radon exposure, one in the range of  $140 \text{ kBq}\cdot\text{m}^{-3}\cdot\text{h}$  to  $650 \text{ kBq}\cdot\text{m}^{-3}\cdot\text{h}$  and the other below  $100 \text{ kBq}\cdot\text{m}^{-3}\cdot\text{h}$ .
- a background measurement of the instruments (sometimes called transit measurement in the case of alpha track detector).

The report file sent to the participants to summarize their results is shown in annex 1.

## 4. Instruments tested

Several types of devices were tested, most of them used alpha track detectors, the other were using electrets. Those detectors are placed in a closed diffusion chamber except for one type which is directly exposed to the atmosphere. The shape, the volume and the material of those diffusion chambers or holders are diverse as shown in annex 2. Also the characteristics of the alpha track detectors placed inside vary: CR-39, LR-115, Makrofol with various thicknesses, detection areas and procedure analyses.

Therefore the range of exposure given by the manufacturers or the laboratories which analyses the detector, can vary a lot. A range value going from 0 to 200 kBq.m<sup>-3</sup>.h is given for the lower value of radon exposure range of measurement (annex 2). In the other hand, the higher value of radon exposure vary between 2 000 kBq.m<sup>-3</sup>.h and 80 000 kBq.m<sup>-3</sup>.h. It should be noted that the range of exposure time depends on the expected exposure level, manufacturers' information on this point is not always available to the user.

Because of confidential rules in some partners' laboratories, only few instruments could be identified by a commercial name and were selected for the analyses in this report. Table 2 provides a summary of these selected instruments; other characteristics can be found in annex 2. It should be noted that, for these selected instruments, the laboratory who read the data or analyzed the detector, is the supplier of the device. Also those instruments are purchased by many laboratories or institutes for long term measurements.

Table 2 – Selected instruments

Type of instrument (commercial name)	Range (from datasheet indications) (in kBq.m <sup>-3</sup> .h)	Time duration (according to manufacturer datasheet indications ) in months	Name of laboratory who analyses the detector
EasyRad	30 - 10 000	2 - 12	Pe@rl
DPR2	50 - 30 000	2 - 12	Algade
DRF	30 - 60 000	2 - 12	Dosirad
KodAlpha	10 - 60 000	2 - 12	Dosirad
Radtrak2	30 – 50 000	3 - 12	Radonova Laboratories AB, Uppsala, Sweden
BfS Makrofol Detector 200131	50 – 10 000	3 - 12 depending on the expected exposure level	Federal Office for Radiation Protection (BfS), Berlin, Germany

## 5. Radon Exposure results

Except for one exposure, the three laboratories used their radon chamber with a stable radon activity concentration throughout the time duration of the exposure. In one laboratory this constant activity is obtained by setting a predefined value in the chamber before the exposure, then automated additional radon is injected to compensate radioactive decay. For the two other laboratories a constant air flow through Ra-226 emanation source with a constant dilution air through the radon chamber is used.

The three laboratories used an alphaGUARD PQ2000 Pro to monitor the radon activity concentration in the chamber. The traceability is obtained, either directly with a CMI Ra-226 source with an emanation certificate or by calibration of the alphaGUARD with an LNHB or PTB radon gas standard.

The main characteristics of the exposures are summarized in table 3 and figure 2.

Temperature and pressure were comparable for all the exposures and vary from 21°C to 25°C and 958 hPa to 1001 hPa respectively. The relative humidity varies from below 5 % to 65%. Duration of exposure were also different going from 7 days to 2 months. The radon exposures vary from 99 kBq.m<sup>-3</sup>.h to 644 kBq.m<sup>-3</sup>.h with a relative uncertainty (k=1) below 5%.

The volume of the reference chambers varies from 34 liters to 30 m<sup>3</sup>.

Table 3 – Exposure data

Exposure code	relative humidity	time duration (days)	Radon exposure (kBq.m <sup>-3</sup> .h) Cref	uncertainty (k=1) (kBq.m <sup>-3</sup> .h)
<b>B1</b>	19%	7.9	203	5
<b>B2</b>	9%	7.0	221	6
<b>B3</b>	26%	7.9	268	7
<b>B4</b>	28%	8.0	644	16
<b>M1</b>	54%	8.0	313	7
<b>M2</b>	<10%	14.0	99	2
<b>I1</b>	< 5%	29.0	141	2
<b>I2</b>	< 5%	13.4	432	5
<b>I3*</b>	< 5%	15.1	428	5
<b>I4</b>	65%	62.0	434	5
<b>Mbackground</b>	<10%	21.0	0	NA
<b>Itransit</b>	/	200.0	0	NA

NA : Not applicable      \*3 times 2 radon levels      /: not indicated

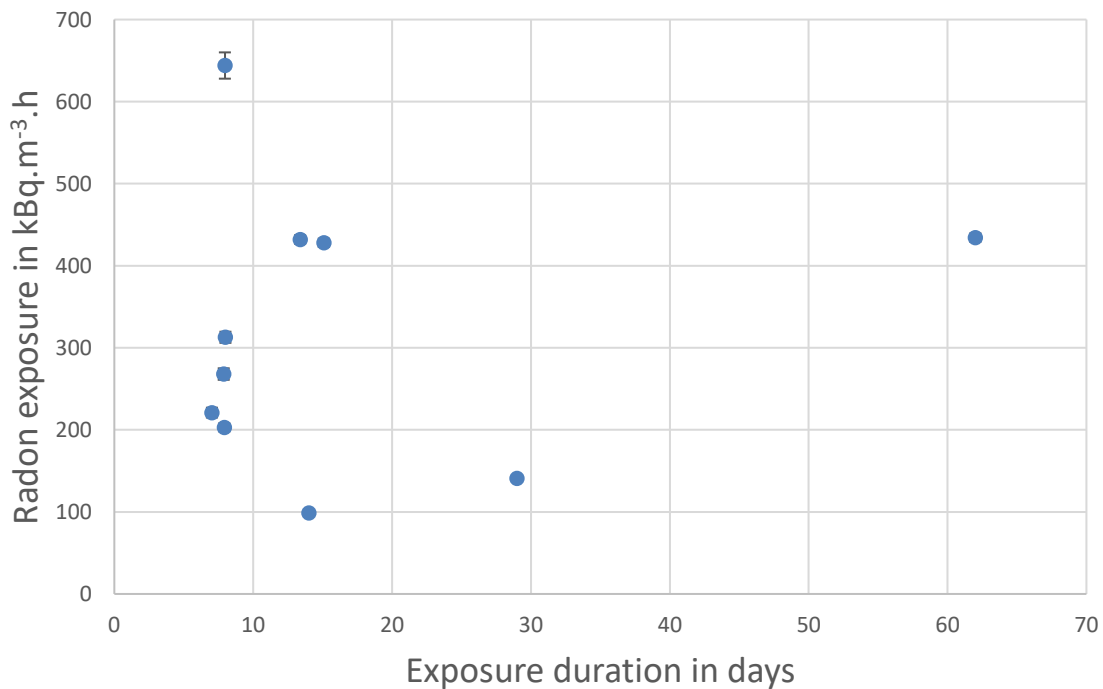


Figure 2 – Radon exposure and time exposure

Exposure I2 and I3 have the same radon exposure for almost the same duration. In exposure I2 the same activity concentration is kept during the exposure. Instead two different radon activity concentrations (around 100 Bq.m<sup>-3</sup> and 1000 Bq.m<sup>-3</sup>) were ascertained successively three time during the exposure I3 in order to simulate rapid changes of radon activity concentration.

In addition the background or transit measurement was investigated in two laboratories.

## 6. Instrument results

Reported results of the selected instruments are given in table 4. In order to maintain the confidentiality of the results, exposures and commercial names of the instruments have been coded. For each exposure or background test and for each different type of apparatus, a set of n instruments were tested.

The arithmetic mean value of the radon exposure in kBq.m<sup>-3</sup>.h, M, measured by the set of n instruments and its combined uncertainty u(M) were calculated by the participants as follow:

$$M = \frac{1}{n} \sum_{i=1}^n m_i ;$$

$$u(M) = \sqrt{\frac{\sum_{i=1}^n u(m_i)^2}{n-1}}, \text{ (at } k=1\text{);}$$

with m<sub>i</sub> and u(m<sub>i</sub>), the measurement result and its combined uncertainty (at k = 1) for one instrument. Note that m<sub>i</sub> and u(m<sub>i</sub>) are given by the laboratory who analyses the detector.

The standard deviation of the mean value, σ(M), was also given by the participants and calculated as follow:

$$\sigma(M) = \sqrt{\frac{\sum_{i=1}^n (m_i - M)^2}{n(n-1)}} ;$$

It can be compared to u(M); if σ(M) > u(M) one can expect a problem in the set of measurement or that the uncertainty, u(m<sub>i</sub>), given by the manufacturer is too low.

In order to compare the measurement result of a set of instruments to the expected true value, traceable to a radon primary standard, the ratio M/C<sub>ref</sub> is used together with the expanded combined uncertainty calculated as follow:

$$U(M/C_{ref}) = 2 \frac{M}{C_{ref}} \times \sqrt{\left(\frac{u(M)}{M}\right)^2 + \left(\frac{u(C_{ref})}{C_{ref}}\right)^2}; \text{ (for } k = 2\text{)}$$

Table 4 – Results of the instruments

Exposure code	Instrument code	n	M (kBq.m <sup>-3</sup> .h)	u(M) (k=1) (kBq.m <sup>-3</sup> .h)	σ(M) (kBq.m <sup>-3</sup> .h)	M/Cref	U(M/Cref) (k=2)
<b>Mbackground</b>	B02	7	3.3	10.5	4.6	NA	NA
<b>ltransit</b>	B02	10	31	/	5	NA	NA
<b>ltransit</b>	E	10	<LD			NA	NA
<b>ltransit</b>	Z01	10	<LD			NA	NA
<b>ltransit</b>	D2	10	<LD			NA	NA
<b>ltransit</b>	D1	10	<LD			NA	NA
<b>M1</b>	B02	5	316.4	21.4	24.8	1.01	0.14
<b>M2</b>	B02	7	112.6	14.6	13.6	1.14	0.30
<b>M2</b>	D01	7	110.3	13.1	10.9	1.12	0.27
<b>I1</b>	E1	10	147	13	8	1.04	0.19
<b>I1</b>	Z01	9	71	/	8	0.50	
<b>I1</b>	D2	10	123	23	8	0.87	0.33
<b>I1</b>	D1	10	137	19	9	0.97	0.27
<b>I1</b>	B02	10	166	22	7	1.18	0.31
<b>I2</b>	E1	10	405	27	7	0.94	0.13
<b>I2</b>	Z01	10	350	50	7	0.81	0.23
<b>I2</b>	D2	10	363	39	20	0.84	0.18
<b>I2</b>	D1	10	388	42	20	0.90	0.19
<b>I2</b>	B02	10	408	36	7	0.94	0.17
<b>I3</b>	E1	10	388	27	8	0.91	0.13
<b>I3</b>	Z01	10	362	51	12	0.85	0.24
<b>I3</b>	D2	10	395	42	27	0.92	0.20
<b>I3</b>	D1	10	366	39	19	0.86	0.18
<b>I3</b>	B02	10	368	31	5	0.86	0.15
<b>I4</b>	E1	10	390	44	17	0.90	0.20
<b>I4</b>	Z01	10	396	55	17	0.91	0.25
<b>I4</b>	D2	10	449	45	13	1.03	0.21
<b>I4</b>	B02	10	423	29	6	0.97	0.13
<b>B1</b>	B02	7	193.4	/	17.7	0.95	
<b>B2</b>	B02	7	205.1	/	14.5	0.93	
<b>B3</b>	B02	7	285	/	22	1.06	
<b>B4</b>	B02	7	701	/	23	1.09	
<b>B1</b>	D01	7	227.3	/	13.5	1.12	
<b>B2</b>	D01	7	247.7	/	13	1.12	
<b>B3</b>	D01	7	295	/	21	1.10	
<b>B4</b>	D01	7	705	/	20	1.09	
<b>B1</b>	Z01	7	223.3	/	43.9	1.10	
<b>B2</b>	Z01	7	250.1	/	36.8	1.13	

/: not indicated      NA: not applicable

The six first lines of table 4 show the results of instruments that were not exposed to radon. All values were below the detection limit except for one instrument of which M was found to be 3.3 kBq.m<sup>-3</sup>.h and 31 kBq.m<sup>-3</sup>.h. The higher value is probably due to a longer period of storage. It should be noted that this higher value is very close to the lower measuring range value of the apparatus.

Note: The transit response of the instrument D01 has not been investigated.

The ratio between the instrument measurements and the expected true value,  $C_{ref}$ , according to the radon exposure is shown in figure 3.

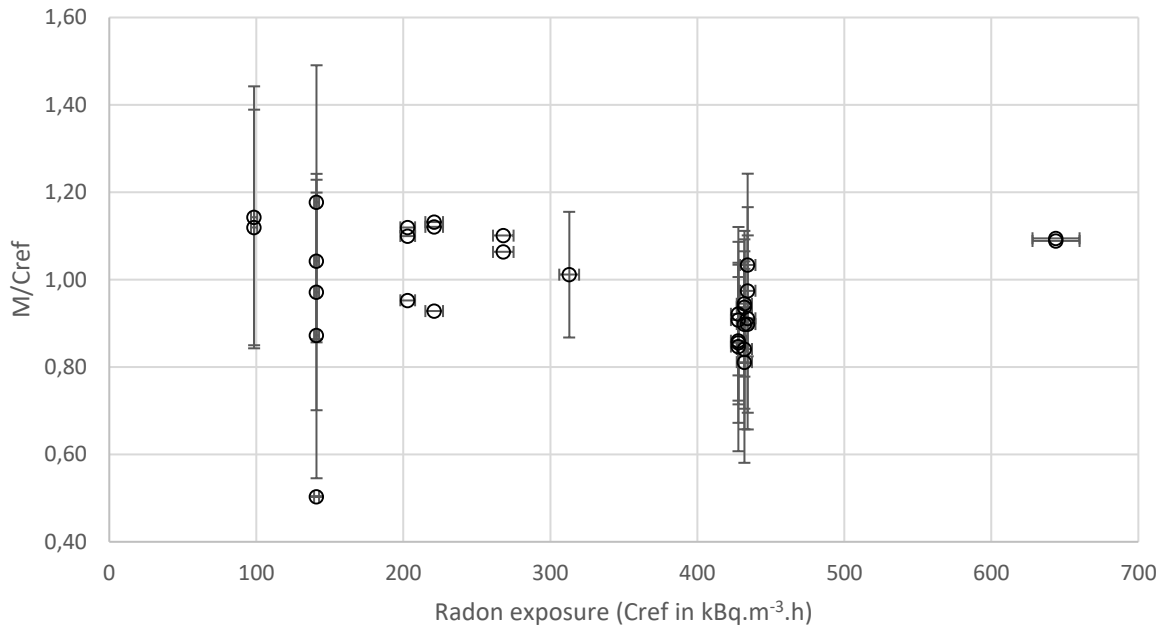


Figure 3 - Ratio between the instrument measurements and the expected true value versus the radon exposure

Except for one set of instruments at low radon exposure, all the mean values of the selected instruments are within the range of twenty percent of the reference value. Dependency on the radon exposure level is not observed. Therefore, for those selected instruments, the linearity response is not an issue inside this range of radon exposure.

The spread of a set of results can be measured by the standard deviation of the population (of  $n$  instruments),  $\sigma(\text{pop})$ , calculated as follow:

$$\sigma(\text{pop}) = \sqrt{n} \sigma(M).$$

Figure 4 shows the relative standard deviation of the population of the selected instruments,  $\sigma(\text{pop})/M$ , in function of the radon exposure. As expected, the relative standard deviation depends on the radon exposure level with a decrease value for higher radon exposure values. Values from some percent to 20 % are observed for at a radon exposure of 430 kBq.m<sup>3</sup>.h. For lower level of radon exposure, relative standard deviations are found to be between 10% and 30%, except for one type of instrument (Z01) where value close to 50% is observed.

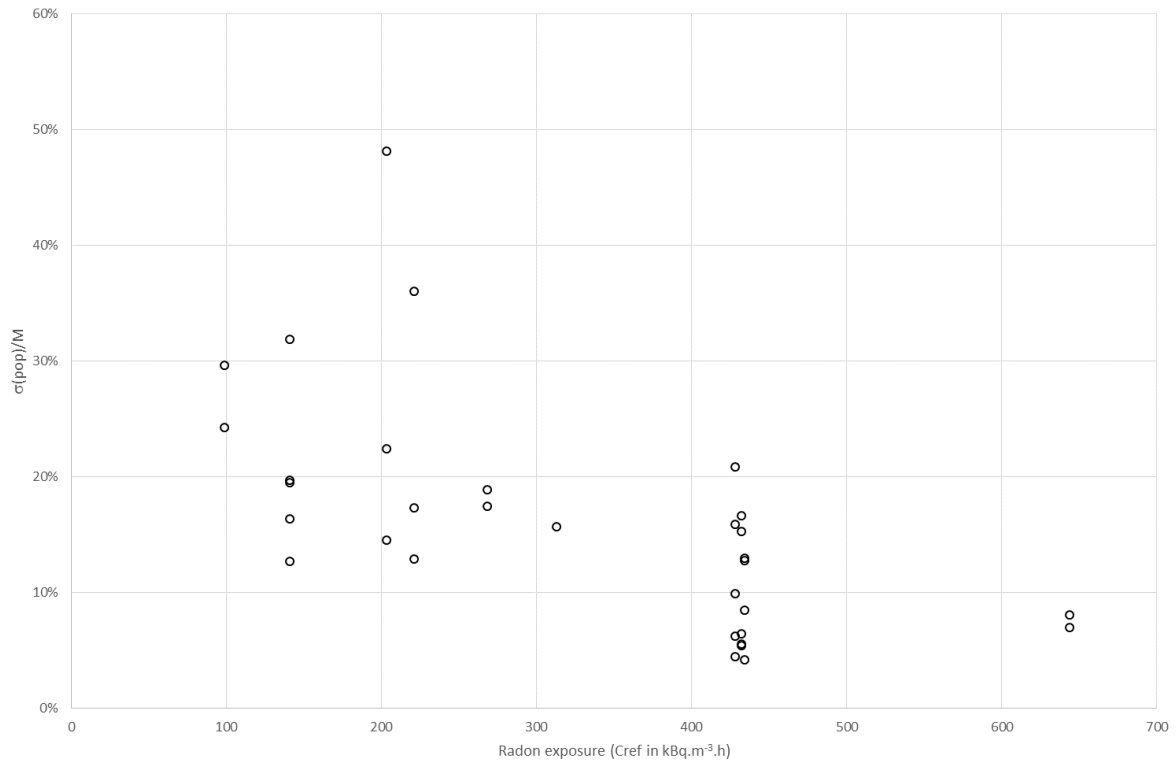


Figure 4 – Relative standard deviation of the population for each type of instruments

Figure 5 shows in detail the result obtained at a radon exposure of  $430 \text{ kBq.m}^{-3}.\text{h}$  during three exposures. Even though the radon exposure level is the same for the three exposures some characteristics differ. All exposures, but I3, had been completed with a constant radon activity concentration through the entire time of exposure. Instead, two different radon activity concentrations (around  $100 \text{ Bq.m}^{-3}$  and  $1000 \text{ Bq.m}^{-3}$ ) were established successively three times during the exposure I3, in order to simulate rapid changes of radon activity concentration. For the exposure I4, the duration of exposure is two months, instead of two weeks for I2 and I3. Also the mean relative humidity is 65% for I4 instead of a dry atmosphere ( $< 5\%$ ) for I2 and I3. No differences on  $M/C_{ref}$  could be observed between these three exposures for the five instruments tested.

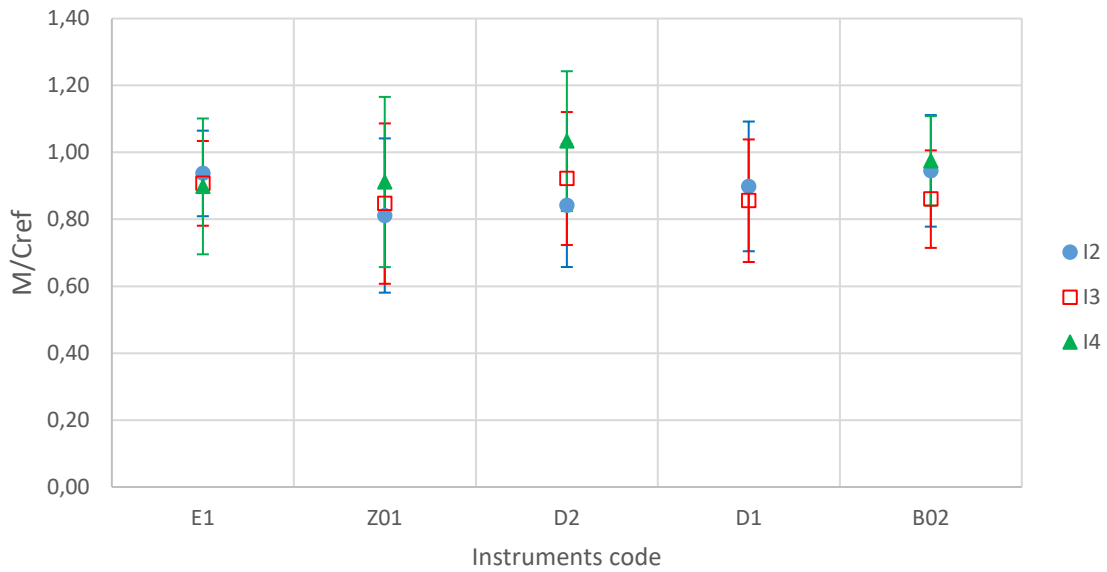


Figure 5 – Results at 430 kBq.m<sup>-3</sup>.h

## 7. Conclusion

Three laboratories participate to the investigation of the accuracy of alpha detectors at low radon exposure. Each laboratory used their own radon chamber with a radon reference atmosphere traceable to a primary radon standard. Radon exposures reference values vary from 99 kBq.m<sup>-3</sup>.h to 644 kBq.m<sup>-3</sup>.h with a relative uncertainty below 5% (at k = 1). The instruments to be tested were exposed over a period of one week to two months. The results of five commercial devices that are used for long term measurement by many laboratories were selected. For each devices a set of 7 or 10 instruments were tested. Ten radon exposures were performed. The mean value of each set of instruments is compared to the radon exposure reference value. All the mean values are in the range of 20% of the reference value except for one instrument at one radon exposure. No dependency on the radon exposure level and on the time duration of the exposure was observed. The spread of the results of a set of instruments was obtained by the standard deviation of the population. As expected, the relative standard deviation grows inversely to the radon exposure level. It was found to be between some percent and 20 % for radon exposure above 400 kBq.m<sup>-3</sup>.h and between 10% and 30% below this value. It should be noted that one device shows a greater dispersion of the results for the low radon exposure.



Annex 2

				Instrument type (design)	Detector	Detector thickness	Total detector area	Analysed detector area	Closed detector (with diffusion barrier)	Range of exposure		
				A	Makrofol	0,3 mm	201 mm <sup>2</sup>	127 mm <sup>2</sup>	Ja / Yes	20 - 5 000 kBq·h·m <sup>-3</sup>		
				A	LR-115	0,3 mm	290 mm <sup>2</sup>	118 mm <sup>2</sup>	Ja / Yes	70 - 7 000 kBq·h·m <sup>-3</sup>	→	
				AA	CR-39	0,9 mm	300 mm <sup>2</sup>	190 mm <sup>2</sup>	Ja / Yes	20 - 20 000 kBq·h·m <sup>-3</sup>		
				AA	CR-39	0,9 mm	100 mm <sup>2</sup>	50 mm <sup>2</sup>	Ja / Yes	20 - 20 000 kBq·h·m <sup>-3</sup>		
				B	CR-39	1,5 mm	440 mm <sup>2</sup>	140 mm <sup>2</sup>	Ja / Yes	20 - 50 000 kBq·h·m <sup>-3</sup>		
				B	CR-39	1 mm	1036 mm <sup>2</sup>	535 mm <sup>2</sup>	Ja / Yes	20 - 50 000 kBq·h·m <sup>-3</sup>	→	
				B	CR-39	1 mm	481 mm <sup>2</sup>	40 mm <sup>2</sup>	Ja / Yes	k.A./ N.s.		
				B	CR-39	1,25 mm	419 mm <sup>2</sup>	120 mm <sup>2</sup>	Ja / Yes	40 - 30 000 kBq·h·m <sup>-3</sup>		
				C	CR-39	1 mm	100 mm <sup>2</sup>	51,7 mm <sup>2</sup>	Ja / Yes	k.A./ N.s.		
				D	Makrofol	0,3 mm	1020 mm <sup>2</sup>	240 mm <sup>2</sup>	Ja / Yes	50 - 10 000 kBq·h·m <sup>-3</sup>	→	
				GA	Elektret (Teflon)	0,127 mm	3421 mm <sup>2</sup>	k.A./ N.s.	Ja / Yes	250 - 16 000 kBq·h·m <sup>-3</sup>		
				GB	Elektret (Teflon)	0,127 mm	3421 mm <sup>2</sup>	k.A./ N.s.	Ja / Yes	50 - 2 000 kBq·h·m <sup>-3</sup>		
				GB	Elektret (Teflon)	0,127 mm	k.A./ N.s.	k.A./ N.s.	Ja / Yes	0 - 240 kBq·h·m <sup>-3</sup>		
				GB	Elektret (Teflon)	k.A./ N.s.	k.A./ N.s.	k.A./ N.s.	Ja / Yes	2 - 11 000 kBq·h·m <sup>-3</sup>		
				GB	Elektret (Teflon)	0,127 mm	k.A./ N.s.	k.A./ N.s.	Ja / Yes	< 2 930 kBq·h·m <sup>-3</sup>		
				L	CR-39	1 mm	100 mm <sup>2</sup>	51,7 mm <sup>2</sup>	Ja / Yes	10 - 80 000 kBq·h·m <sup>-3</sup>	→	
				N	CR-39	1 mm	100 mm <sup>2</sup>	50,9 mm <sup>2</sup>	Ja / Yes	40 - 20 000 kBq·h·m <sup>-3</sup>		
				N	CR-39	k.A./ N.s.	100 mm <sup>2</sup>	52 mm <sup>2</sup>	Ja / Yes	50 - 15 000 kBq·h·m <sup>-3</sup>		
				N	CR-39	1 mm	100 mm <sup>2</sup>	46,8 mm <sup>2</sup>	Ja / Yes	40 - 12 000 kBq·h·m <sup>-3</sup>		
				N	CR-39	k.A./ N.s.	k.A./ N.s.	100 mm <sup>2</sup>	Ja / Yes	k.A./ N.s.		
				N	CR-39	1 mm	100 mm <sup>2</sup>	52 mm <sup>2</sup>	Ja / Yes	12 000 kBq·h·m <sup>-3</sup>		
				N	CR-39	1 mm	100 mm <sup>2</sup>	50 mm <sup>2</sup>	Ja / Yes	40 - 8 000 kBq·h·m <sup>-3</sup>		
				N	CR-39	k.A./ N.s.	100 mm <sup>2</sup>	100 mm <sup>2</sup>	Ja / Yes	12 000 kBq·h·m <sup>-3</sup>		
				N	CR-39	1 mm	100 mm <sup>2</sup>	50 mm <sup>2</sup>	Ja / Yes	40 - 8 000 kBq·h·m <sup>-3</sup>		
				N	CR-39	1 mm	100 mm <sup>2</sup>	k.A./ N.s.	Ja / Yes	12 000 kBq·h·m <sup>-3</sup>		
				Z	LR-115	0,012 mm	227 mm <sup>2</sup>	100 mm <sup>2</sup>	Ja / Yes	50 - 30 000 kBq·h·m <sup>-3</sup>	→	
				Z	LR-115	0,012 mm	227 mm <sup>2</sup>	113 mm <sup>2</sup>	Ja / Yes	50 - 10 000 kBq·h·m <sup>-3</sup>		